NASA Contractor Report 159361

PRELIMINARY DESIGN CHARACTERISTICS OF A SUBSONIC BUSINESS JET CONCEPT EMPLOYING AN ASPECT RATIO 25 STRUT-BRACED WING

R. V. Turriziani, W. A. Lovell, G. L. Martin,
J. E. Price, E. E. Swanson, and G. F. Washburn

(NASA-CR-159361) PRELIMINARY DESIGN CHARACTERISTICS OF A SUBSONIC BUSINESS JET CONCEPT EMPLOYING AN ASPECT RATIO 25 STRUT BRACED WING (Kentron International, Inc.) 101 p HC A06/MF A01 CSCL 01A G3/02

N81-11013

Unclas 29275

KENTRON INTERNATIONAL, INC.
Hampton Technical Center
an LTV company
Hampton, Virginia 23666

NASA Contract NAS1-16000
October 1980

National Aeronautics and
Space Administration
Langley Research Center
Hampton, Virginia 23665

SUMMARY

A study was conducted to determine the fuel efficiency advantages of replacing the conventional wing on a transatlantic-range business jet with a larger, strut-braced, aspect ratio 25 wing. Lifting struts were selected for the study airplane based on an induced drag improvement over non-lifting struts.

The strut-braced wing airplane cruises at higher altitudes and lower speeds than the conventional wing configuration due to the significantly higher cruise lift coefficients required to realize the much higher lift-to-drag ratio potential of the high aspect ratio wing. Two engines were considered, the baseline engine and a higher thrust engine to attain higher cruise altitudes. Also, due to its larger wing, the strut-braced wing airplane has a much lower wing loading than the conventional wing airplane. Although strut-bracing reduces the total weight for a given wing planform, the larger, high aspect ratio wing weighs more than the conventional wing. The improved aerodynamic performance, however, more than compensates for this weight penalty.

Fuel savings were determined for a range of payloads, operating weights, and cruise speeds and for both engines. With both airplanes flying the same payload-range, a fuel savings in excess of twenty percent is realized with the strut-braced wing design. However, the strut-braced wing airplane will be more expensive to build, and, due to the lower cruise speeds, less productive than the conventional wing configuration.

INTRODUCTION

This study has been conducted as part of an on-going effort to evaluate different approaches toward improving the fuel efficiency of aircraft. The

present study consists of an evaluation of two subsonic business jets incorporating an aspect ratio 25, strut-braced high wing. The baseline airplane for the study is a low, cantilever wing business jet with transatlantic range. Each aircraft was configured for a flight crew of two and accommodations for a maximum of 13 passengers. As much of the baseline airplane fuselage as feasible was retained for the strut-braced wing configurations.

Two strut-braced wing configurations were developed differing only in the engine used. In the first version a relatively high thrust engine was chosen in order to attain very high cruise altitudes while in the second the baseline airplane engine was used. For convenience the two airplanes are referred to as the SB-1 and SB-2, respectively. In addition to the obvious struts and braces, the wings of the strut-braced and baseline airplanes are quite different except for their streamwise thickness and planform taper ratios. The strut-braced wing has an aspect ratio of 25 and naturally laminar airfoils, while the baseline wing has an aspect ratio of 9.77 and supercritical airfoil sections. The strut-braced wing is unswept whereas the quarter-chord sweep of the baseline wing is 23 degrees.

The study was done in two phases. In the first, the maximum takeoff gross weight of the strut-braced wing airplanes was limited to that of the baseline airplane and the effect on range was noted. In the second part, the strut-braced wing configurations were required to fly the same payload-range mission as the baseline airplane, and the fuel requirements were determined and compared to the baseline airplane. An additional study variable, applicable to both of the above phases, was passenger accommodations. A weight increment was established to account for the accommodations required for each passenger. These weights were handled in two ways during the payload/range analysis: (1) the operating weight was adjusted as the number of passengers changed; (2) the operating weight was held constant at the value for 13 passengers, irrespective of the actual number of passengers.

Included in this study were configuration definition and layout; weight and drag estimations; design of wing struts and braces from loads, weights, and aerodynamic viewpoints; the estimation of installed engine data; and mission performance.

SYMBOLS AND DEFINITIONS

Where applicable, values are given in this report in both International System Units (SI) and U.S. Customary Units. All calculations were made in U.S. Customary Units.

A	aspect ratio
b	wing span, m (ft)
C_L	lift coefficient, L/qS
C_D	drag coefficient, D/qS
C_{D_i}	induced drag coefficient
C_{D_p}	parasite drag coefficient
C_{D_M}	compressibility drag coefficient
C_f	average skin-friction coefficient, F/qS_{wet}
c.g.	center-of-gravity, percent MAC
C_n	yawing moment coefficient, yawing moment/$qS_w b$
c_r	rudder chord
c_{vt}	vertical tail chord
D	drag, N (lbf)
e	Oswald's airplane efficiency factor, induced-drag efficiency factor
EAS	equivalent airspeed, m/s (knots)

F	equivalent flat plate area, $C_f S_{wet}$, $C_D S$, m^2 (ft^2)
h_p	pressure altitude, m (ft)
HP	horsepower
L	lift, N (lbf)
LFC	laminar flow control
M	Mach number
MAC	mean aerodynamic chord, m (ft)
N_c	bending moment at wing station c, m-N (in-lbf)
q	dynamic pressure, Pa (lbf/ft^2)
R_e	Reynolds number
S	reference area, m^2 (ft^2)
t/c	thickness to chord ratio
TOGW	takeoff gross weight, N (lbf)
$\bar{v}$	horizontal tail volume coefficient
W	weight, N (lbf)
y	spanwise chord location relative to airplane centerline, m (ft)
ΔC_{D_p}	lift-dependent parasite drag coefficient

δ_r rudder deflection, deg

η semi-span fraction

Subscripts:

min minimum

s strut

w wing

wet wetted area

AIRPLANE DEVELOPMENT

Design Criteria

A number of design criteria were established for this study. The baseline airplane and mission ground rules were identical to the non-LFC business jet of reference 1. The baseline fuselage, insofar as possible, was to be used by the strut-braced configurations including accommodations for a cr. . of two and 13 passengers. The wing was to have an aspect ratio of 25 and NACA naturally laminar airfoils. Engine selecti.n was to be limited to those currently available. The baseline airplane engine was to be the second study engine for the strut-braced wing airplane.

Payload-range comparisons were to be made between the baseline and strut-braced wing configurations, with the maximum takeoff gross weight of the strut-braced wing airplanes limited to that of the baseline airplane, 86.3 kN (19 400 lbf). Fuel required comparisons were to be made between the baseline and strut-braced wing business jets with both aircraft flying the payload-range of the baseline airplane. Both the payload-range and the fuel required comparisons were to be made at long-range and high-speed cruise conditions, and with the airplane operating weight adjusted for passenger accommodations, as in the study of reference 1.

Configuration Description

The baseline airplane for this study is from figure 1 of reference 1 and is presented in this report in figure 1.

The two business jets configured for this study have the same strut-braced wing, fuselage, empennage, and landing gear, but differ in the engine used. The SB-1 version uses the General Electric TF34-GE-100 engine, while the SB-2 employs the Garrett AiResearch TFE731-2-2B engine scaled to the thrust level of the TFE731-3 engine. Both airplanes are strut-braced high-wing configurations with two engines attached to the aft fuselage and with the horizontal stabilizer mounted on top of the vertical fin. General arrangements of the two airplanes are shown in figures 2 and 3. The main physical characteristics of the baseline and strut-braced wing airplanes are summarized in table I.

The fuselage for the two strut-braced configurations is that of the baseline airplane modified for wing and landing gear relocations. The fuselage accommodates a crew of two and a maximum of 13 passengers with an 86 cm (34 in) seat pitch. The fuselage length is 16.46 m (54 ft), and the maximum diameter is 1.83 m (6 ft) with a center cabin aisle height of 152 cm (60 in). The passenger cabin includes a toilet, vanity cabinet, and refreshment console. A luggage compartment with a volume of 1.39 m^3 (49 ft^3) is located in the aft fuselage.

The wing selected for the two strut-braced airplanes has 0° sweep at the quarter-chord and natural laminar-flow airfoils with an average thickness ratio of 12.2 percent. The wing has a reference area (trapezoidal) of 51.10 m^2 (550 ft^2) with a taper ratio of .400 and an aspect ratio of 25. The wing is braced with a single strut stabilized by two side braces.

The empennage for the two strut-braced configurations is larger than that for the baseline airplane of figure 1. Sizing was based on static stability and control criteria for the landing and takeoff modes of flight. The horizontal tail has an area of 7.06 m^2 (76 ft^2), and the vertical tail an area of 6.64 m^2 (71.5 ft^2).

The landing gear for the two strut-braced wing airplanes has a single-wheel nose strut and two double-wheel main struts. The main landing gear is located

at the rear fuselage pressure bulkhead so that the gear assembly can retract inside the fuselage aft of the pressure bulkhead.

A fuel holding and distribution tank of 852 liters (225 gallons) is located in the aft fuselage. The remaining fuel, 2847 liters (752 gallons), is carried in integral wing tanks. With the JP-4 fuel used in this study, at a density of .779 kg/liter (6.5 lbm/gal), the airplane fuel capacity is 2.88 Mg (6 350 lbm).

STRUCTURAL AND WEIGHT ANALYSIS

Because there is little weight data on wings with aspect ratios greater than 12, structural strength and deflection studies were conducted to support the wing and airplane weight analyses. The results of the structural studies are presented first, followed by the weight-analysis results.

The detailed structural and weight analysis approach taken for determining the weight of the strut-braced wings is given in Appendix C of reference 2. This approach consists of first determining the weight of the cantilever wing utilizing a statistical mass properties computer program. The strength and deflection characteristics of both cantilever and strut-braced wings are then determined with the SPAR Structural Analysis System of reference 3. Next, utilizing the wing and skin sizing data from the SPAR program and the strut-sizing data determined by the methods given in Appendix C of reference 2, the net weight saving of the strut-braced wing over the cantilever wing is established. This net weight saving is subtracted from the weight of the cantilever wing resulting in the strut-braced wing weight.

Throughout the structural study the following parameters were used: fuel in the wing up to the maximum of 2.22 Mg (4890 lbm) and .66 Mg (1460 lbm) in the fuselage; ultimate load factor of 3.75; and a wing with an aspect ratio of 25 and an area of 51.1 m^2 (550 ft^2). The SB-2, 86.7 kN (19 500 lbf), configuration was used as the vehicle for basic structural studies. The structural weights for the heavier SB-1, 97.9 kN (22 010 lbf), configuration were estimated based on the SB-2 structural study.

Structural Configuration and Model

The SPAR Structural Analysis System cantilever and strut-braced models are shown in figure 4. The wing is identical for both the cantilever and strut-braced configurations and is fabricated from conventional high-strength 7075-T6 aluminum alloy. The wing box consists of wing skins stabilized by stringers, full-depth ribs, and two spars located along the 15 percent and 65 percent chord lines. The 1.52 mm (.06 in) thick leading- and trailing-edge skins carry only pressure loads and were modeled to carry no wing bending or shear loads. To facilitate the analysis, the spars and ribs were held at a constant gauge of 2.54 mm (.10 in).

A detailed design of the struts was conducted to optimize the strut configuration for minimum weight. The details of the method are given in Appendix C of reference 2. The struts are lifting struts and are attached to the bottom side of the fuselage and to the lower wing-skin at a wing rib and are stabilized by lateral braces attached to the wing as shown in figures 2 through 4. Based on the study of reference 2, the strut attachment to wing location was selected at η = .429. The 7075-T6 aluminum-alloy strut is of sheet-stringer construction and utilizes two spars, as shown in figure 5. The struts have a 0.61 m (24 in) chord and a t/c of 12 percent based on aerodynamic requirements.

To design the struts with the desired chords, thickness-chord ratio, and reasonable weights for the strut length required, it was necessary to stabilize the single strut with one or two side braces. The struts without the side stabilizing braces would be unstable in column bending even with solid aluminum structural boxes. Appendix C of reference 2 presents details of the method used to design the braces. The braces are symmetrical airfoil shaped aluminum skins with a t/c of 12 percent and a chord length of 0.1 m (4 in).

Loads

Airloads were calculated for cruise at the +2.5g and -1g (limit) maneuver conditions and are shown in table II. For both the cantilever and strut-braced wing configurations, airload distributions were assumed to be constructed halfway between the elliptical and actual planform geometry distributions, where the ordinates of the loading were selected so that each distribution gave the

same total load. The strut was designed to carry 13.9 percent of the wing airload.

The wing box is, in general, critical for the +2.5g maneuver condition while the strut is critical for the -1g condition. For the latter condition the strut must carry combined bending and axial compression loads. The airloads cause the wing to bend, producing strut axial compression. Fairly high compression loads were also calculated in the strut for the +2.0g taxi condition. The side stabilizing braces were determined to be critical from compression loads resulting from a 2.5g positive flight maneuver. Both rigid body and dynamic components were included for the taxi condition. Utilizing a typical landing gear time-history input, the wing dynamic response loads and deflections were not significant in comparison to the rigid body component.

Structural Results

The wing bending and shear loads are shown in figures 6 and 7, respectively. These loads are based on the airloads given in table II for the wing and strut. The wing bending resultant loads, N_c, presented in table III are based on these wing bending moment curves. For this unswept wing the torsional loads are small and were not considered. The strut stiffens the wing and reduces the deflections with the η = .429 strut, as shown in figure 8. The deflections could be further reduced by utilizing a longer but heavier strut.

Weight Results

Table III presents the detailed wing weight saving for a strut-braced wing over a cantilever design. The net weight saving is equal to the wing-skin saving, 3.82 kN (859 lbf), less the weight of the struts and braces, 1.02 kN (230 lbf) as presented later in this section, or 2.79 kN (629 lbf). The effective wing skin thickness, $\bar{t}$, was calculated utilizing equation 7.17 of reference 4:

$$\bar{t} = C_c L_o + \frac{N_c}{F_{co}} ULF, \text{ where:}$$

$\bar{t}$ = wing skin thickness

C_c = constant = .002

L_o = rib spacing = .381 m (15 in)

N_c = running load

F_{co} = strength allowable

ULF = ultimate load factor of 1.5

An ultimate strength allowable of 379.3 MPa (55 000 psi) was used in the above calculation.

Struts of two different chords were analyzed. The 0.61 m (24 in) chord strut was selected based on aerodynamic benefits and minimal weight penalty over one with a smaller chord. The two side-brace configuration was selected since the combined strut and braces weight was about 18 percent less than the weight of the single side-brace design. The strut length associated with attachment to the wing at η = .429 resulted in a good compromise between wing weight and tip deflection.

The strut system weight per side was determined to be as follows: strut, .37 kN (83.3 lbf); braces (2), .02 kN (3.5 lbf); and attachments .12 kN (28.2 lbf), for a total of .51 kN (115 lbf). This results in a total airplane strut system weight of 1.02 kN (230 lbf).

The airplane group weights (which include wing weights) are shown in table IV for the SB-1 airplane and in table V for the SB-2 airplane. The weights of the baseline airplane from reference 1 are included in table IV. The weight per square foot of the strut-braced wings is approximately equal to that of the baseline airplane wing. The SB-1 and SB-2 unit weights are 286.3 Pa (5.98 psf) and 247.8 Pa (5.53 psf), respectively, compared to the baseline airplane value of 271.5 Pa (5.67 psf). The weights presented for the strut-braced configurations

correspond to the cases where, with maximum payload, the takeoff gross weight matches that of the baseline airplane or is that required to fly the range of the baseline airplane. The one exception to this is the cantilever SB-2 data in table V which is included to show the weight saving in going from the cantilever wing to the strut-braced design. The mission fuel has no significance other than to put the cantilever configuration at the same gross weight as the strut-braced wing airplane. Note that the strut-braced wing weight is 17 percent less than that of the cantilever wing. The SB-1 airplane has similar savings.

The general conclusion of this weight study is that strut bracing of this high aspect ratio wing saves weight. Basing wing-weight estimates on wing-box strength analysis is valid where little statistical weight data is available. These preliminary strength analyses must be used with judgment, for there is a great deal of non-optimum (not primary load-strength related) weight which must be added to determine the wing weight. Further detailed wing design studies are required to define this non-optimum wing weight. It would appear that a large portion of the non-optimum weight penalty may occur near the root of the wing; therefore, the penalty would be relatively less with increasing aspect ratio.

Balance Results

The SB-1 and SB-2 configurations were checked for center-of-gravity (c.g.) range. For both airplanes, the c.g. for all payload/fuel conditions remained in the required range of 27 to 60 percent of the mean aerodynamic chord, as discussed in the stability and control section of this report.

PROPULSION ANALYSIS

As required by the study criteria, the strut-braced wing airplane was evaluated with two currently available engines. The anticipated high-altitude cruise requirements led to the selection of the General Electric TF34-GE-100 engine which has both relatively high-altitude capability and thrust levels at altitude consistent with the study aircraft requirements. This model is designated SB-1. The second engine is the same as that in the baseline airplane--the Garrett AiResearch TFE731-2-2B scaled to the thrust level of the TFE731-3

(ref. 1). This approach was necessary due to the unavailability of TFE731-3 performance data. SB-2 is the model designation with this engine.

General Electric TF34-GE-100 Engine

Description. - The TF34-GE-100 is a two-spool turbofan with separate fan and primary exhaust nozzles. This engine is equipped to provide compressor airbleed and shaft power for aircraft services.

At sea level static, standard day conditions, the design performance is: 40.26 kN (9050 lbf) net engine thrust; a specific fuel consumption (SFC) of .0377 kg/hr/N (.37 lbm/hr/lbf); and a corrected airflow of 151 kg/sec (333 lbm/sec). The bare engine weight is 6.35 kN (1427 lbm) which does not include airframe accessories, inlet, nozzles, thrust reverser, or cowling.

Performance. - Uninstalled engine performance at standard day conditions, for the desired airplane operating envelope, was extracted from the specifications of reference 5 and the supplementary data of reference 6. Although engine performance data provided by the General Electric company terminated at 18 29 km (60 000 ft) such data was extended to 19.81 km (65 000 ft) by extrapolation. The 19.81 km (65 000 ft) performance data was considered as an absolute limit above which further performance extrapolations would be questionable.

The installed performance as provided for this study was developed by reducing the uninstalled gross thrust by five percent with no change in fuel flow or ram drag at all operating conditions. This method of correcting uninstalled performance, for the installation effects of inlet recovery, power extraction, and service airbleed, was used since reference 5 did not provide the correction factors necessary to adjust for these effects. The five percent thrust degradation was considered to be a reasonable penalty based on comparisons of similar engines for similar applications.

Installed engine performance for maximum climb thrust and fuel flow as a function of altitude and Mach number is provided in figure 9. Maximum and part-power cruise fuel flow as a function of thrust and Mach number are provided for the nominal cruise altitudes in figure 10.

Nacelle. - The engine as provided by General Electric does not include the inlet nozzle, thrust reverser, or cowling. Therefore, using the data provided in reference 5, a nacelle was developed for the engine as shown by the sketch in figure 11.

Garrett AiResearch TFE731-2-2B Engine

Description. - The TFE731-2-2B is a lightweight, two-spool geared transonic stage, front-fan, jet-propulsion engine. It has the capability of providing compressor airbleed and shaft power for aircraft services.

At design operating conditions of sea level static and flat-rated ambient temperature of 22°C (72°C) the following engine performance is provided. At takeoff power, limited to five minutes, the net thrust is 15.57 kN (3 500 lbf) with a specific fuel consumption of .0514 kg/hr/N (.504 lbm/hr/lbf). At maximum continuous power, the net thrust is 14.46 kN (3 250 lbf) with a specific fue consumption of .0508 kg/hr/N (.498 lbm/hr/lbf). The corrected engine airflow rate is 51.3 kg/sec (113 lbm/sec).

Performance. - The uninstalled engine performance (ref. 7), at standard day operating conditions, was corrected using the methods of reference 8 for the following installation effects at all operating conditions. High pressure service airbleed or the maximum allowable airbleed, whichever is less, is 0.23 kg/sec (0.5 lbm/sec). The shaft power extraction is 14.9 kw (20 HP), and the inlet pressure recovery is 0.99.

The installed thrust is provided in graphical form for the airplane operating envelope. The maximum climb rated thrust and fuel flow as functions of altitude and Mach number are presented in figure 12. Maximum and part-power cruise fuel flow, as a function of thrust, Mach number and altitude, is presented in figure 13. Performance data presented at 16.76 km (55 000 ft) altitude is extrapolated and should be considered as the upper altitude limit of engine operation.

The data in figures 12 and 13 were adjusted to the level of the TFE731-3 engine by applying a scaling factor. The scaling method employed was that of adjusting the thrust and fuel flow provided by the ratio of the sea level static design thrusts of the two engines. The thrust levels are 16.46 kN (3 700 lbf)

for the TFE731-3 and 15.57 kN (3 500 lbf) for the TFE731-2-2B; the scaling factor was 1.057.

Nacelle. - Scaling of the TFE731-2-2B nacelle for the TFE731-3 engine was not necessary since both engines have the same basic overall dimensions. Based on the dimensions provided in reference 7, an air intake, nozzle and cowling were fitted to the TFE731-2-2B engine. The air intake was sized to provide two percent more airflow than required by the engine to provide for nacelle ventilation and cooling. The nozzles were designed to be co-axial with co-planar exits. A sketch of the resulting nacelle with tabulated dimensions is provided as figure 14. The bare engine weight is 3.27 kN (736 lbf) for the TFE731-E engine.

AERODYNAMIC ANALYSIS

Wing Design

The initial aerodynamic effort in this study was to determine the area, planform, and airfoil sections for an aspect ratio 25 wing. The area was selected to achieve a high cruise L/D. The increase in wing weight with increases in wing area was an indirect consideration. The strut-braced wing configuration had not been established at this point, and therefore aerodynamic data generated for the baseline airplane study of reference 1 was utilized for the wing sizing.

Wing area. - An average cruise $C_{D_{p_{min}}}$ = .0250 was estimated with one-third (.00833) attributable to the wing, leaving .01667 for the remainder of the airplane. These values were used for the first study wing area, 27.87 m^2 (300 ft^2). As the wing areas were increased, their drag was assumed to be proportional to their areas, and therefore the respective wing $C_{D_{p_{min}}}$'s remained .00833. The drag of the remainder of the airplane was assumed to be independent of wing area. This produced a constant equivalent flat plate drag area (F) for the airplane minus wing. This procedure resulted in the total airplane $C_{D_{p_{min}}}$'s presented in figure 15. For this phase of the study, the total airplane drag coefficient was represented by the following equation:

$$C_D = C_{D_{p_{min}}} + \frac{C_L^2}{\pi A e}$$

The resulting variation of L/D with C_L is presented in figure 16, based on an assumed e = .96.

A preliminary study of naturally laminar airfoil sections was conducted to determine the maximum cruise C_L's at the Mach numbers of interest (.60 to .75) before significant drag rises would be encountered. From the data in references 9 to 13, it appeared that lift coefficients in the 0.7 to 0.8 range would be feasible. From figure 16 an area of 51.10 m^2 (550 ft^2) was selected as a compromise between higher L/D's and anticipated heavier weights of the larger wings. The choice was in part based on selecting an L/D of about 30, which was considered to be a reasonable L/D objective for the strut-braced wing configuration.

To finalize the wing area selection it was necessary to evaluate the flight speeds and altitudes required to attain the desired lift coefficients. For a representative cruise C_L of 0.7, the flight conditions are presented in figure 17 for a number of weights. These flight conditions are reasonable except at the lighter weights, which are limited by the altitude capability of the engine. In such cases, for a specific cruise Mach number, the airplane is forced to fly at lower lift coefficients with a resulting reduction in L/D. As figure 17 illustrates, operation at the desired lift coefficients and at moderate business-jet cruise Mach numbers requires altitudes well above those for current business jets. The engine in the required thrust class with the highest altitude capability was the General Elecric TF34-GE-100. The maximum operational altitude for this engine is 19.81 km (65 000 ft). The study was later expanded to include the baseline airplane engine, the Garrett AiResearch TFE731-3, which is limited to 16.76 km (55 000 ft) but was not considered in wing area selection.

Wing airfoils and sweep. - The study criteria required NACA naturally laminar airfoil sections for the wing. The airfoil selection was made on the basis of the most favorable drag characteristics at the expected cruise lift coefficients and Mach numbers. The airfoils and associated aerodynamic characteristics were obtained from wind tunnel tests reported in references 9 through 13. The sections selected were the 64_1-4[illegible] for the wing root and 64_1-410

at the wing tip, resulting in a weighted average t/c of 12.2 percent. This t/c selection simplified the design of the airplane by allowing an unswept wing to be used, while still permitting the expected long-range cruise Mach numbers to be flown without encountering compressibiity drag. Note that although the cruise Mach numbers for the strut-braced wing airplane were expected to be lower than those for the baseline airplane, the higher operating lift coefficients required by the strut-braced wing configuration ruled out an increase in wing t/c.

Drag Analysis

The drag characteristics of the strut-braced wing airplanes were determined with methods previously used for the baseline airplane (ref. 1) where applicable. As shown in figures 2 and 3, the two strut-braced wing configurations are identical except for the engine nacelles and engine struts. The total drag of each of the three airplanes is represented by the following equation:

$$C_{D_{total}} = C_{D_{p_{min}}} + \Delta C_{D_p} + C_{D_i} + C_{D_M}$$

Presentation of $C_{D_{total}}$ for each strut-braced wing airplane requires two plots; figures 18 and 19 for the SB-1 and figures 20 and 21 for the SB-2. Figures 18 and 20 present the basic lift-drag polars and are based on Reynolds numbers corresponding to 129 m/s EAS (250 kts), the climb speed. The effects of Reynolds number over the remainder of the flight envelope are presented in figures 19 and 21. Each of the drag items is discussed in the following sections.

Minimum parasite drag - The minimum parasite drag coefficients were determined by standard methods, accounting for the drag items shown in tables VI through VIII. The baseline airplane data was developed during the study of reference 1. The drag values are presented in the form of equivalent flat plate area ($C_D S_w$) and are based on $C_L = 0$, and representative long-range cruise altitudes and Mach numbers. Note that the drag areas of the SB-1 and SB-2, at their different cruise speeds and altitudes, are the same except for the engine strut and nacelle. This is due to the offsetting effects on the skin friction coefficient (C_f) of changes in Reynolds number and percent laminarization.

Wing: The minimum parasite drag coefficient of the wing average aerodynamic section (64_1-412) was determined by combining 64-212 data (ref. 9) with camber effects from reference 10. Using this test data and other 64-4xx airfoil data (ref. 12) figure 22 was generated showing the extent of natural laminar flow achievable as a function of Reynolds number (Appendix A of ref. 2). In long-range cruise, laminar flow on average extends over approximately 62 percent of the wing chord length for the SB-1 and 60 percent for the SB-2. These laminar flows, which are based on smooth-airfoil test data, require more precise fabrication than current industry practice. Due to the shorter chord length, higher cruise altitudes and lower cruise Mach numbers, the strut-braced wing operates at Reynolds numbers that are less than half those of the baseline airplane wing. The lower Reynolds numbers lead to greater percentages of laminar flow, but also result in higher laminar and turbulent friction drag coefficients.

Supercritical airfoils were used for the baseline airplane wing enabling speeds up to the high-speed cruise Mach number of 0.80 without encountering compressibility drag. This wing was considered to be fully turbulent (ref. 1). As a result, the baseline wing has a minimum parasite drag per unit area about 46 percent greater than the strut-braced wing (tables VI and VII) although the baseline airplane cruises at higher Reynolds numbers. Viewed another way, the wing of the strut-braced airplane has 89 percent greater area than the baseline airplane wing, but its minimum parasite drag area is only 24 percent greater.

Wing struts and braces: The strut with two braces was chosen over the single brace configuration since it was significantly lighter and the impact on drag is small. The strut has approximately the same airfoil (64_1-412) as the average wing section. The braces have symmetrical 64-012 airfoils.

The parasite drag of the struts and braces was established as it was for the wing. Due to the lower Reynolds numbers, laminar flow extended further on the struts and braces than the wing. The interference effects included in tables VII and VIII were estimated based on wind-tunnel tests (ref. 14) wherein the interference effects are reduced to a 10 percent increase in the drag of the isolated strut and braces. For this application, this allowance was increased to 20 percent.

The resulting drag breakdowns are presented in tables VII and VIII. Note that because of the offsetting effects of increased laminarity and decreased Reynolds number on C_f, $C_{D_{p_{min}}}$ of the struts and braces remained essentially constant throughout the cruise envelope.

The struts and braces combined comprise 6.8 percent of the SB-1 total $C_{D_{p_{min}}}$ and 7.3 percent of the SB-2 total $C_{D_{p_{min}}}$, at the cruise conditions of tables VII and VIII.

Remainder of the airplane: Other than the wing, wing struts, and braces of the SB-1 and SB-2 aircraft, the remaining parts of the aircraft were considered to be in fully turbulent flow. The contributions to the basic minimum parasite drag coefficients are contained in figures 18 through 21.

Variation of parasite drag with lift. - The variation of parasite drag with lift includes angle-of-attack dependent friction drag, pressure drag, and the effects of a non-elliptical load distribution on the wing. This increment (ΔC_{D_p}) was based in part on jet-transport flight test data and includes correlations for the effects of airfoil camber, wing sweep, and thickness ratio.

Induced drag. - In the bookkeeping associated with the method which generated the preceding ΔC_{D_p}, the airplane Oswald efficiency factor "e" becores unity. The actual value is obtained through the use of the C_{D_p} term. This applies to the configurations with and without struts, but, as will be discussed later, the struts produce an additional effect on induced drag.

The decision to utilize a lifting rather than non-lifting strut and the methodology to evaluate the wing-strut combination was based on Appendix B of reference 2. At the aircraft design lift coefficient the spanwise loading along the strut span is made uniform by a moderate strut twist. This loading then blends into the wing loading from the strut-wing intersection to the wingtip. Hence, there is no trailing vorticity sheet for the exposed strut, and the wing-strut acts as a kinked-wing biplane.

The derivation of wing-strut L/D was based on starting with an elliptical wing loading before introducing the strut effects. This is compatible with the drag breakdown format being used for the strut-braced wing airplanes where C_{D_i} is based on e = 1.0. The strut has been placed such that it and the wing are at the estimated best long-range cruise C_L (.65) simultaneously. With this method it is possible to calculate the strut lift coefficient (C_{L_s}) corresponding to a particular wing lift coefficient (C_{L_w}). The relationship of these lift coefficients, all based on the wing reference area, is presented in figure 23 for a number of strut to wing area ratios. Note that the wing area (S_w) is the projected wing area and the strut area (S_s) is measured normal to its surface. From Appendix B of reference 2, the induced drag efficiency factor for the wing-strut combination is:

$$e = 1 - \frac{S_s}{S_w} \frac{C_{L_s}}{C_{L_w}} \cos\gamma$$

where γ is the angle between the wing and the strut measured in the front view and C_{L_s} is based on the strut reference area. The variation of "e" with S_s/S_w with total airplane lift coefficient is presented in figure 24. The lift-drag ratios were then calculated, using a representative cruise $C_{D_{p_{min}}} = .0166$ for the airplane without struts and adding the appropriate minimum parasite drag increment for each strut size. The resulting values of L/D were plotted against two different lift coefficients (wing C_L and wing plus strut C_L) in figure 25.

Figure 25(a) shows the systematic variation of L/D, increasing with increasing S_s/S_w, as a function of C_{L_w}. In actual flight, the total C_L must be considered and the struts contribute significantly to the total airplane C_L. Therefore the overall effect of the struts on L/D is as presented in figure 25(b). This illustrates the net result of the offsetting effects on drag due to the struts (increased minimum parasite drag and increased efficiency factor). As figure 25(b) indicates, moderate size struts can be added to an aspect ratio 25 wing with little degradation of the airplane L/D. The lift contribution of the struts allow the airplane to cruise at higher lift coefficients than without

the struts before encountering undesirable airfoil drag characteristics associated with high C_L-moderate Mach number operation.

The results of this study were used to select a strut size and to evaluate the aerodynamic characteristics of the wing-strut combination. Structural requirements defined the attachment point of the strut to the wing. Since it was shown that strut size did not have a significant effect on L/D, a strut size was selected with the same t/c as the average wing t/c. This resulted in a strut with the same drag rise characteristics as the wing and still large enough to generate a significant amount of lift.

The strut-wing area ratio selected was .170, but to account for interference effects the strut was reduced in length, for analytical purposes, resulting in $S_s/S_w = .139$. The induced drag was based on this reduced area ratio; but the minimum parasite drag of the struts was based on their total area ($S_s/S_w = .170$). For the incompressible flight regime, angle-of-attack dependent drag coefficients, (ΔC_{D_p} plus C_{D_i}) are presented in figure 26, which demonstrates the aerodynamics advantage of the aspect ratio 25 wing over the aspect ratio 9.77 design.

Compressibility drag. - The naturally laminar NACA airfoils have a much earlier drag rise than the supercritical airfoils used in the baseline airplane wing. Compressibility drag was zero for the entire speed range of the baseline airplane (ref. 1). The data sources of the compressibility drag increment for the strut-braced wing were references 9 and 10. The magnitude of C_{D_M} was such that it affected the selection of high-speed cruise Mach numbers.

Effect on wing sizing. - A comparison of the final L/D's (fig. 25b) to those determined in the wing sizing phase of the study (fig. 16) indicates excellent agreement. Therefore the wing is properly sized to meet the L/D objective as stated in the wing area section of this report.

Stability and Control

A cursory stability and control analysis of the strut-braced wing business jet was conducted in order to determine the required horizontal and vertical tail areas. All tail sizing was based on static stability and control criteria for

takeoff and landing. The TF34-GE-100 engine was used for empennage sizing for both strut-braced configurations. This results in a slightly larger empennage than needed for the SB-2 configuration due to its lower engine-out moment.

The aft location of the main landing gear on the strut-braced wing configurations causes a relatively large amount of longitudinal control power to be required for rotation during takeoff. This defines the forward center-of-gravity limit as shown on figure 27. The aft center-of-gravity limit is based on maintaining a ten-percent mean aerodynamic chord (MAC) static margin. A center-of-gravity range of 50.8 cm (20 in) was deemed adequate to allow for variations in loading. The minimum horizontal tail area which meets all these criteria is 46 percent larger than the horizontal tail of the baseline airplane. The controllable center-of-gravity range is from 27 to 60 percent of the MAC, further rearward than usual due to the large empennage. For the vertical tail, an area 70 percent greater than that of the baseline airplane is needed to provide sufficient positive directional stability for the strut-braced wing configurations. The rudder size is based on the ability to maintain a straight path during takeoff with one engine inoperative. Figure 28 presents the directional control capability of the airplane for several chord ratios and rudder deflections. A chord ratio of 0.3 and a maximum rudder deflection of ±30 degrees was selected as indicated.

PERFORMANCE AND ANALYSIS

Takeoff and Landing Performance

It was concluded in reference 1 that takeoff and landing performance of the baseline airplane would be comparable to existing business jets. Compared to the baseline airplane, the strut-braced wing configurations have greatly reduced wing-loadings and equal or higher thrust-weight ratios. These factors will enhance the takeoff and landing performance of the strut-braced wing airplanes. The SB-1 and SB-2 may have such a strong capability in these areas that it may be possible to eliminate high-lift devices.

Mission Performance

The mission performance of the strut-braced wing aircraft was determined for two differing criteria. In the first case, the baseline airplane maximum gross

weight [86.3 kN (19 400 lbf)] was used as the maximum gross weight for the strut-braced wing configurations. The operating empty weights of the strut-braced wing aircraft are treater than that of the baseline airplane; therefore, at constant TOGW the available fuel is reduced. The range capability with this reduced fuel was determined and compared to the baseline airplane range for each payload.

The second approach was directly related to fuel efficiency in that the strut-braced wing airplanes were made to fly the same payload-range as the baseline airplane, as previously established in reference 1. The fuel required to fly these missions was determined and compared to that of the baseline airplane.

Payload-range capabilities were calculated using the same mission ground rules as were used for the baseline airplane (ref. 1). Climb performance was based on a speed schedule consisting of a constant equivalent airspeed segment [129 m/s (250 kts)] followed by a segment at cruise Mach number. The cruise segment was analyzed in the cruise-climb mode at the best Breguet range-factor altitude or at the cruise ceiling when so limited. The reserve fuel allowance was equal to that needed for 45 minutes of additional cruise.

An additional variable affecting payload-range performance was the accommodations provided for the passengers. Two methods were employed to account for these items. In the first case the full accommodations (for 13 passengers) remained aboard the airplane as the number of passengers was reduced and is referred to on the figures as "passenger accommodations for 13 passengers". The second method removed the accommodations provided for each passenger as the passenger was removed from the payload. On the appropriate figures, this case is referred to as "with passenger accommodations adjusted for number of passengers". The weight increment for accommodations is part of the operating weight [445 N (100 lbf) per passenger]. Payload, although referred to as "passengers", actually consists of passengers plus luggage [756 N (170 lbf) plus 133 N (30 lbf) per passenger].

Cruise speed selection. - Long-range and high-speed cruise Mach numbers were selected based on the variation of range with cruise Mach number. The corresponding ranges are presented in figure 29 and were based on gross weights where passenger accommodations were adjusted for number of passengers. The fuel loads were varied with number of passengers (payload), and were based on the

requirements at average cruise Mach numbers for flying the baseline airplane range.

The long-range speeds selected were those resulting in greatest range except in the case of the SB-1 airplane, where a little higher speed was selected to provide a lower blocktime with a negligible effect on range. The speeds selected were M = .65 for the SB-1 and M = .55 for the SB-2 compared to M = .71 for the baseline airplane.

High-speed cruise Mach numbers were selected such that the increased speed reduced range by approximately 10 percent. The resulting cruise speeds were M = .70 for the SB-1 and .65 for the SB-2. The corresponding speed for the baseline airplane is M = .80.

Pay oad versus range. - The payload-range capabilities, with maximum gross weight limited to 86.3 kN (19 400 lbf), are presented in figures 30 and 31. The baseline airplane curves are from reference 1. Differences in operating weight between the various configurations is reflected in fuel available (fig. 32). The aerodynamic improvement of the SB-2 over the baseline airplane outweighs the reduction in fuel and increase in operating weight up to a payload of approximately 11 passengers. However, in the case of the SB-1 airplane, the weight increase over the baseline airplane is of such magnitude that the available fuel is severely limited; in spite of the improved aerodynamics the range is drastically reduced. Maximum fuel for the baseline airplane is 3.45 Mg (7 600 lbm) while for the strut-braced wing airplanes it is 2.88 Mg (6 350 lbm).

Fuel efficiency. - The fuel savings with the strut-braced wing aircraft developed in this study are significant. One of the factors constraining the fuel saving is the altitude limitation resulting from the use of available engines. The effect of this limitation is illustrated in figure 33 which presents long-range cruise C_L and L/D of the SB-1 and SB-2. It can be seen that as the airplanes become lighter, with decreasing numbers of passengers, the difference between C_L and L/D at start and end of cruise increases. This large difference is a consequence of cruising at lower than optimum altitude and, therefore, at higher dynamic pressures. The net result is a decrease in both C_L and L/D. This effect is illustrated on figure 34, which presents curves (dashed lines) representing the C_L's and corresponding L/D's that occur at the

start and end of the cruise segement. These curves are based on all the payloads included in the study and are shown relative to those based on the drag polars. The range of cruise altitudes is also indicated on these figures.

In spite of the engine limitation effects, the aerodynamic benefits of the strut-braced wing designs are quite large compared to the baseline airplane. A summary of the long-range and high-speed cruise L/D's is presented in figure 35 for all models. The narrow C_L range of the baseline airplane reflects the fact that the airplane was not cruise-ceiling limited and, therefore, was consistently able to attain its best Breguet range factor altitude, which is essentially a constant C_L operation. The average increases in long-range L/D, over the baseline airplane, are 82 percent and 77 percent for the SB-1 and SB-2, respectively. The average L/D improvement at high-speed cruise conditions is 84 percent for the SB-1 and 67 percent for the SB-2.

A typical variation with payload of average cruise specific fuel consumption and gross weight is presented in figure 36. Compared to the baseline airplane, the SB-2 weight increase due to its larger wing area is largely off-set by the reduced fuel requirement. The SB-1 is substantially heavier than the baseline airplane and the SB-2, due almost entirely to its larger engines. The resultant wing loadings are 1.92 Pa (40.0 psf) for the SB-1 and 1.70 Pa (35.5 psf) for the SB-2, compared to 3.19 Pa (66.7 psf) for the baseline airplane. These wing loadings represent a reduction from the baseline of 40.0 percent and 46.7 percent for the SB-1 and SB-2, respectively.

The results of the mission calculations which form the main objective of this study are summarized in figures 37 through 38. The plots present the fuel required to fly the range of the baseline airplane, versus payload, at the stated conditions. The corresponding ranges are from figures 30 through 31. The fuel savings, in percentage form, did not vary much with payload, accommodations, or cruise Mach number. The average reduction in fuel required is 22.5 percent ± 2 percent and applies to both the SB-1 and SB-2 airplanes. An additional comparison was made whereby the long-range baseline airplane mission was flown at high-speed cruise Mach numbers by the strut-braced airplanes. This would be done to reduce block times, but the fuel savings decrease to an average value of 16.5 percent $\pm$ 1 percent. The takeoff gross weights for these missions are presented in figures 39 and 40.

Productivity and Cost Considerations

As detailed in the preceding "cruise speed selection" section, the cruise speeds of the strut-braced wing airplanes are substantially lower than those of the baseline airplane. The lower cruise speeds result in longer trip times and therefore, reduced aircraft productivity. The strut-braced configuration with the higher cruise speed has a significantly larger engine which contributes additional cost. Furthermore, both strut-braced wing configurations have higher operating empty weights than the baseline airplane. Since construction costs tend to vary directly with weight, the strut-braced wing aircraft will probably have a greater initial cost. Additional costs will also be because of surface tolerance requirements for natural laminar flow airfoils with the need for more stringent construction practices. These factors, all of which adversely impact operating costs, must be weighed against the fuel savings indicated in this study.

CONCLUDING REMARKS

A study has been conducted to evaluate a transatlantic-range business jet with a strut-braced high aspect ratio wing and to compare its performance to a similar business jet with a conventional wing. With both airplanes flying the same payload-range, a substantial fuel savings is realized with the strut-braced wing design. These savings are possible over a wide range of payloads, operating weights and cruise speeds and for several engines. The strut-braced wing airplane cruises at higher altitudes and lower speeds than the conventional wing configuration due to significantly higher cruise lift coefficients. These lift coefficients are required to realize the much higher L/D potential of the high aspect ratio wing. Also, due to its larger wing, the strut-braced wing airplane has a much lower wing loading than the conventional wing airplane. Although strut-bracing reduces the total weight for a given wing planform, the larger, high aspect ratio wing weighs more than the conventional wing. The improved aerodynamic performance, however, more than compensates for this weight penalty. Due to the wing size and complexity, the strut-braced wing airplane will be more expensive to build, and, due to the lower speeds, less productive than the conventional wing configuration.

REFERENCES

1. Turriziari, R. V., Lovell, W. A., Price, J. E., Quartero, C. B., and Washburn, G. F.: Preliminary Design Characteristics of a Subsonic Business Jet Concept Employing Laminar Flow Control, NASA CR-158958, September 1978.

2. Smith, P. M., Lovell, W. A., Price, J. E., and Washburn, G. F.: A Study of High-Altitude Manned Research Aircraft Employing Strut-Braced Wings of High-Aspect-Ratio, NASA CR-159262, 1980.

3. Whetstone, W. A.: SPAR Structural Analysis System Reference Manual, System Level 14, NASA CR-145098, 1979.

4. Shanley, F. R.: Weight-Strength Analysis of Aircraft Structures, Second Edition, Dover Publications.

5. Coalson, M. A.: Prime Item Development Specification for Engine, Aircraft Turbofan TF34-GE-100, CI NO. 10E23A1. General Electric Company Specification No. CP45E0002, Code Identification 99207, Part 1 of 2, Revision C, June 1, 1977.

6. Harris, W. A.: Supplementary TF34 Engine Performance, the General Electric Company, August 4, 1978.

7. Brandys, E. L. and Viquesney, J. L.: 731 Turbofan Engine, Preliminary Installation Manual. IM-8001, October 4, 1971.

8. Clarke, P. J.: Performance Correction Procedure for A. Research Model TFE731-2-2B Turbofan Engine (Gates Learjet Corporation). PE-8119-R, June 30, 1970.

9. Van Dyke, Milton D.: High-Speed Subsonic Characteristics of 16 NACA 6-Series Airfoil Sections, NACA Technical Note 2070, March 1952.

10. Summers, James L. and Treon, Stuart L.: The Effect of Amount and Type of Camber on the Variation with Mach Number of the Aerodynamic Characteristics of a 10 Percent Thick NACA 64A-Series Airfoil Section, NACA Technical Note 2096, May 1950.

11. Stivers, Louis S., Jr.: Effects of Subsonic Mach Numbers on the Forces and Pressure Distributions on Four NACA 64A-Series Airfoil Sections at Angles of Attack as High as 28, NACA Technical Note 3162, March 1954.

12. Abbott, Ira H., Von Doenhoff, Albert E., and Stivers, Louis S., Jr.: Summary of Airfoil Data, NACA Report 824, 1945.

13. Loftin, Laurence K., Jr. and Smith, Hamilton A.: Aerodynamic Characteristics of 15 NACA Airfoil Sections at Seven Reynolds Numbers from 0.7×10^6 to 9.0×10^6, NACA Technical Note 1945, October 1949.

14. Jobe, Charles E., Kulfan, Robert M. and Vachal, John D.: Wing Planforms for Large Military Transports, Journal of Aircraft. Vol. 16, July 1979, pp. 425-432.

TABLE I. - PHYSICAL CHARACTERISTICS

	Configuration		
	Baseline	SB-1	SB-2
WING			
Area, m^2 (ft^2)	27.03 (291)		51.10 (550)
Aspect ratio	9.77		25
Sweep @ 1/4 chord, deg	23		0
Span, m (ft)	16.25 (53.33)		33.74 (117.25)
Taper ratio	.388		.400
MAC, m (ft)	1.77 (5.82)		1.52 (4.98)
Streamwise t/c, root	.12		.14
, tip	.12		.10
NACA airfoil section, root	(special		64$_1$-414
, tip	supercritical)		64$_1$-410
HORIZONTAL TAIL			
Area, m^2 (ft^2)	4.83 (52)		7.06 (76)
Aspect ratio	5.36		5.36
Sweep @ 1/4 chord, deg	25		25
Span, m (ft)	5.09 (16.70)		6.15 (20.18)
Taper ratio			
VERTICAL TAIL			
Area, m^2 (ft^2)	3.90 (42)		6.64 (71.5)
Aspect Ratio	1.54		1.59
Sweep @ 1/4 chord, deg	35		35
Span, m (ft)	2.44 (8.0)		3.25 (10.66)
Taper ratio	.423		.450

TABLE I. - Concluded

	Configuration		
	Baseline	SB-1	SB-2
FUSELAGE			
Length, m (ft)	16.46 (54.0)	16.46 (54.0)	
Diameter, m (ft)	1.83 (6.0)	1.83 (6.0)	
WING STRUT			
Length, m (ft)	-	7.11 (23.33)	
Chord length, m (ft)	-	.61 (2)	
NACA airfoil section	-	64_1-412	
WING BRACES			
Lengths, m (ft)	-	1.22 (4)	
m (ft)	-	.61 (2)	
Chord length, m (ft)	-	.10 (.33)	
NACA airfoil section)	-	64-012	
NACELLE			
Length, m (ft)	2.74 (9.0)	3.43 (11.24)	2.74 (9.0)
Diameter, m (ft)	1.07 (3.5)	1.35 (4.42)	1.07 (3.5)

TABLE II. - AIRLOADS

LOAD CONDITION	WING AIRLOADS (per one side of airplane)		STRUT LOADS (per strut)			
			Air		Axial	
	kN	lbf	kN	lbf	kN	lbf
Cantilever						
* 2.5 g maneuver	105.62	23744	-	-	-	-
* -1.0 g maneuver	- 52.81	-11872	-	-	-	-
Strut-braced, n = .429						
* 2.5 g maneuver	90.42	20328	12.57	2826	319.52	71831
* -1.0 g maneuver	-36.17	- 8132	- 5.03	-1130	-127.66	-28700
** 2.0 g taxi	0	0	0	0	-138.95	-31237

* Less 2.22 kN (500 lbf) taxi and climb fuel.

** Full wing fuel condition, 2.218 Mg (4890 lbm).

TABLE III. - WING SKIN WEIGHT SAVING DUE TO STRUT-BRACING

Wing Station η	Bending Resultant ΔN_c		Skin Thickness $\Delta \bar{t}$		Skin Weight ΔW	
	kN/m	lbf/in	mm	in	kN	lbf
0 - .1	1665	9505	6.60	.260	1.27	285.7
.1 - .2	1496	8541	5.92	.233	1.07	240.0
.2 - .3	1189	6788	4.72	.186	.79	178.1
.3 - .4	695	3969	2.74	.108	.43	96.9
.4 - .5	162	925	.660	.026	.10	21.6
.5 - .6	153	874	.610	.024	.08	18.1
.6 - .7	95	543	.381	.015	.04	10.1
.7 - .8	64	366	.254	.010	.03	6.1
.8 - .9	24	137	.076	.003	.01	1.9
.9 - 1.0	7	41	.025	.001	0	0.6
				TOTAL	3.82	859.0

NOTE: The deltas shown are between the cantilever and strut-braced wings.

TABLE IV. - SB-1 AIRPLANE WEIGHTS

	Baseline (ref. 1)		SB-1			
			* Baseline TOGW		** Baseline Range	
	kN	lbf	kN	lbf	kN	lbf
Structure						
- excluding wing	12.59	2830	14.68	3300	15.44	3470
- wing	7.34	1650	14.28	3210	14.63	3290
Propulsion	8.05	1810	14.46	3250	14.77	3320
Systems	17.26	3880	17.30	3890	17.75	3990
Weight Empty	45.24	10170	60.72	13650	12.59	14070
Operating items	2.80	630	3.07	690	3.07	690
Operating weight empty	48.04	10800	65.79	14340	65.66	14760
Payload (maximum)	11.57	2600	11.57	2600	11.57	2600
Zero fuel weight	59.61	13400	75.36	16940	77.23	17360
Mission fuel	26.69	6000	10.94	2460	20.68	4650
Takeoff gross weight	86.30	19400	86.30	19400	97.91	22010

*Takeoff gross weight held equal to baseline's.

**Takeoff gross weight for range equal to baseline's.

TABLE V. - SB-2 AIRPLANE WEIGHTS

	Cantilever SB-2		Strut-braced SB-2			
			* Baseline TOGW		** Baseline Range	
	kN	lbf	kN	lbf	kN	lbf
Structure						
- excluding wing	12.63	2840	12.68	2850	12.68	2850
- wing	16.32	3670	13.52	3040	13.52	3040
Propulsion	8.59	1930	8.59	1930	8.59	1930
Systems	17.30	3890	17.30	3890	17.30	3890
Weight Empty	54.84	12330	52.09	11710	52.09	11710
Operating items	3.07	690	3.07	690	3.07	690
Operating weight empty	57.91	13020	55.16	12400	55.16	12400
Payload (maximum)	11.57	2600	11.57	2600	11.57	2600
Zero fuel weight	69.48	15620	66.73	15000	66.73	15000
Mission fuel	17.26	3880	19.57	4400	20.01	4500
Takeoff gross weight	86.74	19500	86.30	19400	86.74	19500

* Takeoff gross weight held equal to baseline's.

** Takeoff gross weight for range equal to baseline's.

TABLE VI. - MINIMUM PARASITE DRAG OF BASELINE BUSINESS JET AT M = .71 AND 15.24 km (50 000 ft)

Airplane Part	Wetted Area	Reynolds Number	Drag Item	Coeff. C_f	Equivalent Flat Plate Area	
					m^2	ft^2
Wing	52.76 m^2 (568 ft^2)	4.79 x 10^6	Uncorr. flat plate	.00315	.166	1.79
			Supervelocity		.034	.37
			Pressure drag		.002	.02
			Wing/Body interf.		.006	.07
			Excrescences		.013	.14
			Surface roughness		.005	.05
					.227	2.44
Horizontal Tail	9.75 m^2 (105 ft^2)	2.62 x 10^6	Uncorr. flat plate	.00350	.034	.37
			Supervelocity		.005	.05
			Pressure drag		.000	.00
			Interference		.002	.02
			Excrescences		.003	.03
			Surface roughness		.001	.01
					.046	.49
Vertical Tail	9.10 m^2 (98 ft^2)	4.41 x 10^6	Uncorr. flat plate	.00319	.029	.31
			Supervelocity		.004	.04
			Pressure drag		.000	.00
			Interference		.002	.02
			Excrescences		.003	.03
			Surface roughness		.001	.01
					.038	.41

TABLE VI. - Continued

Airplane Part	Wetted Area	Reynolds Number	Drag Item	Coeff. C_f	Equivalent Flat Plate Area	
					m^2	ft^2
Fuselage	68.75 m^2 (740 ft^2)	4.55×10^7	Uncorr. flat plate	.00221	.152	1.64
			3-dim. effect		.001	.01
			Supervelocity		.008	.09
			Pressure drag		.002	.02
			Non-optimum shape		.003	.03
			Cockpit drag		.023	.25
			Pressurization		.008	.09
			Excrescences		.009	.10
			Surface roughness		.005	.05
					.212	2.28
Engine Struts	2.78 m^2 (30 ft^2)	5.64×10^6	Uncorr. flat plate	.00307	.008	.09
			Supervelocity		.001	.01
			Pressure drag		.000	.00
			Excrescences		.001	.01
			Surface roughness		.001	.01
					.011	.12
Nacelles	15.79 m^2 (170 ft^2)	7.58×10^6	Uncorr. flat plate	.00292	.046	.50
			3-dim. effect		.000	.00
			Supervelocity		.013	.14
			Excrescences		.009	.10
			Surface roughness		.001	.01
			Loss of lip suct.		.007	.08
			Boattail drag		.008	.09
			Interference		.027	.29
					.112	1.21

TABLE VI. - Concluded

Airplane Part	Wetted Area	Reynolds Number	Drag Item	Coeff. C_f	Equivalent Flat Plate Area	
					m^2	ft^2
Trim					.003	.03
Air Condition, etc.					.005	.05
Total Airplane					.653	7.03

TABLE VII. - MINIMUM PARASITE DRAG OF SB-1 CONFIGURATION AT M = .65 AND 18.29 km (60 000 ft)

Airplane Part	Wetted Area	Reynolds Number	Drag Item	Coeff. C_f	Equivalent Flat Plate Area	
					m^2	ft^2
Wing	103.96 m^2 (1119 ft^2)	2.19×10^6	Uncorr. flat plate	.00211	.219	2.36
			Supervelocity		.043	.46
			Pressure drag		.003	.03
			Wing/Body interf.		.001	.01
			Excrescences		.008	.09
			Surface roughness		.007	.07
					.281	3.03
Horizontal Tail	14.40 m^2 (155 ft^2)	1.80×10^6	Uncorr. flat plate	.00378	.055	.59
			Supervelocity		.009	.10
			Pressure drag		.001	.01
			Interference		.002	.02
			Excrescences		.005	.05
			Surface roughness		.002	.02
					.073	.78
Vertical Tail	13.56 m^2 (146 ft^2)	2.89×10^6	Uncorr. flat plate	.00346	.047	.51
			Supervelocity		.008	.09
			Pressure drag		.000	.00
			Interference		.002	.02
			Excrescences		.004	.04
			Surface roughness		.002	.02
					.063	.68

TABLE VII. - Continued

Airplane Part	Wetted Area	Reynolds Number	Drag Item	Coeff. C_f	Equivalent Flat Plate Area	
					m^2	ft^2
Fuselage	69.40 m^2 (747 ft^2)	2.58×10^7	Uncorr. flat plate	.00242	.168	1.81
			3-dim. effect		.001	.01
			Supervelocity		.009	.10
			Pressure drag		.002	.02
			Non-optimum shape		.004	.04
			Cockpit drag		.023	.25
			Pressurization		.008	.08
			Excrescences		.010	.11
			Surface roughness		.005	.05
					.231	2.49
Engine Struts	2.23 m^2 (24 ft^2)	2.95×10^6	Uncorr. flat plate	.00345	.007	.08
			Supervelocity		.001	.01
			Pressure drag		.000	.00
			Excrescences		.001	.01
			Surface roughness		.001	.01
					.010	.11
Nacelles	22.20 m^2 (239 ft^2)	5.37×10^6	Uncorr. flat plate	.00311	.070	.75
			3-dim. effect		.000	.00
			Supervelocity		.021	.23
			Excrescences		.014	.15
			Surface roughness		.002	.02
			Loss of lip suct.		.012	.13
			Boattail drag		.020	.21
			Interference		.043	.46
					.182	1.96

TABLE VII. - Concluded

Airplane Part	Wetted Area	Reynolds Number	Drag Item	Coeff. C_f	Equivalent Flat Plate Area	
					m^2	ft^2
Wing Struts	17.22 m^2 (185 ft^2)	.956 x 10^6	Uncorr. flat plate	.00236	.041	.44
			Supervelocity		.007	.08
			Surface roughness		.001	.01
			Interference		.009	.10
					.059	.63
Wing Braces	.74 m^2 (8 ft^2)	.159 x 10^6	Uncorr. flat plate	.00346	.003	.03
			Supervelocity		.001	.01
			Surface roughness		.000	.00
			Inteference		.001	.01
					.004	.04
Trim					.004	.04
Air Condition, etc.					.005	.05
Total Airplane					.911	9.81

TABLE VIII. - MINIMUM PARASITE DRAG OF SB-2 CONFIGUPATION AT M = .55 AND 16.76 km (55 000 ft).

Airplane Part	Wetted Area	Reynolds Number	Drag Item	Coeff. C_f	Equivalent Flat Plate Area	
					m^2	ft^2
Total airplane minus engine struts and nacelles		Equivalent flat plate area is identical to SB-1 at .65 m and 18.29 km (60 000 ft). Table VIII.			.719	7.74
Engine Struts	2.78 m^2 (30 ft^2)	8.89×10^6	Uncorr. flat plate	.00281	.009	.10
			Supervelocity		.001	.01
			Pressure drag		.000	.00
			Excrescences		.001	.01
			Surface roughness		.001	.01
					.012	.13
Nacelles	15.79 m^2 (170 ft^2)	1.19×10^7	Uncorr. flat plate	.00269	.051	.55
			3-dim. effect		.000	.00
			Supervelocity		.013	.14
			Excrescences		.010	.11
			Surface roughness		.002	.02
			Loss of lip suct.		.007	.08
			Boattail drag		.008	.09
			Interference		.027	.29
					.119	1.28
Total Airplane					.850	9.15

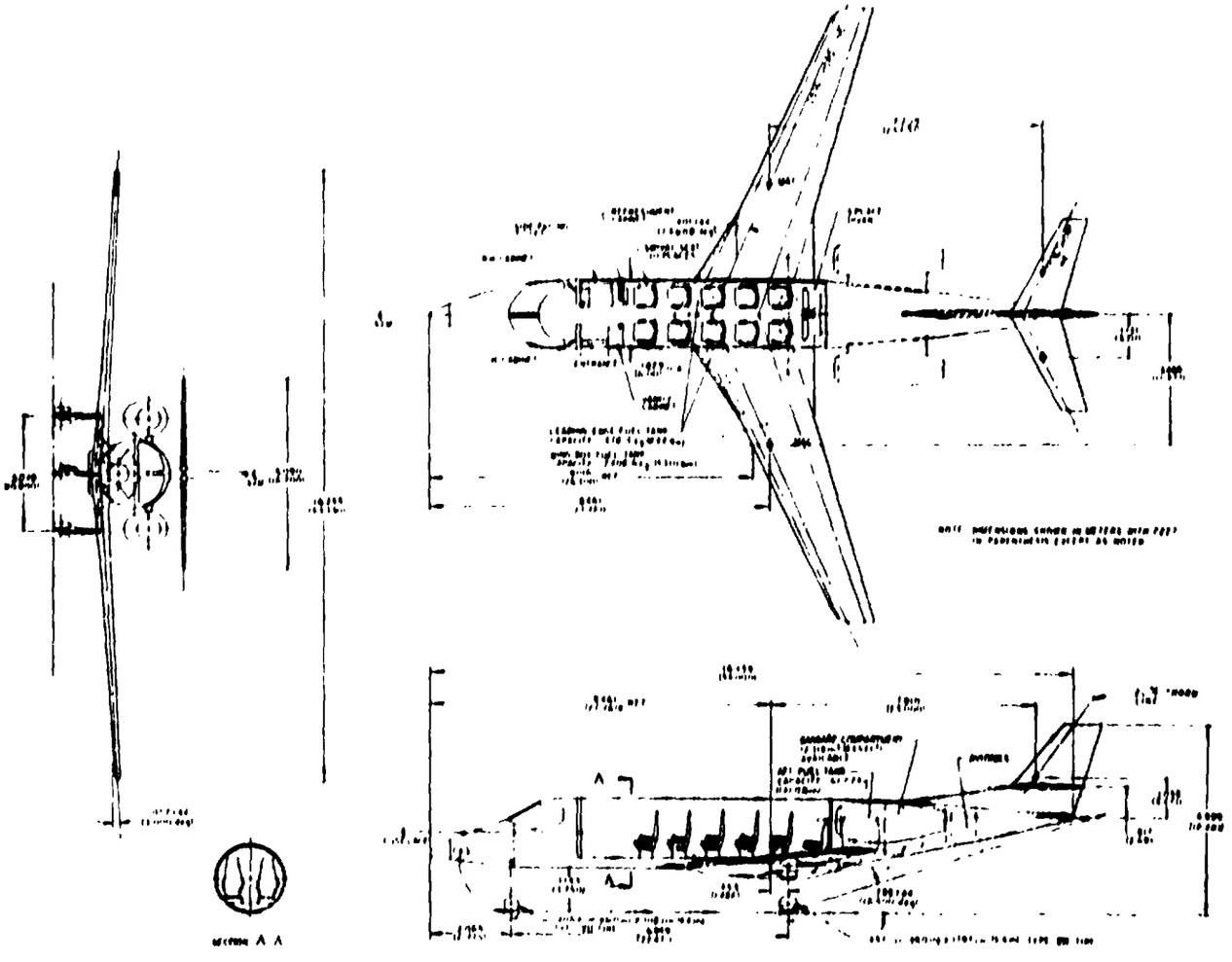

Figure 1. - General arrangement of baseline business jet with TFE731-3 engines.

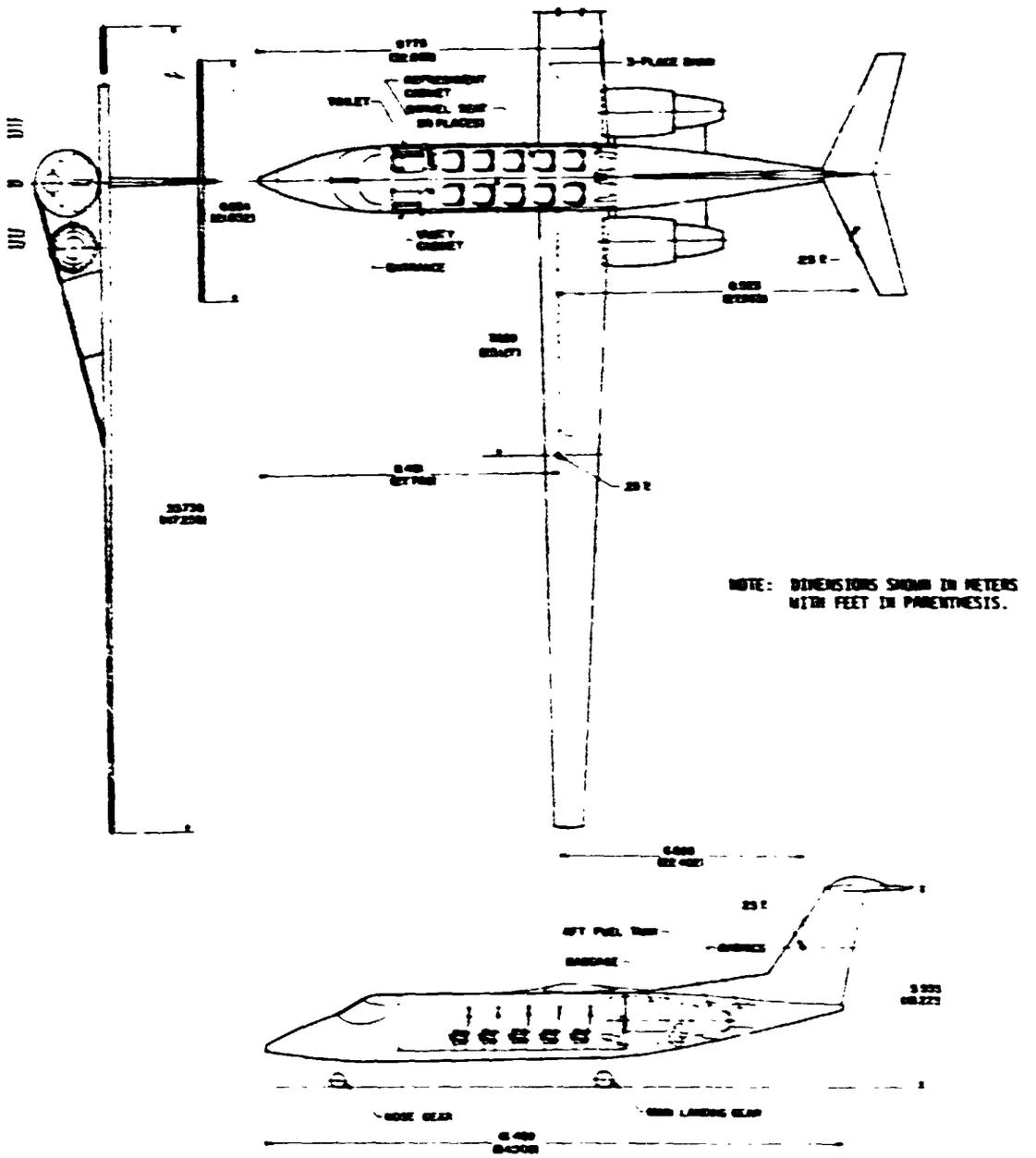

Figure 2. - General arrangement of strut-braced wing business jet with TF34-GE-100 engines (model SB-1).

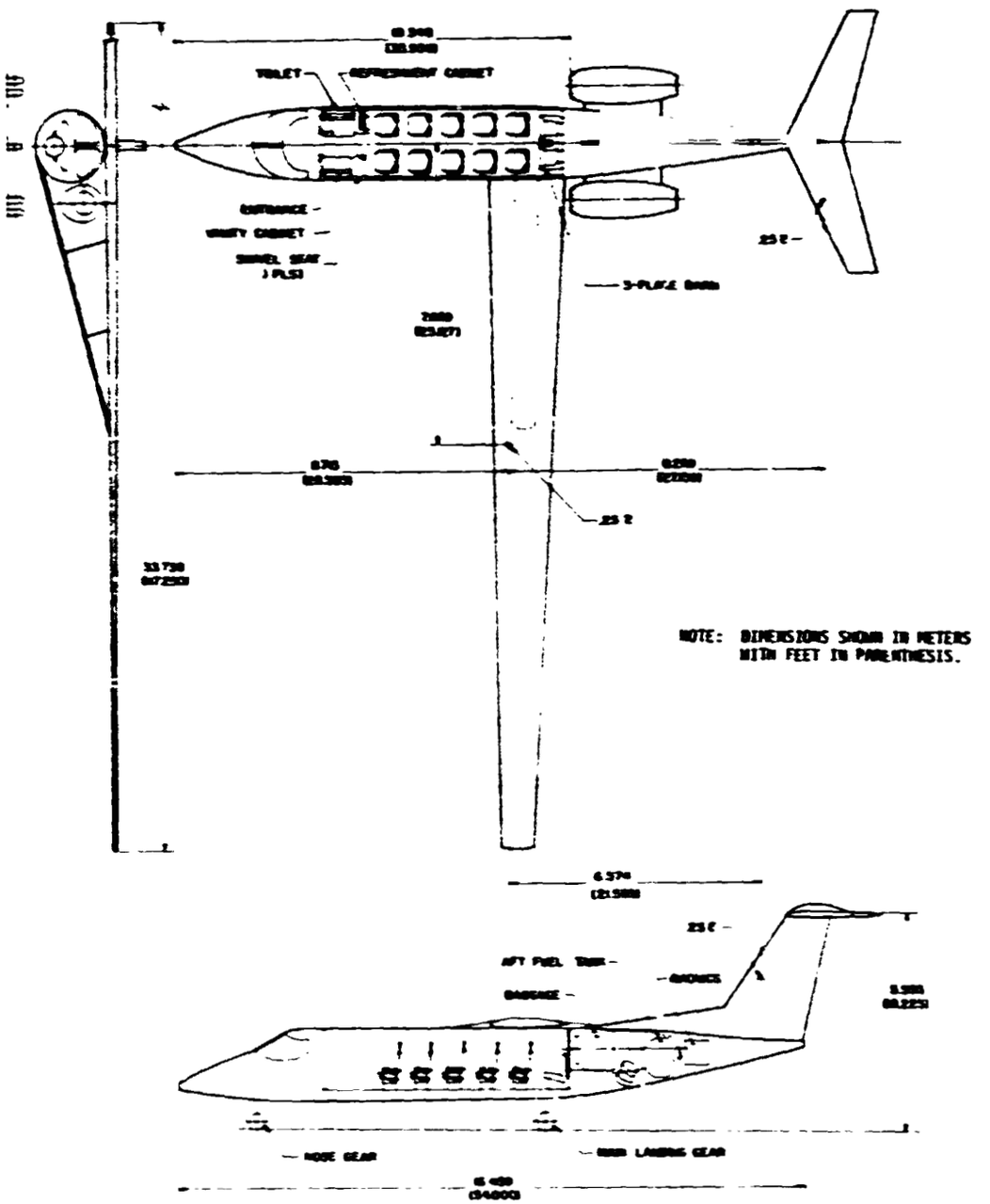

Figure 3. - General arrangement of strut-braced wing business jet with TFE731-3 engines (model SB-2).

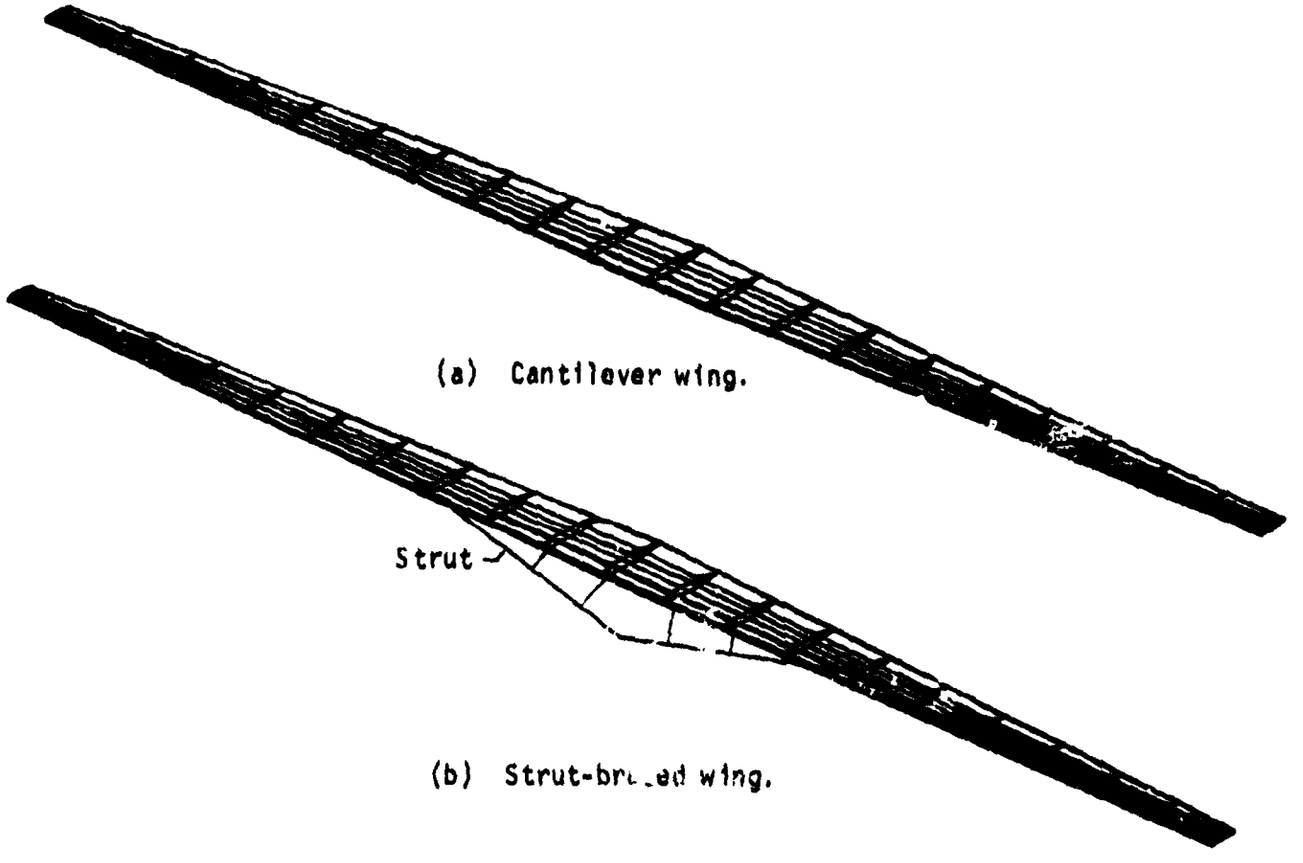

(a) Cantilever wing.

(b) Strut-braced wing.

Figure 4. - Structural wing models.

Note: All material is aluminum.

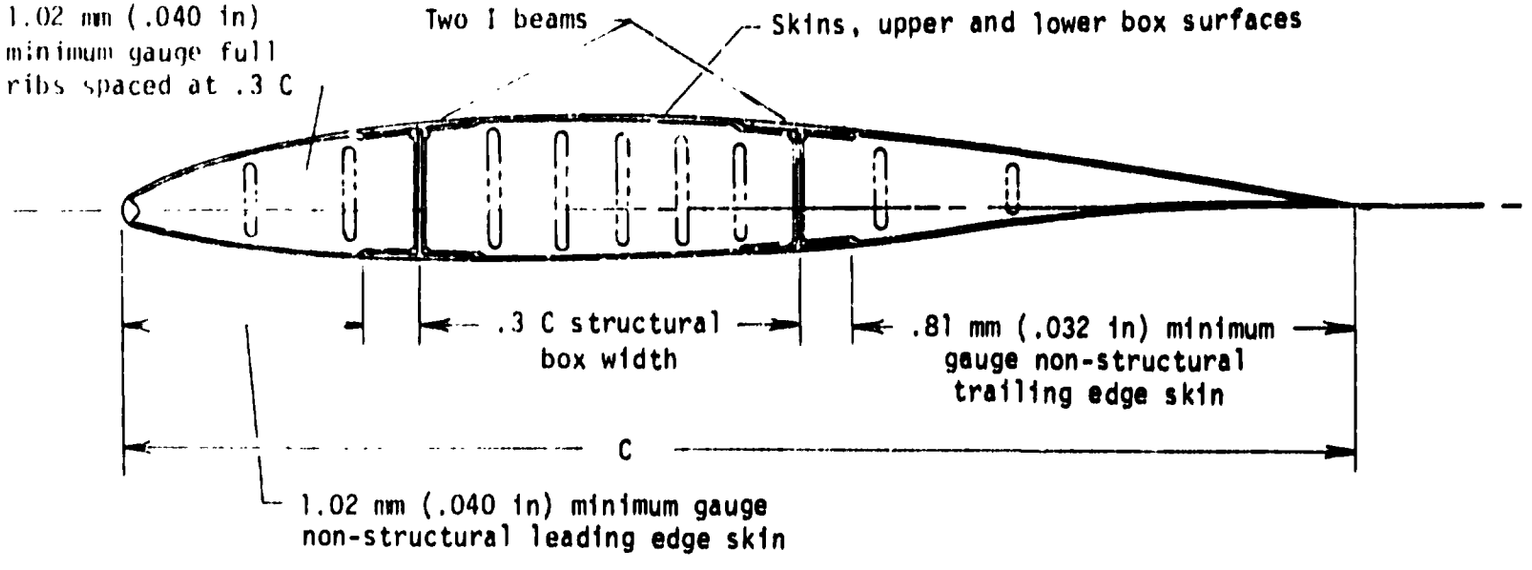

Figure 5. - Typical wing strut two beam structural box and secondary structure.

Fuel = 1.77 Mg(3900 lbm), at maneuver conditions.

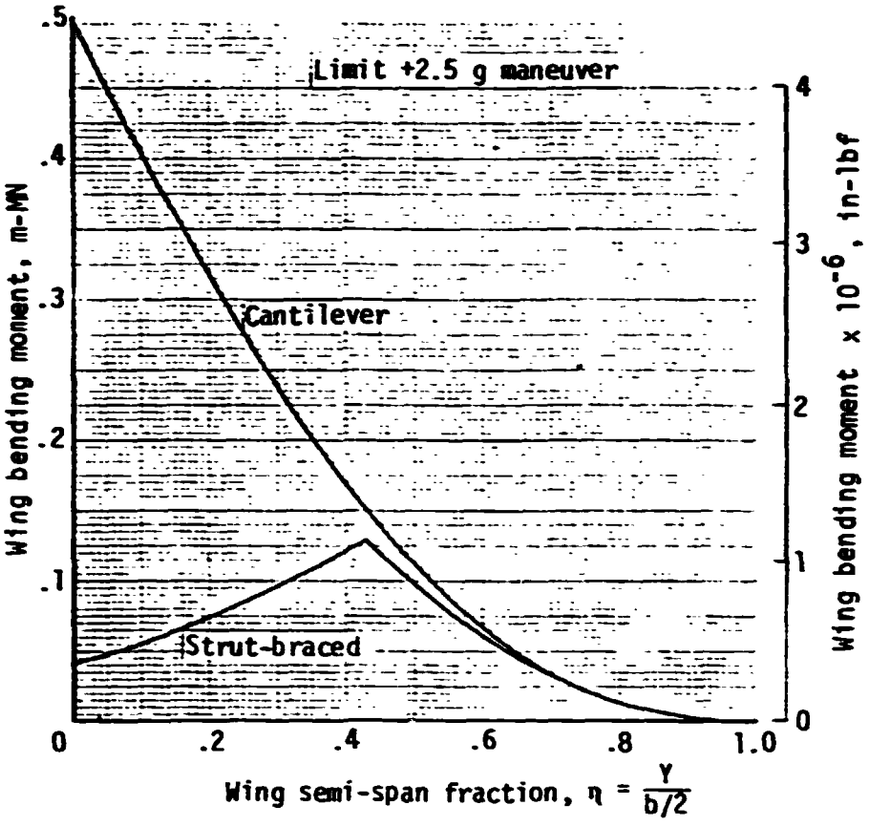

Figure 6. - Wing bending moments of cantilever and strut-braced wings on 86.3 kN (19 400 lbf) SB-2 airplane.

Fuel = 1.77 Mg (3 900 lbm), at maneuver conditions.

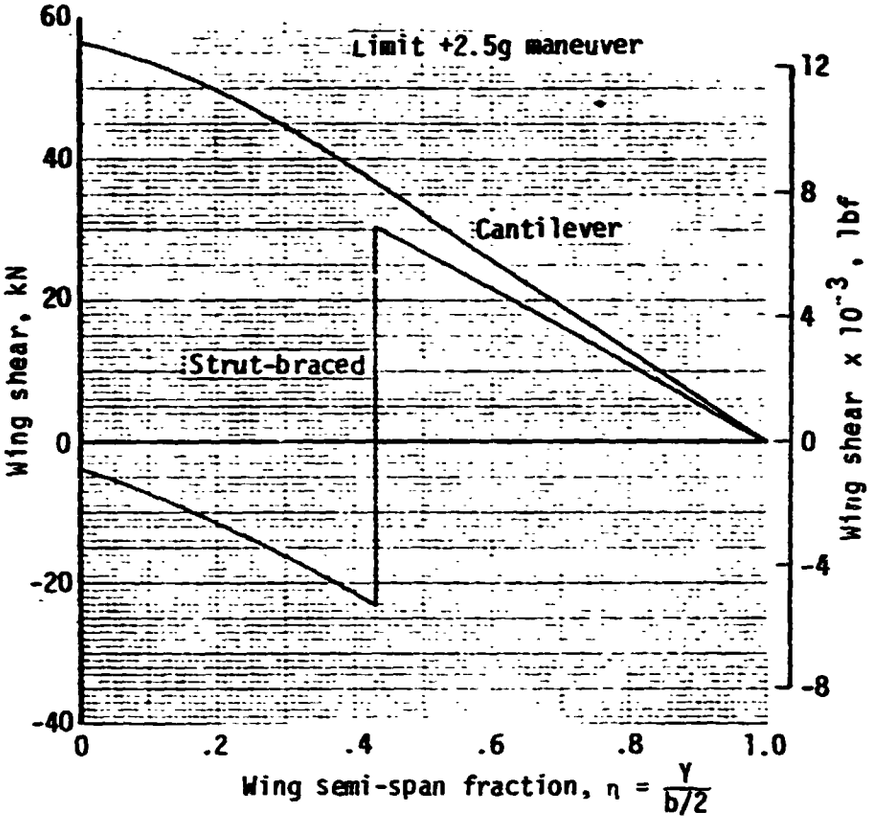

Figure 7. - Wing shear of cantilever and strut-braced wings on 86.3 kN (19 400 lbf) SB-2 airplane.

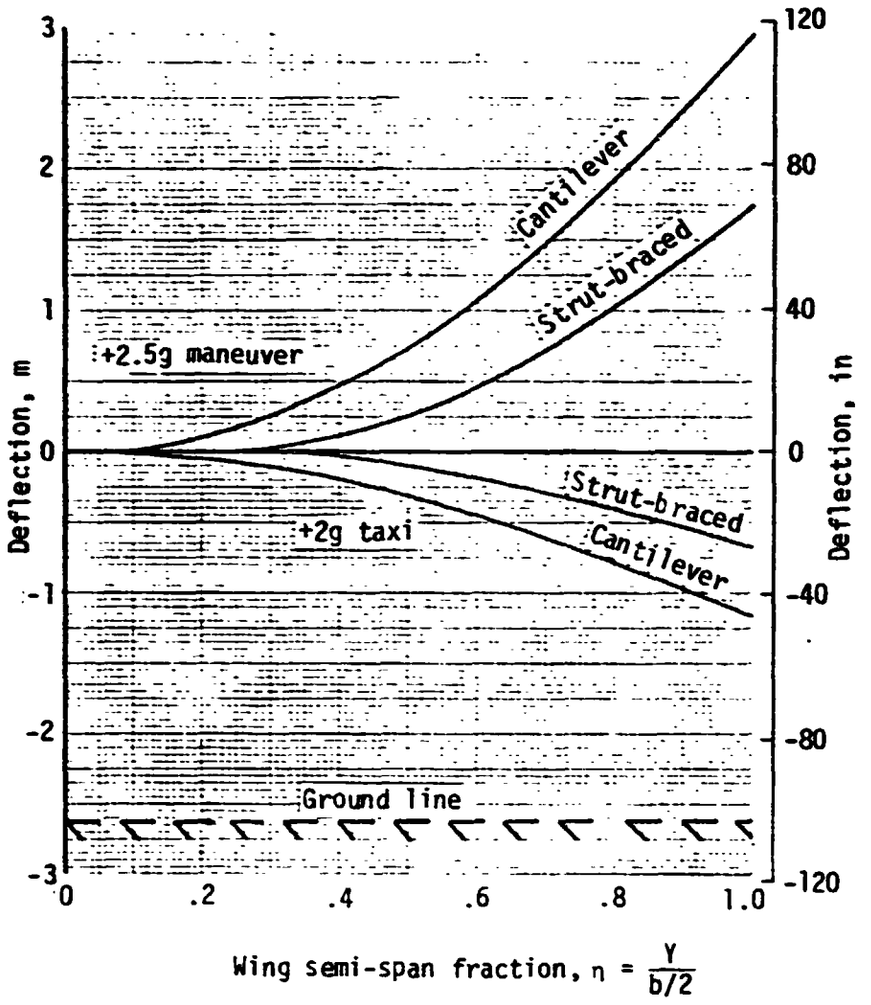

Figure 8. - Wing deflection of cantilever and strut-braced wings on 86.3 kN (19 400 lbf) SB-2 airplane.

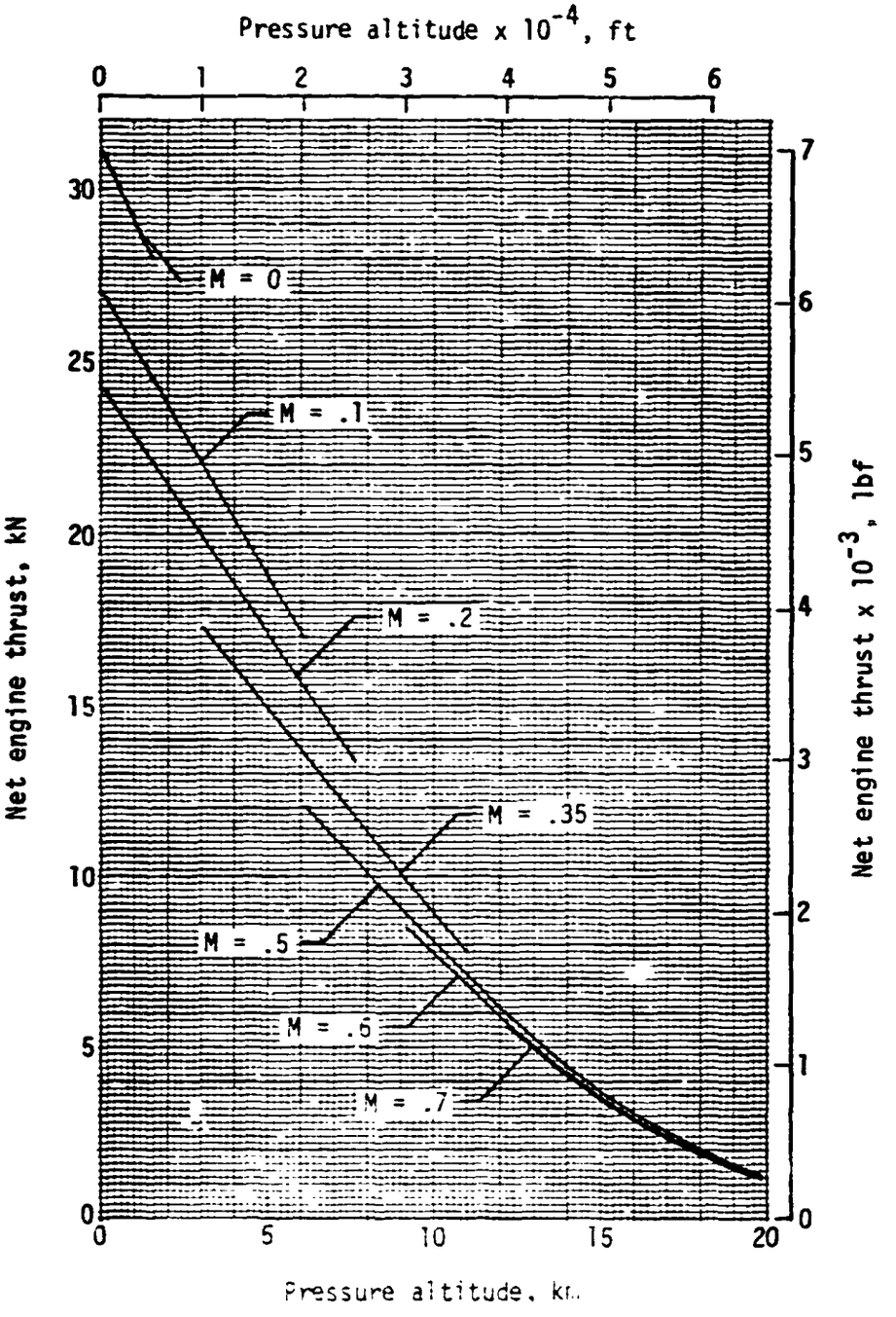

(a) thrust.

Figure 9. - Installed performance of TF34-GE-100 engine; maximum climb rating at standard atmospheric conditions.

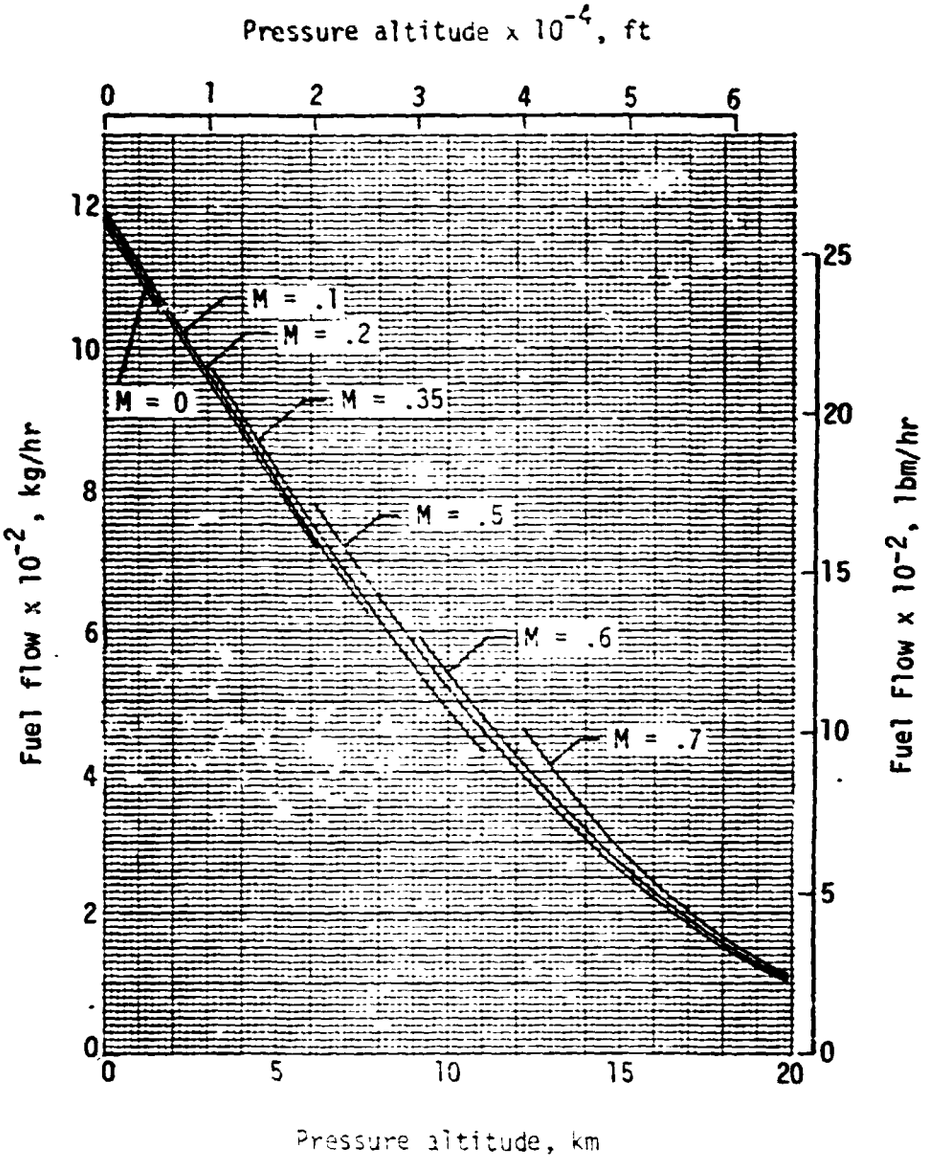

(b) Fuel flow.

Figure 9. - Concluded.

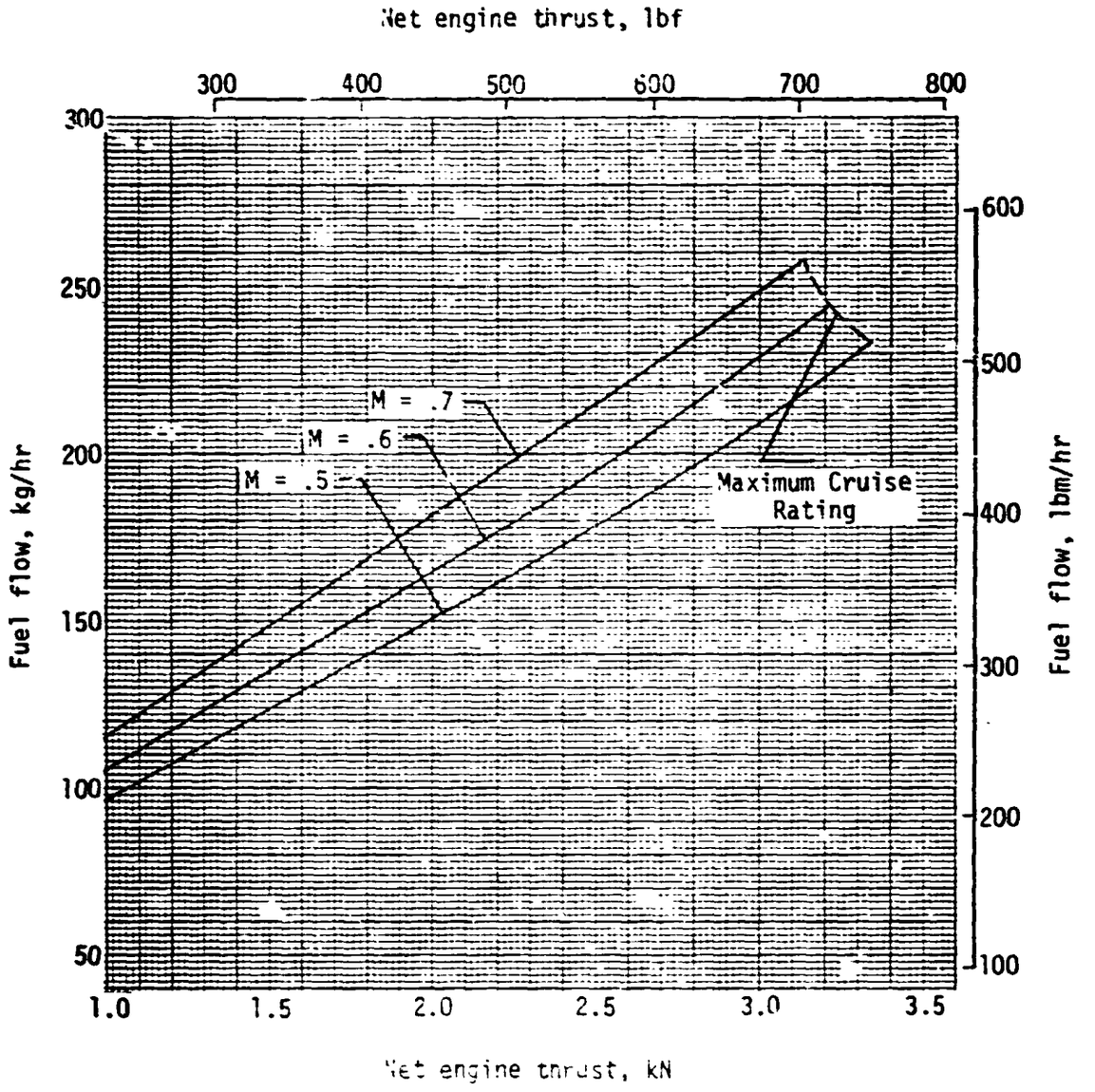

(a) h_p = 15.24 km (50 000 ft)

Figure 10. - Installed performance of TF34-GE100 engine; thrust and fuel flow for maximum and part power cruise at standard atmospheric conditions.

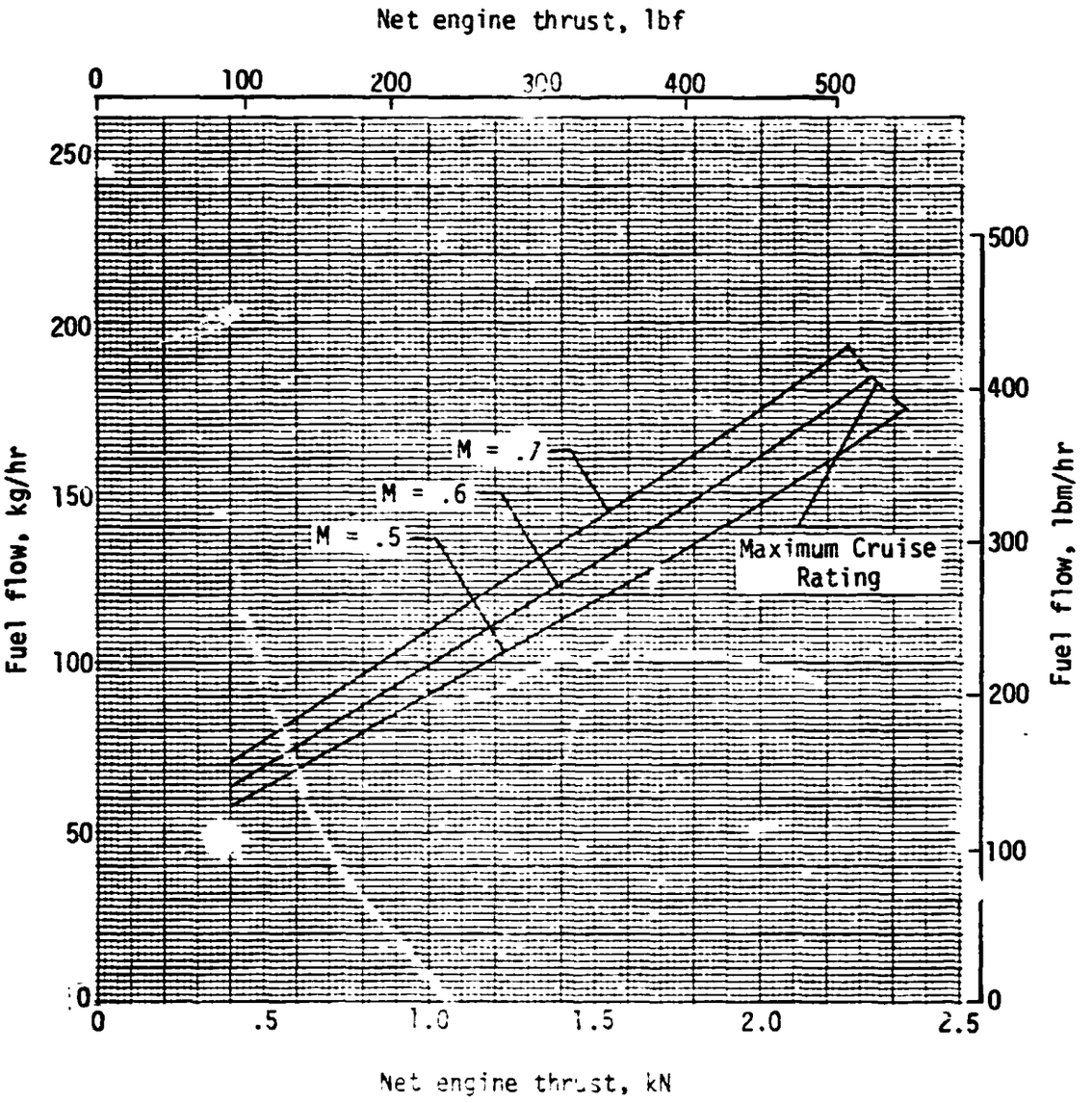

(b) h_p = 16.76 km (55 000 ft)

Figure 10. - Continued

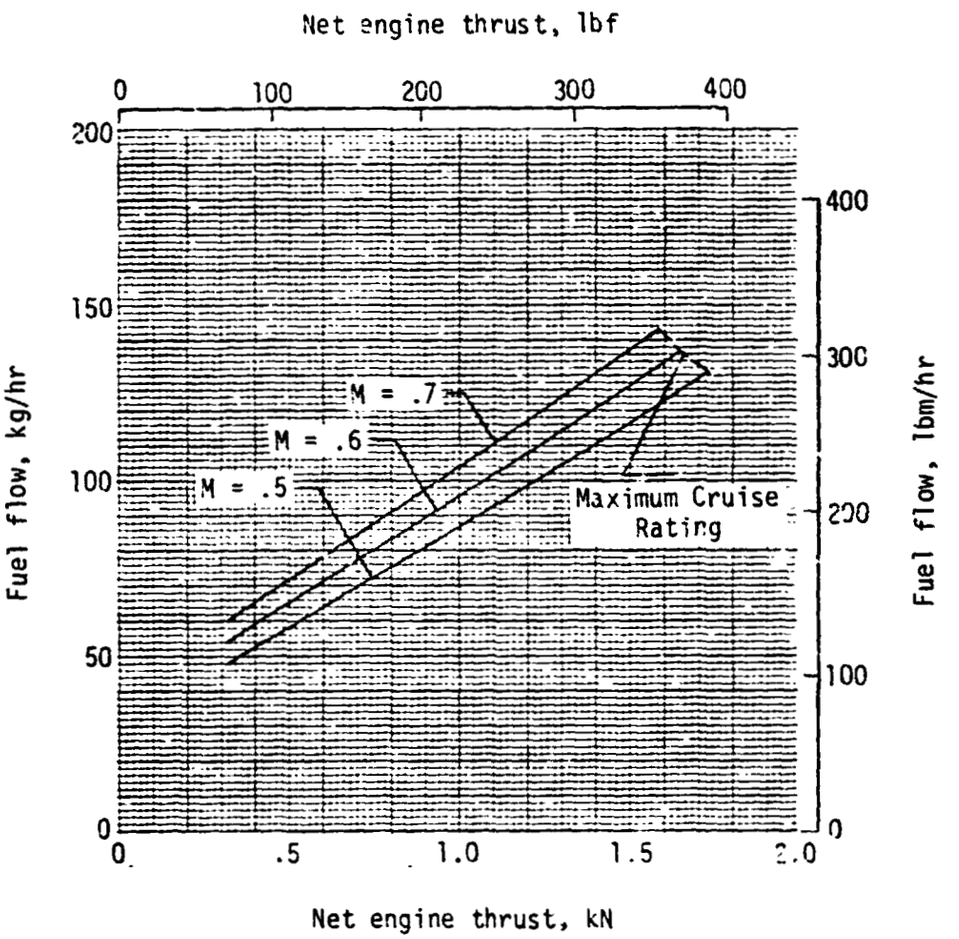

(c) h_p = 18.29 km (60 000 ft).

Figure 10. - Continued.

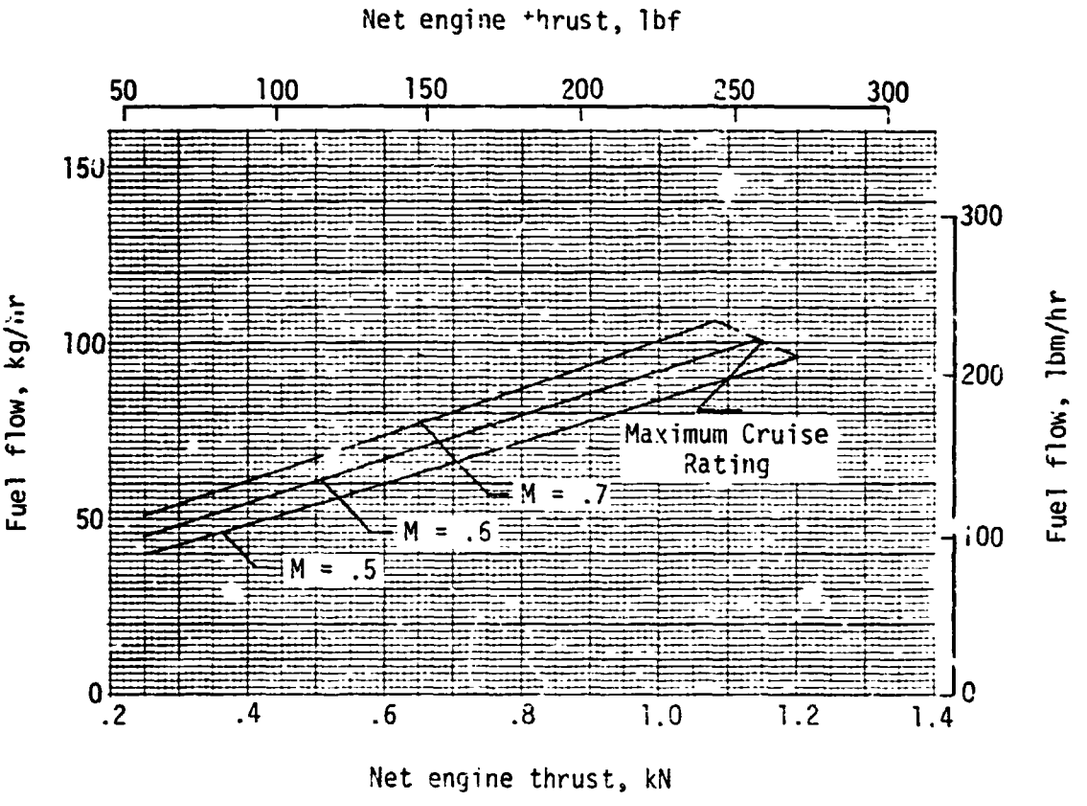

(d) h_p = 19.81 km (65 000 ft)

Figure 10. - Concluded.

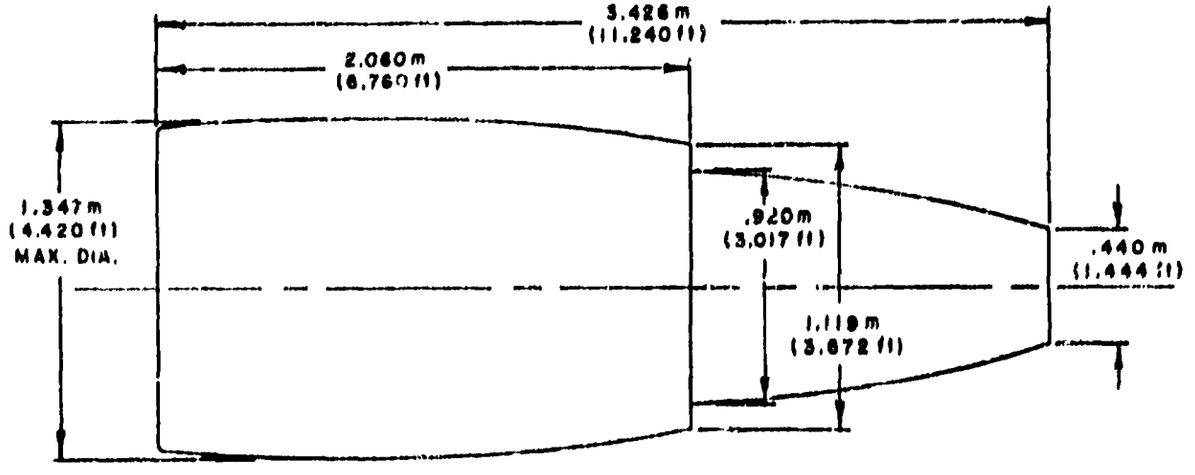

Figure 11. - TF34-GE-100 turbofan engine nacelle.

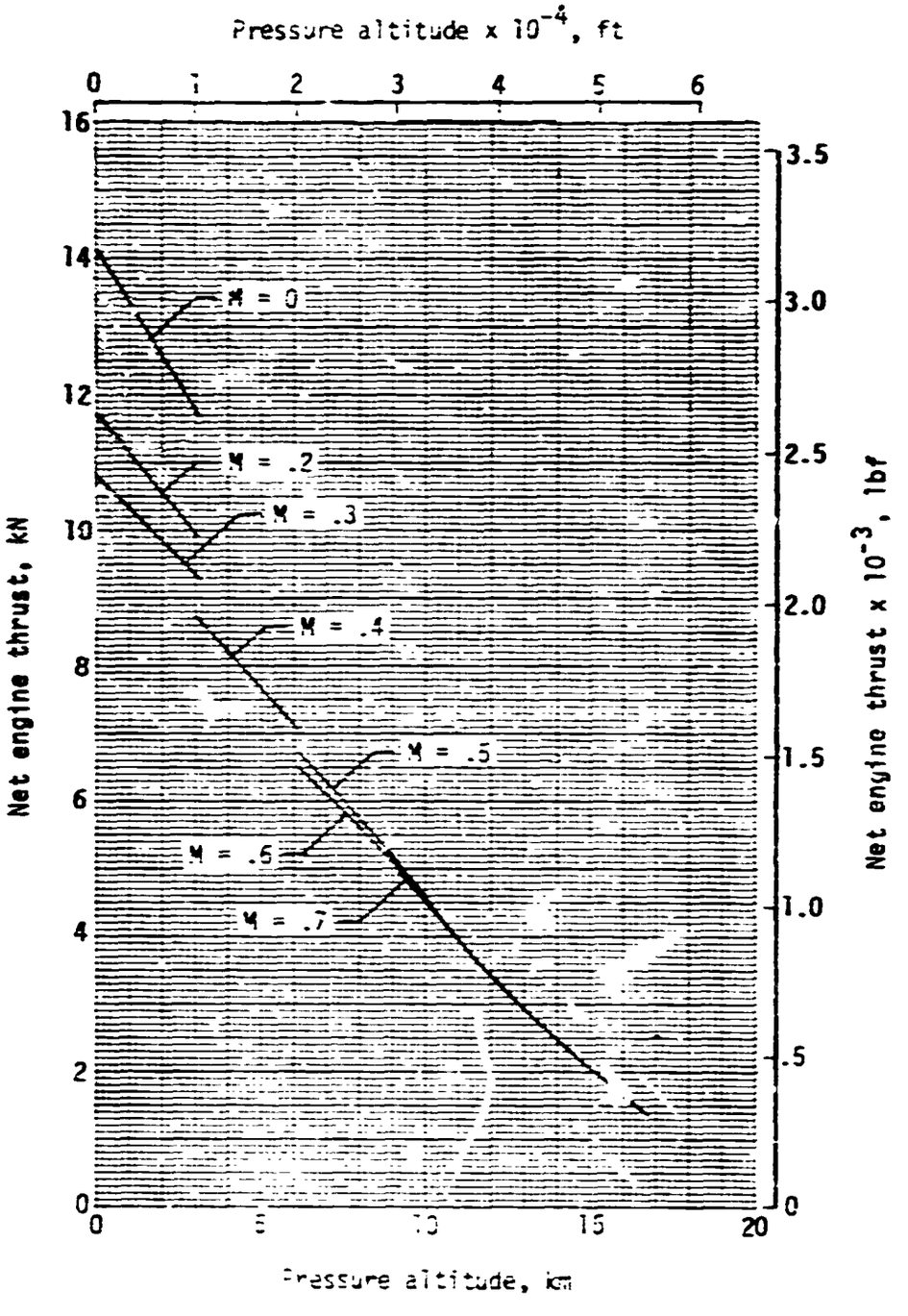

a, Thrust.

Figure 12. - Installed performance of TFE731-2-2B engine; maximum climb rating at standard atmospheric conditions.

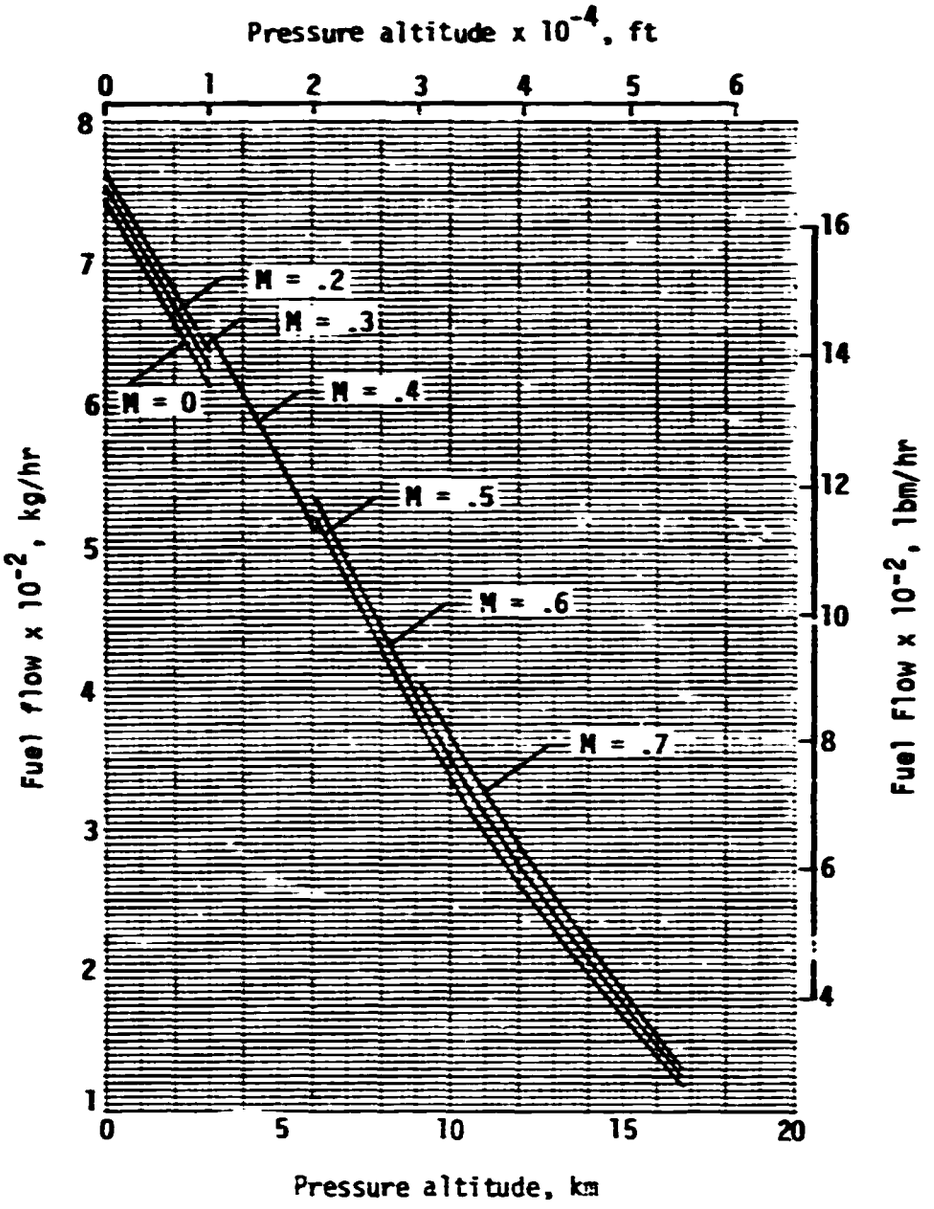

(b) fuel flow.

Figure 12. - Concluded.

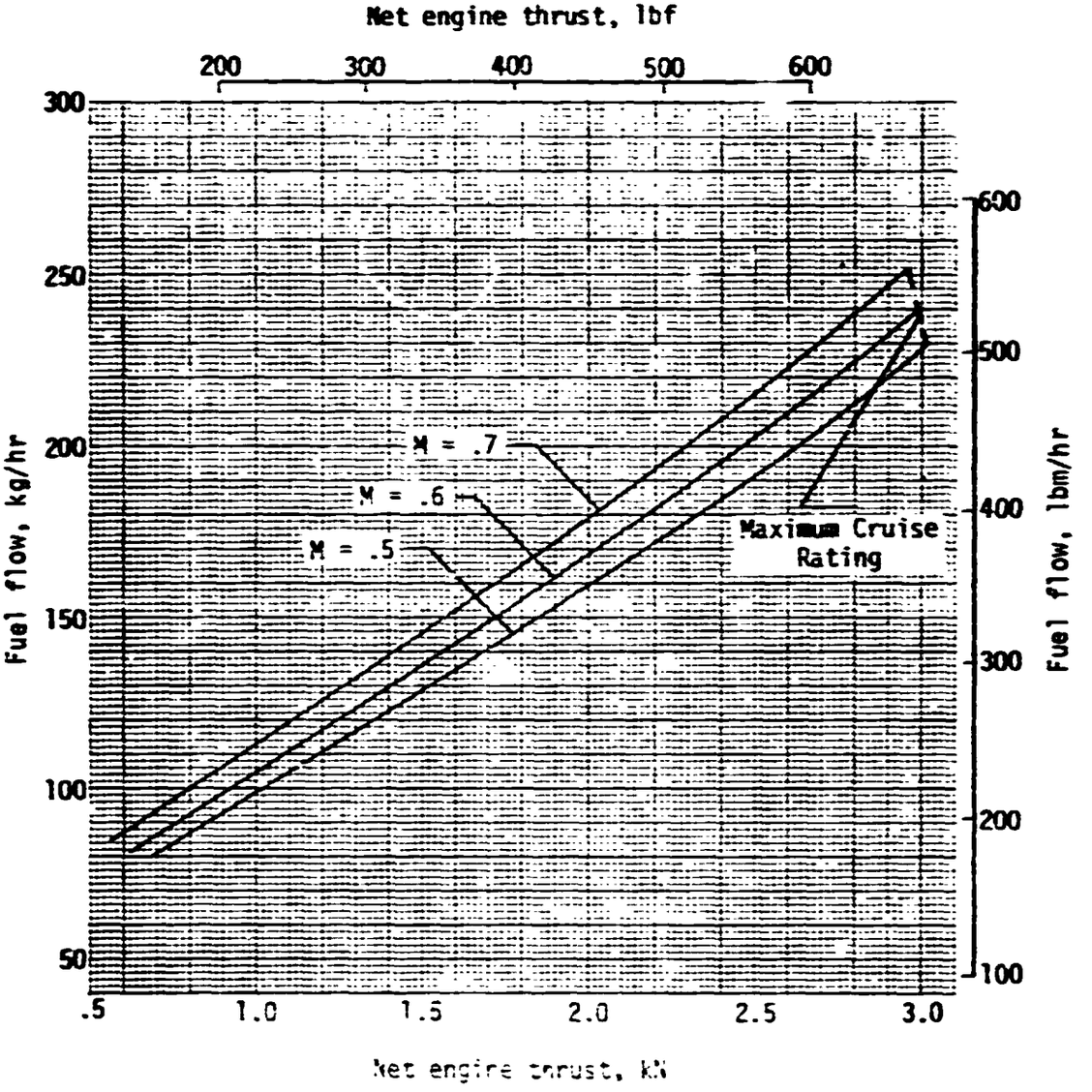

(a) h_p = 12.19 km (40 000 ft).

Figure 13. - Installed performance of TFE731-2-2B engine; thrust and fuel flow for maximum and part power cruise at standard atmospheric conditions.

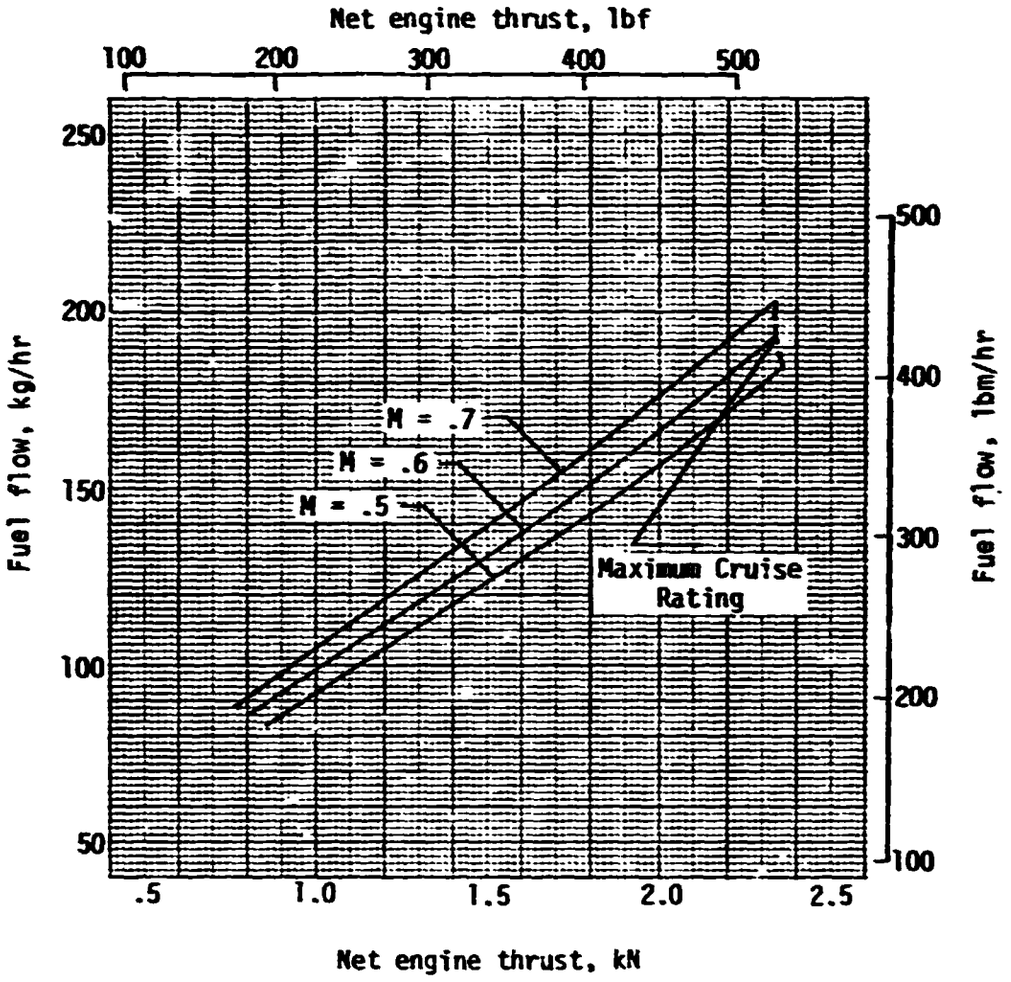

(b) h_p = 13.72 km (45 000 ft).

Figure 13. - Continued.

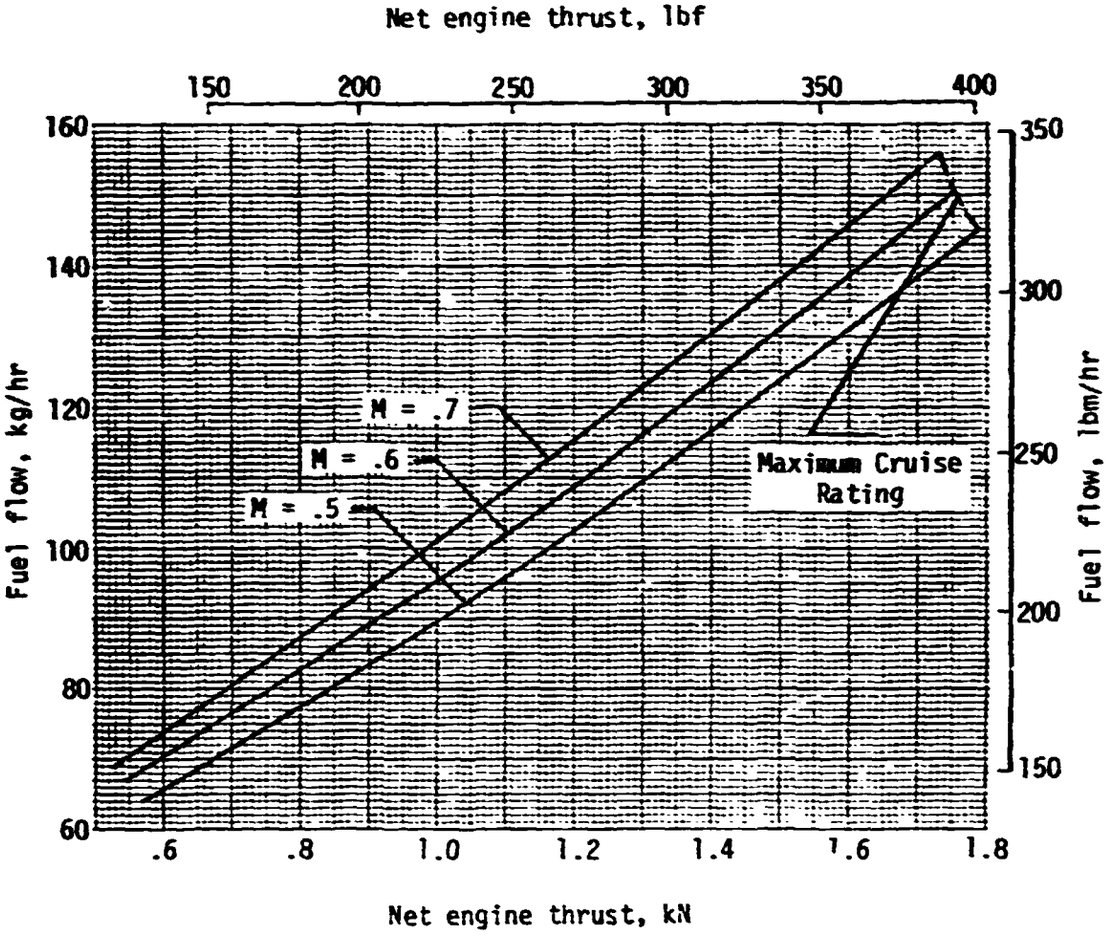

(c) h_p = 15.24 km (50 000 ft).

Figure 13. - Continued.

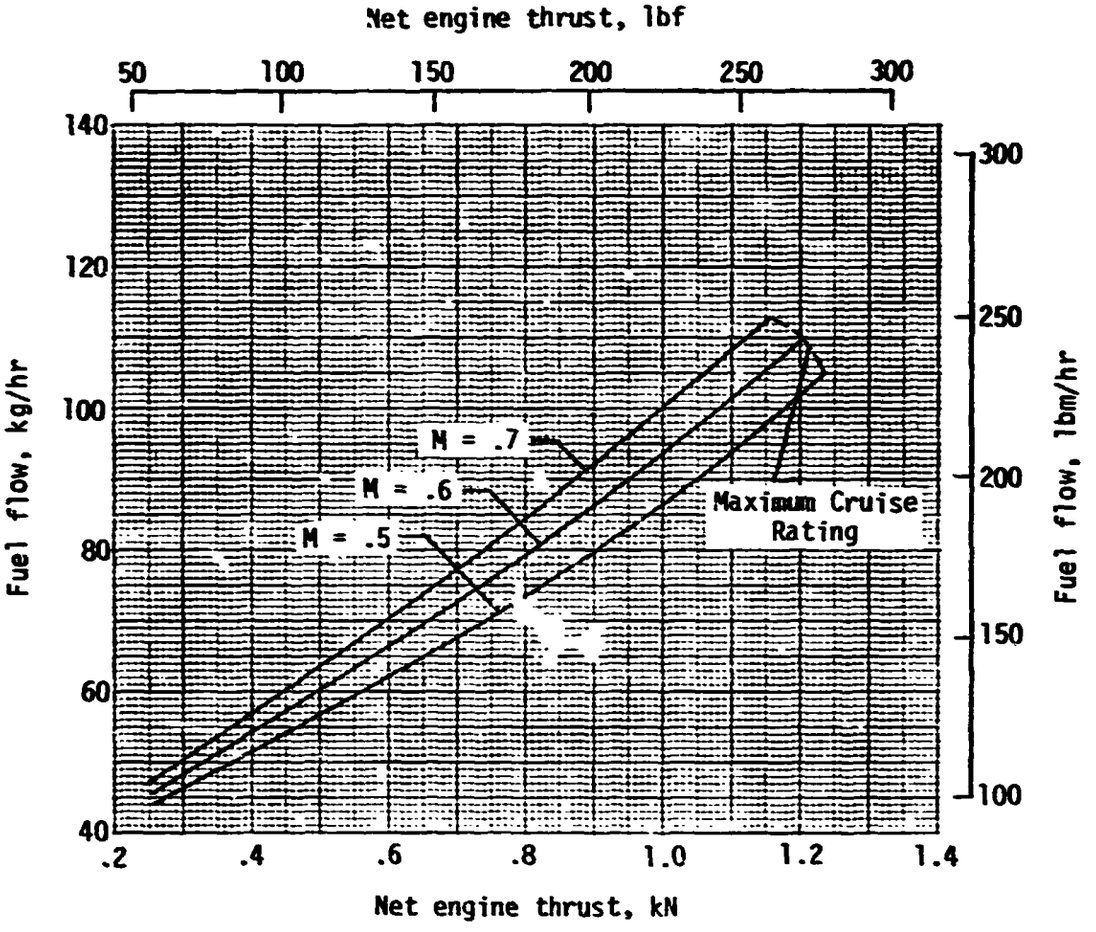

(d) h_p = 16.76 km (55 000 ft).

Figure 13. - Concluded.

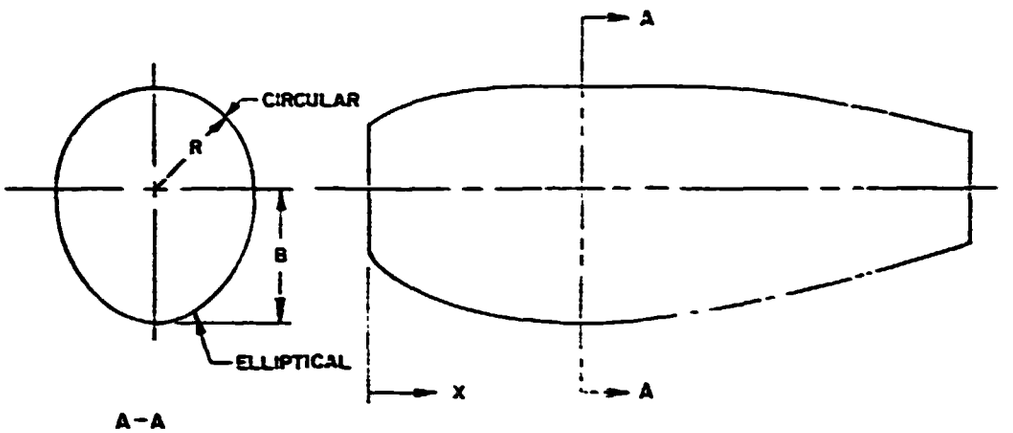

X		R		B	
ft	m	ft	m	ft	m
0	0	.937	.286	.937	.286
.167	.051	1.063	.324	1.125	.343
.500	.152	1.204	.367	1.367	.417
.833	.254	1.313	.400	1.538	.469
1.250	.381	1.404	.428	1.692	.516
1.667	.508	1.463	.446	1.804	.550
2.083	.635	1.492	.455	1.875	.572
2.458	.749	1.504	.458	1.917	.584
2.833	.863	1.504	.458	1.942	.592
3.575	1.090	1.504	.458	1.950	.594
4.275	1.303	1.504	.458	1.908	.582
4.967	1.514	1.504	.458	1.813	.553
5.467	1.666	1.488	.454	1.725	.526
5.917	1.804	1.438	.438	1.633	.498
6.600	2.012	1.338	.408	1.471	.448
7.433	2.266	1.179	.359	1.254	.382
8.283	2.525	.992	.302	1.033	.315
9.033	2.753	.810	.247	.810	.247

Figure 14. - TFE731-2-2B and TFE731-3 turbofan engine nacelle.

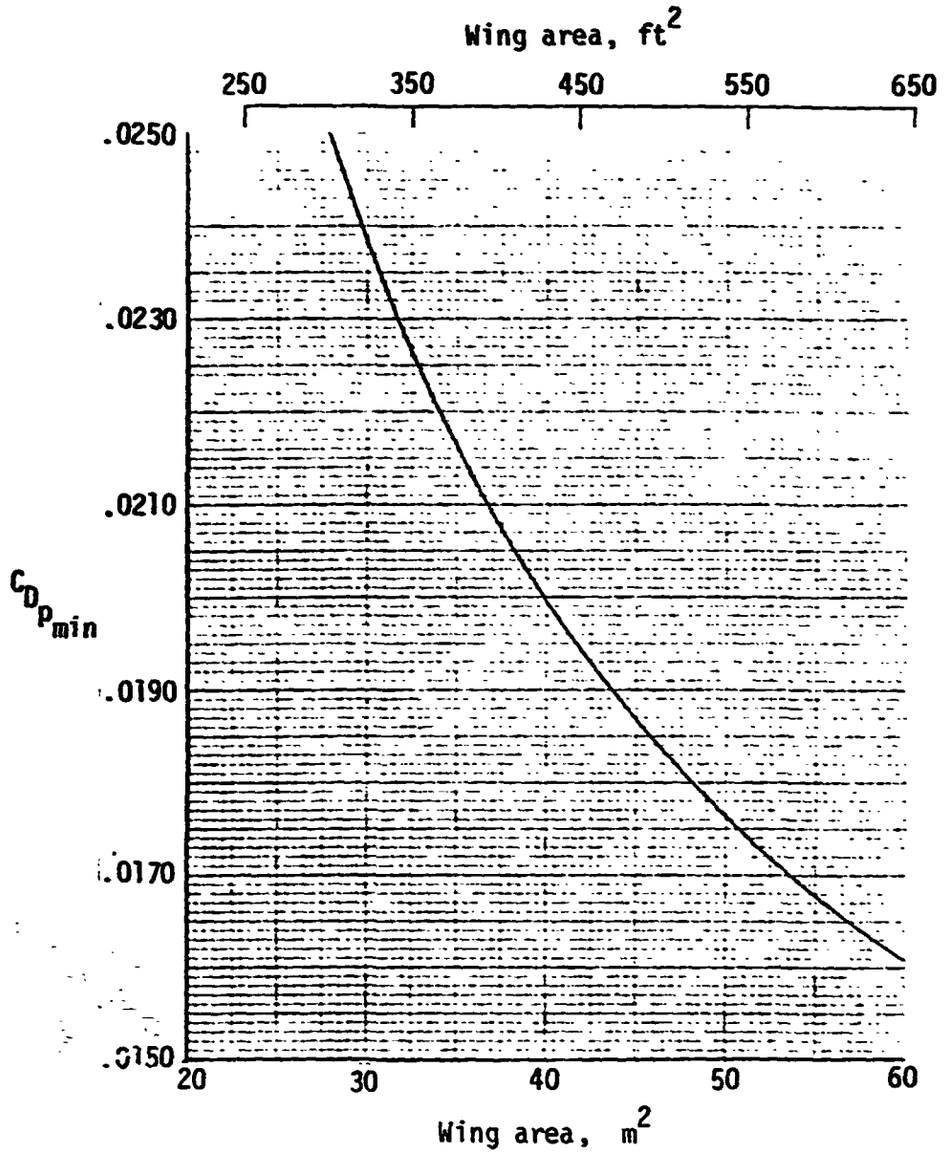

NOTE: These $C_{D_{p_{min}}}$'s were used for wing sizing only and were based on preliminary drag estimates.

Figure 15. - Minimum parasite drag coefficient versus wing area.

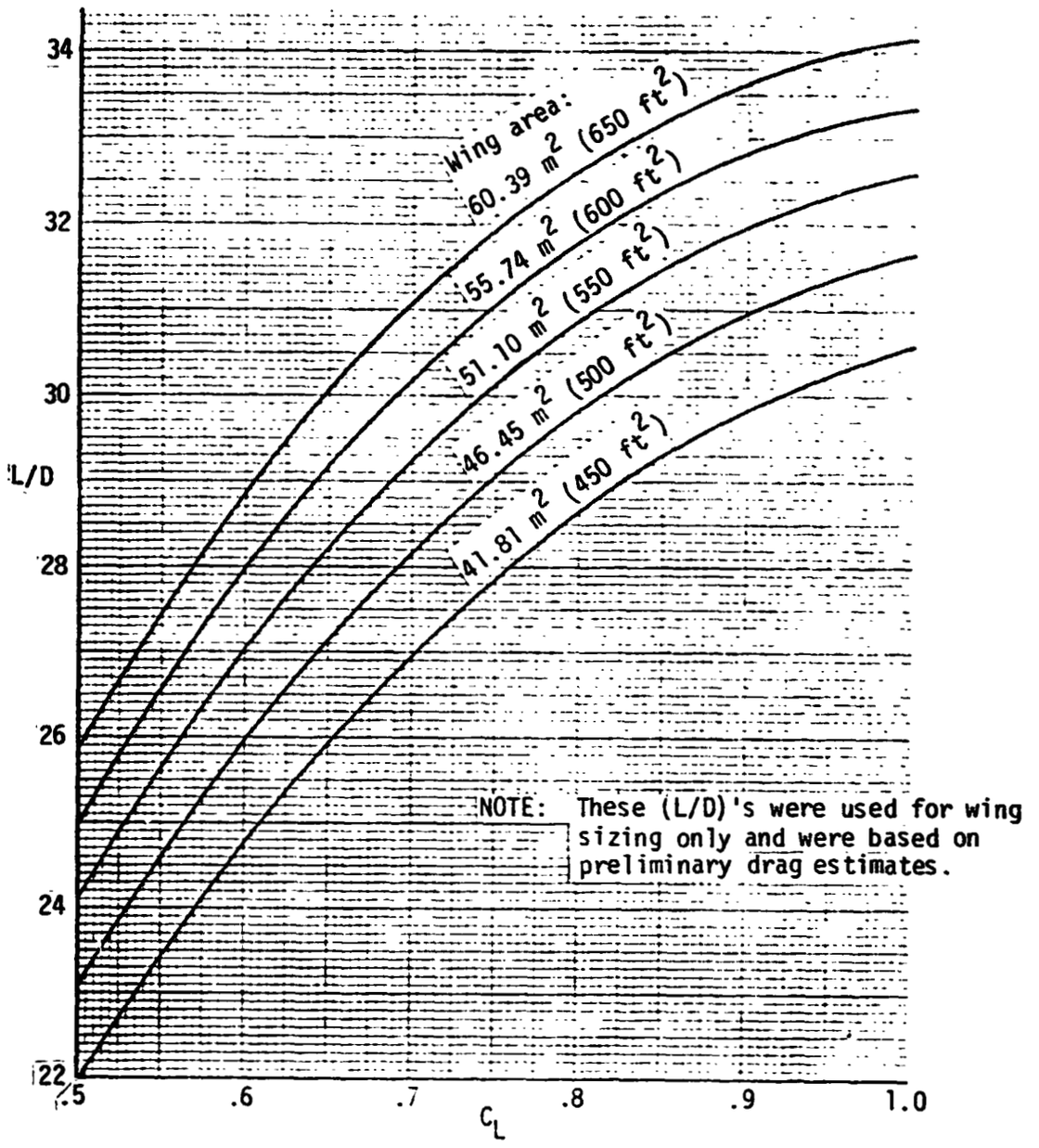

Figure 16. - Wing sizing study - variation of L/D with wing area and C_L.

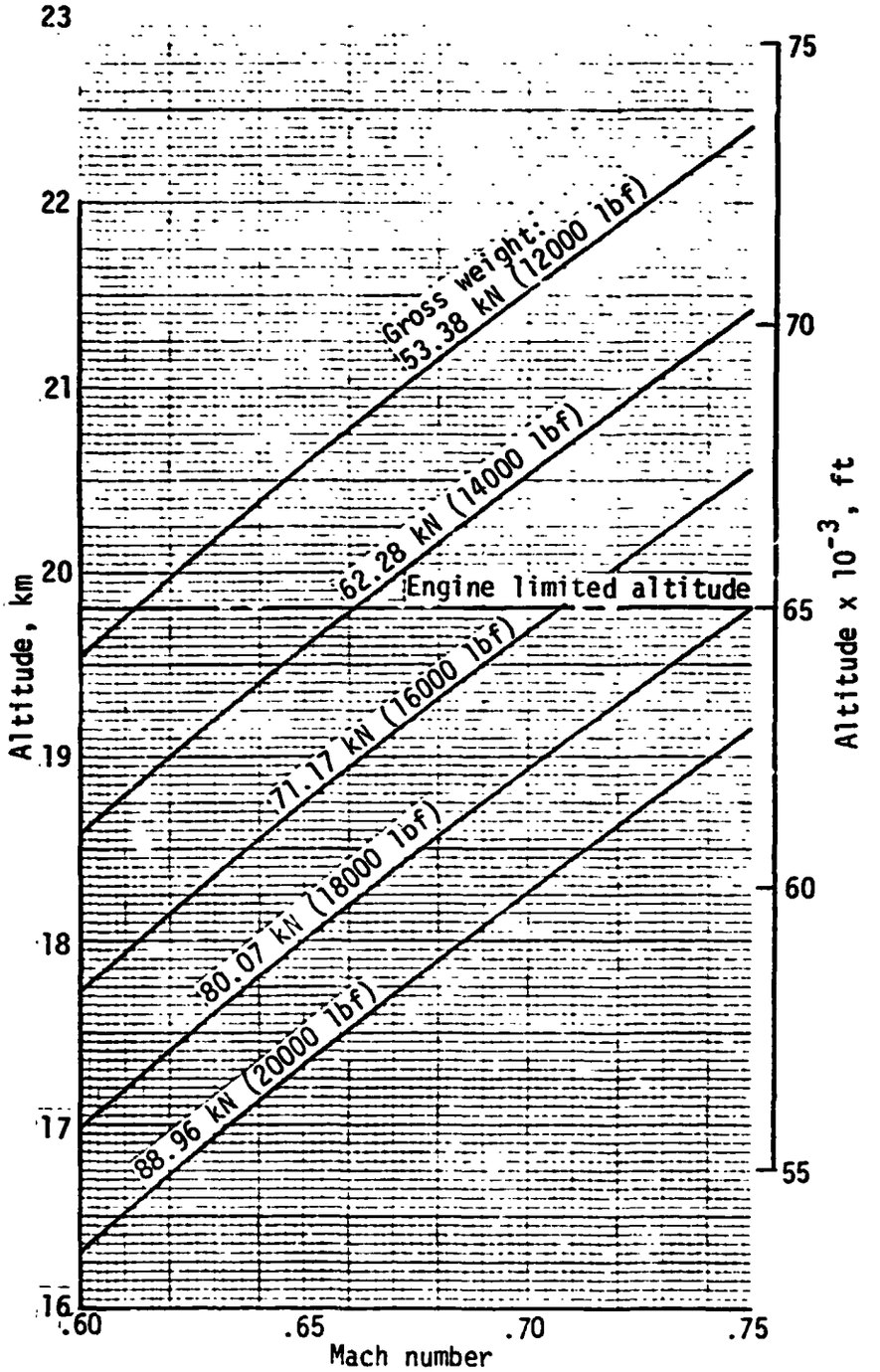

Figure 17. - Cruise flight conditions with C_L = 0.7 and wing area equal to 51.10 m^2 (550 ft^2).

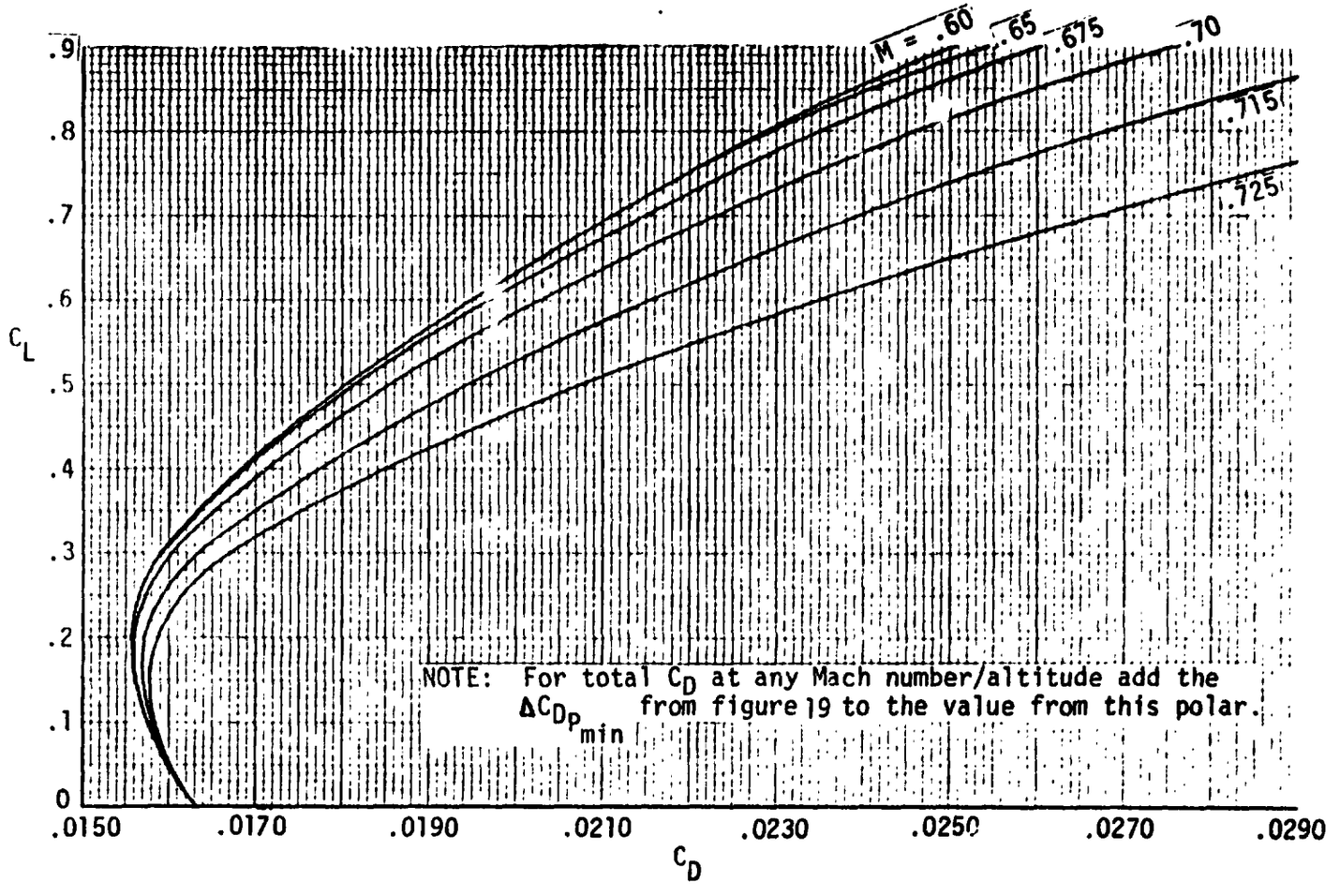

Figure 18. - Drag polars for the strut-braced wing airplane with TF34-GE-100 engines (SB-1), at an equivalent airspeed of 129 m/s (250 kts).

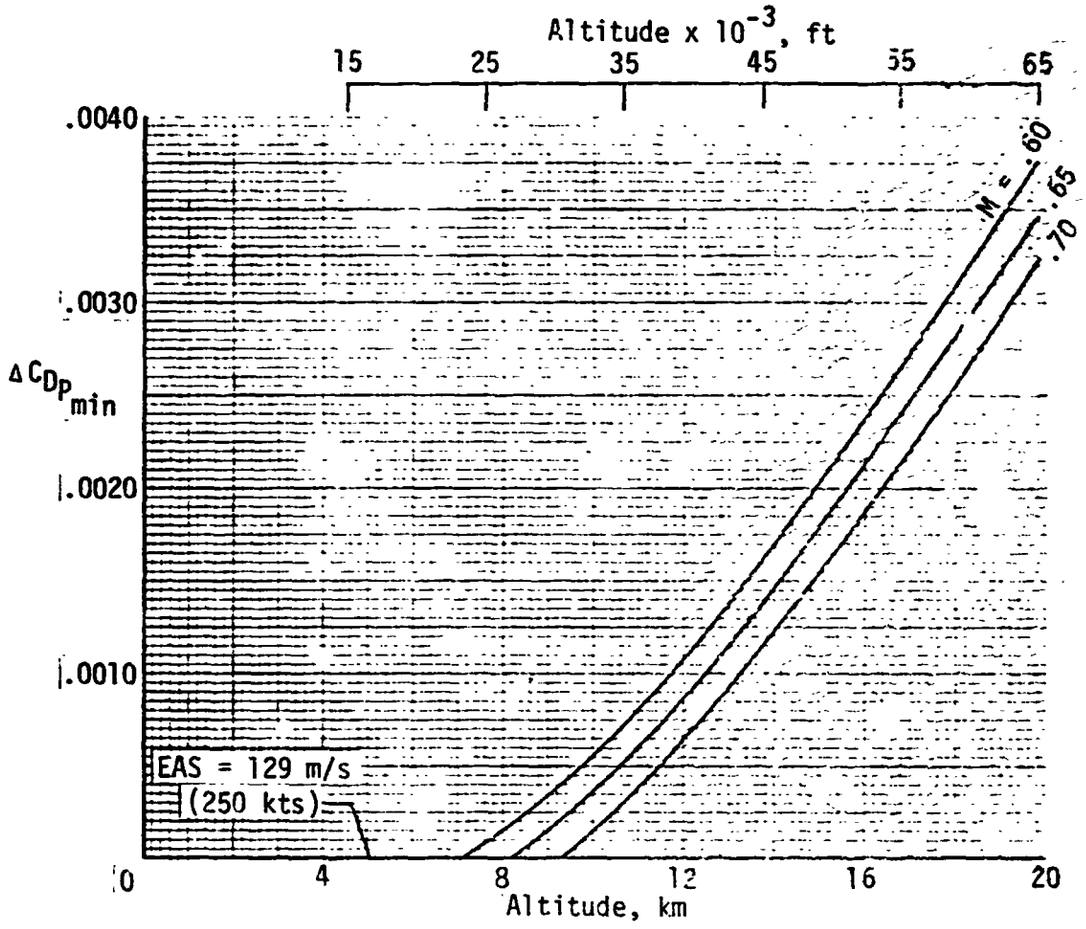

Figure 19. - Incremental minimum parasite drag coefficient due to Reynolds number, for the strut-braced wing airplane with TF34-GE-100 engines (SB-1).

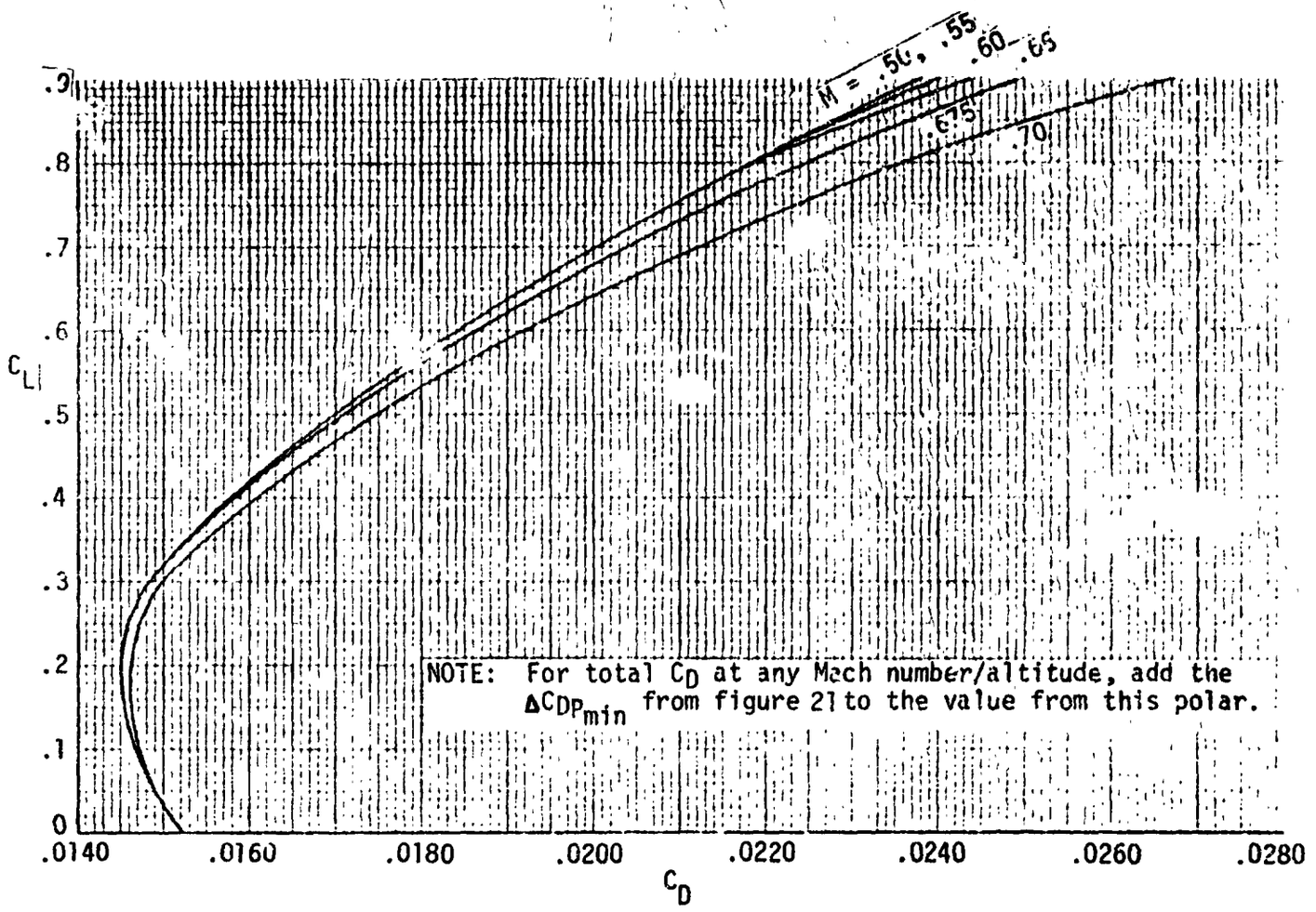

Figure 20. - Drag polars for the strut-braced wing airplane with TFE731-3 engines (SB-2), at an equivalent airspeed of 129 m/s (250 kts).

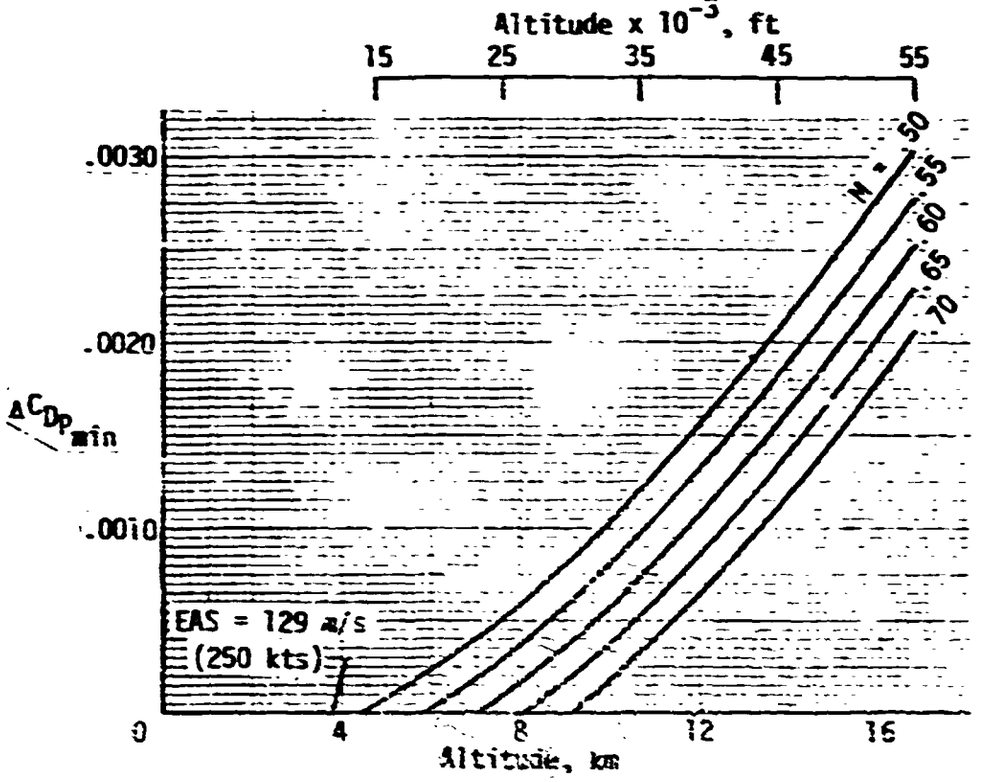

Figure 21. - Increment of minimum parasite drag coefficient due to Reynolds number, for the strut-braced wing airplane with TFE731-3 engines (SB-2).

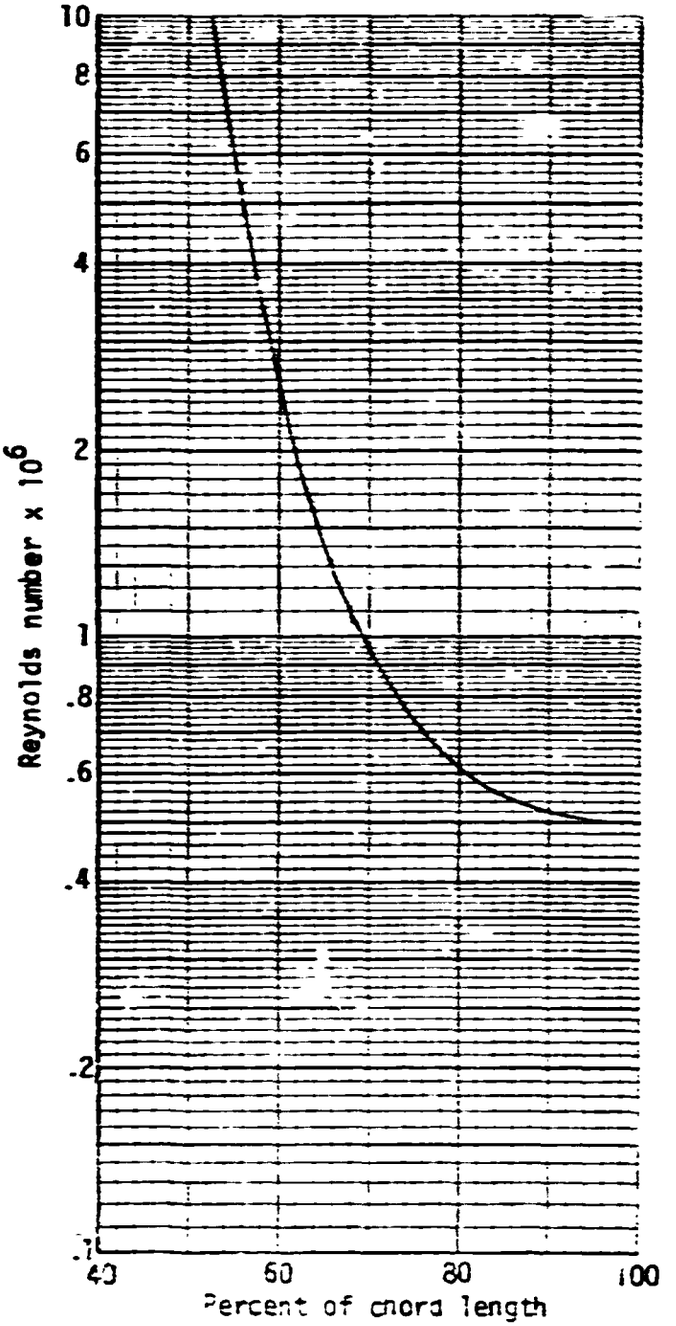

Figure 22. - Achievable smooth airfoil laminarization.

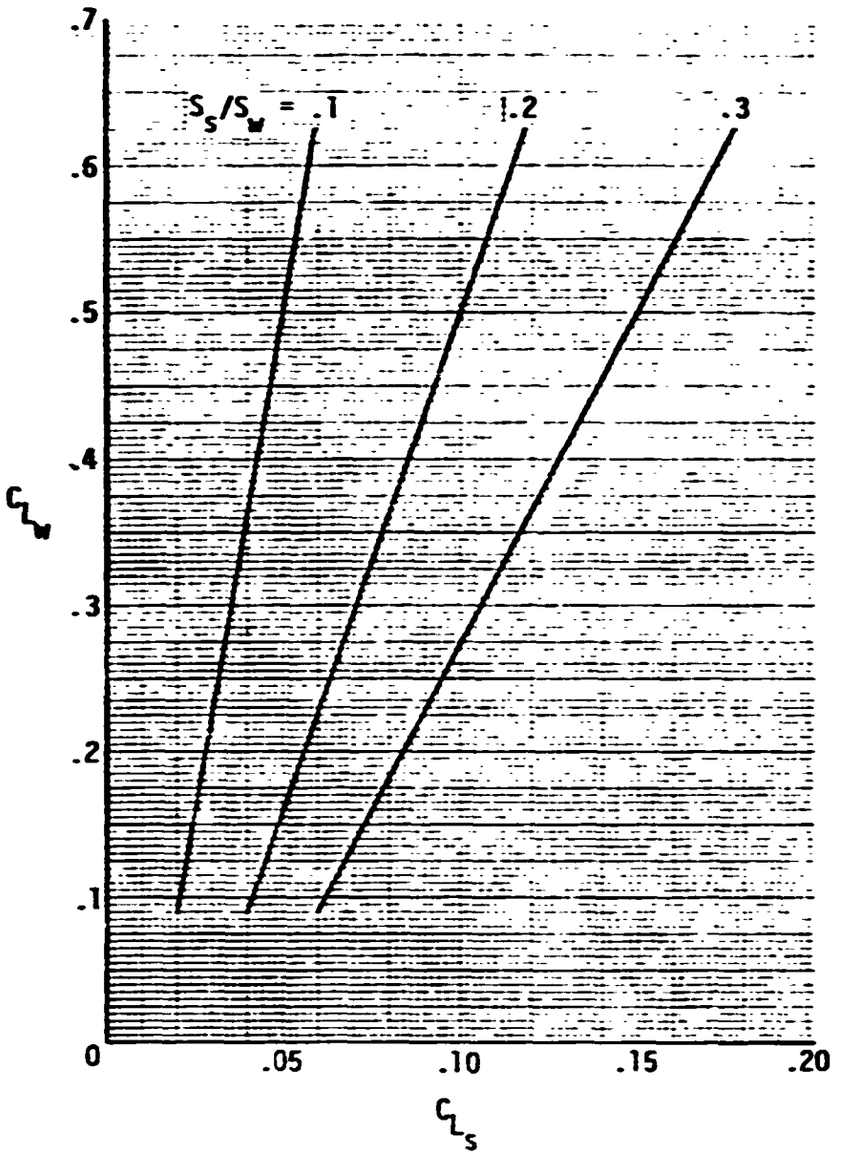

Figure 7 . - Relationship of strut lift coefficient to wing lift coefficient.

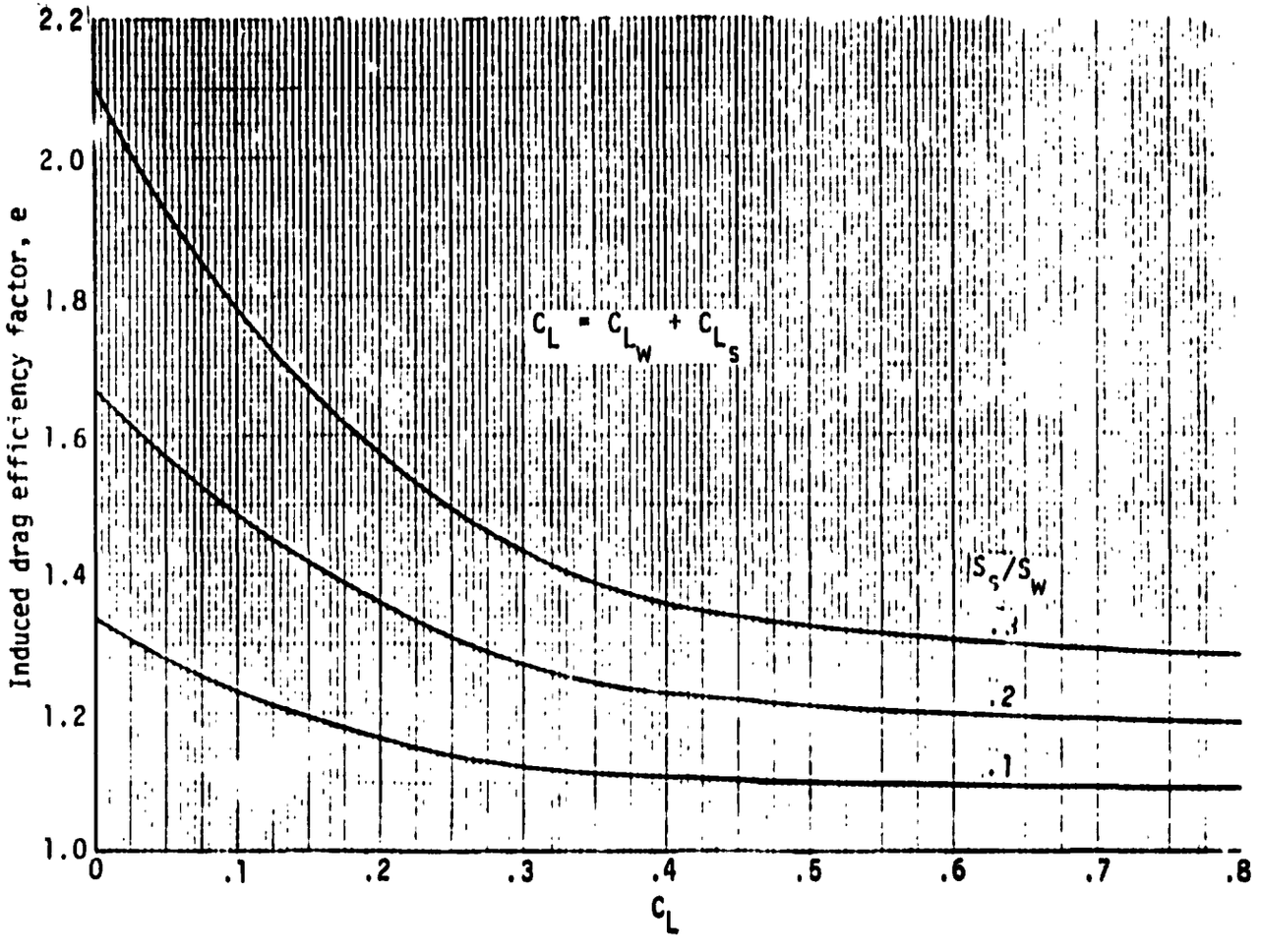

Figure 24. - Induced drag efficiency factor (e) for several wing-strut combinations - S_W = 51.10 m^2 (550 ft^2) and AR = 25.

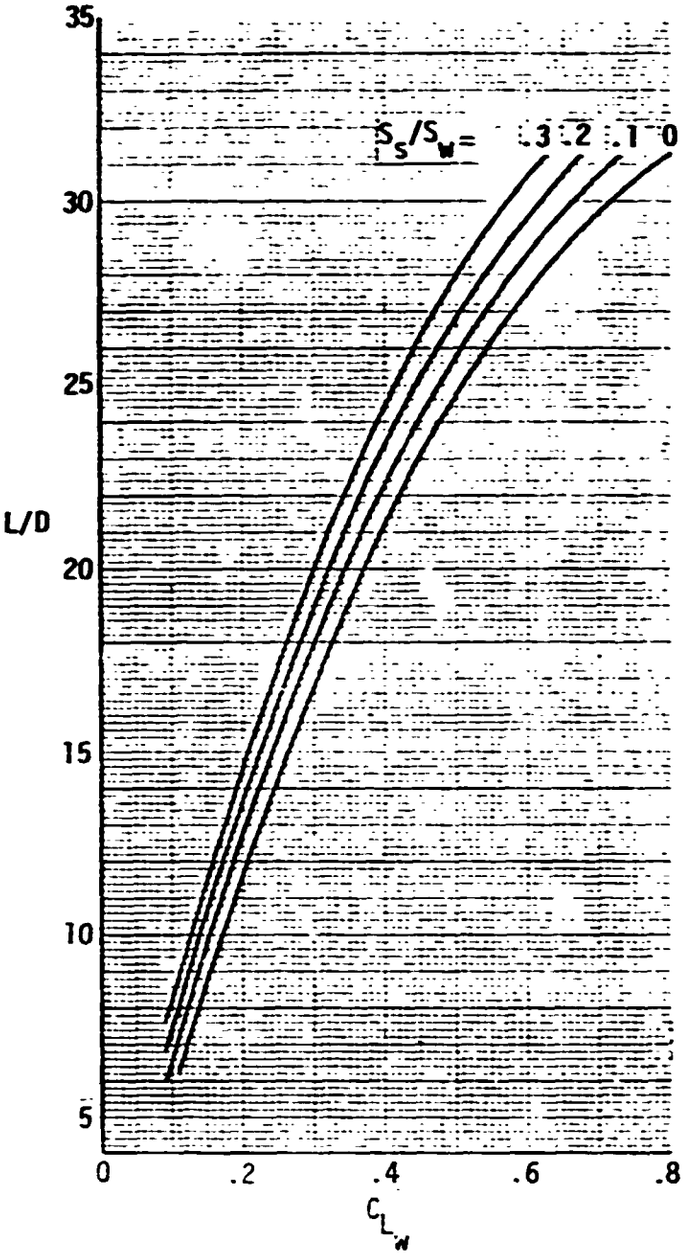

(a) wing lift coefficient.

Figure 25. - Lift-drag ratio with and without struts - $C_{D_{P_{min}}}$ = .0166 (without struts) - S_w = 51.10 m^2 (550 ft^2).

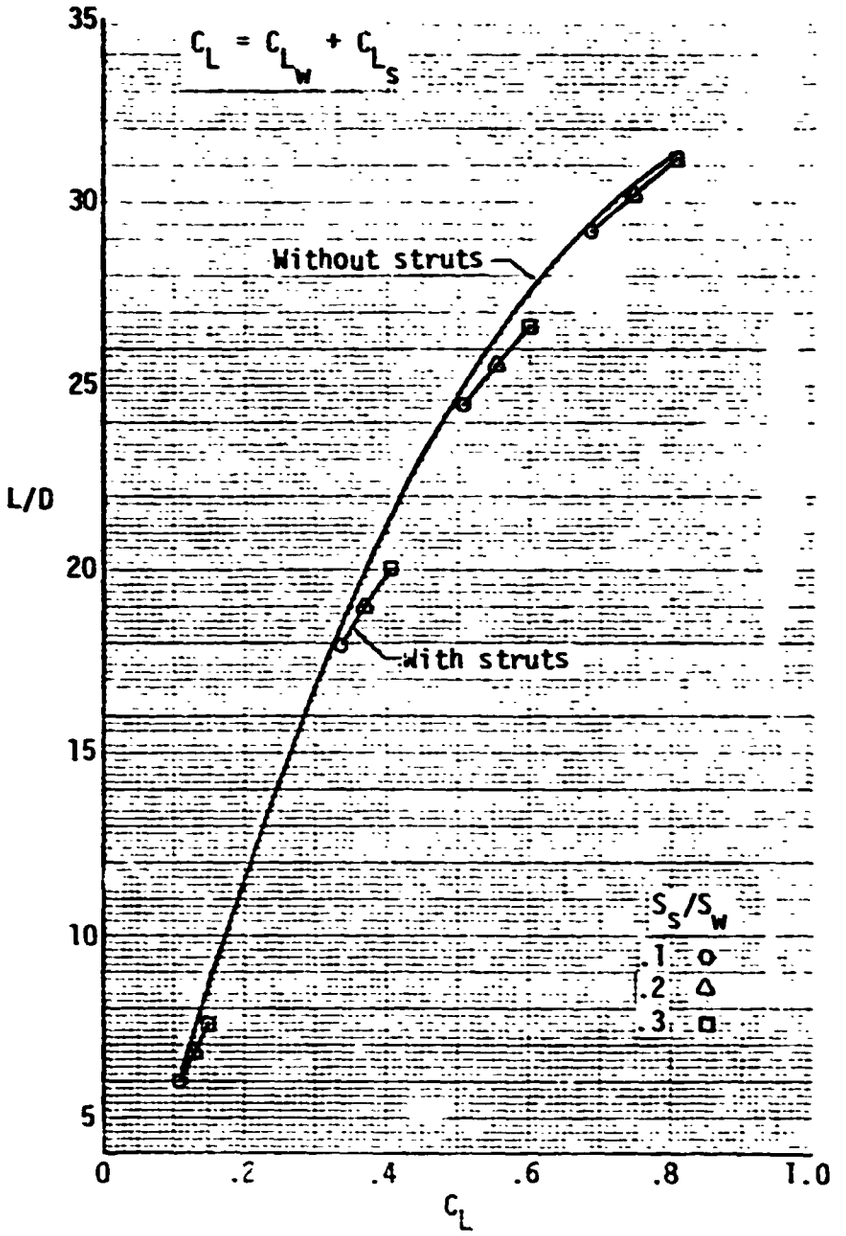

(b) total lift coefficient.

Figure 25. - Concluded.

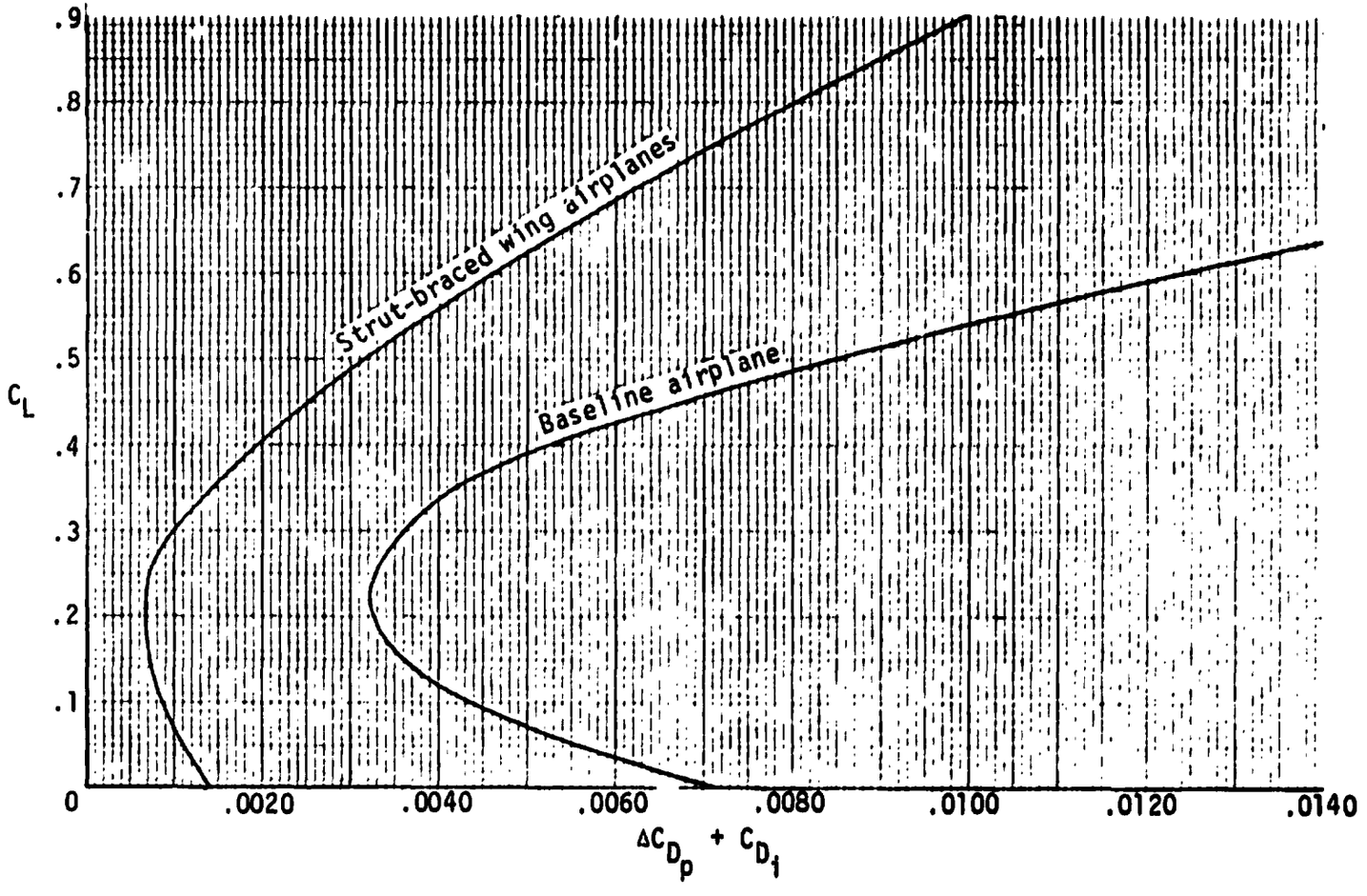

Figure 26. - Variation of parasite plus induced drag with lift, of the baseline and strut-braced wing configurations.

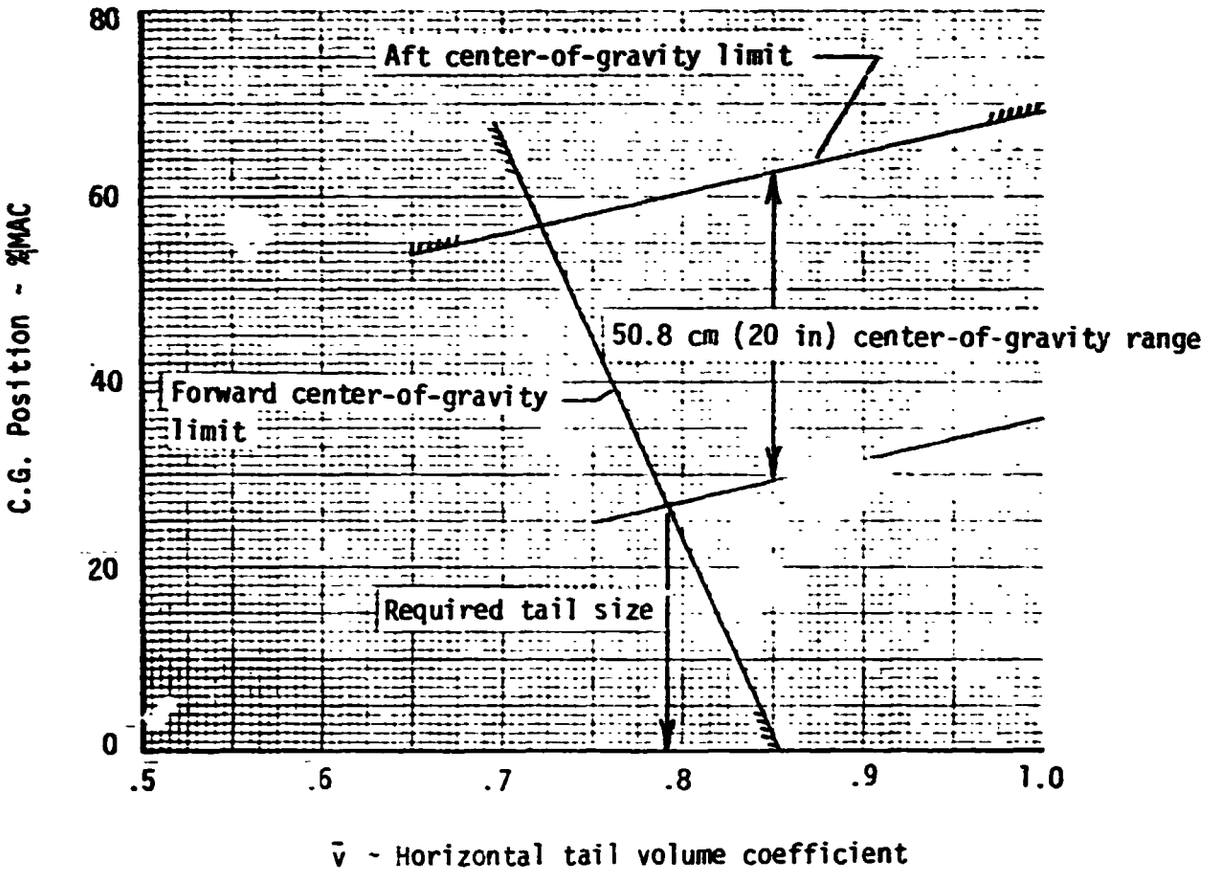

Figure 27. - Center-of-gravity limits for takeoff and landing.

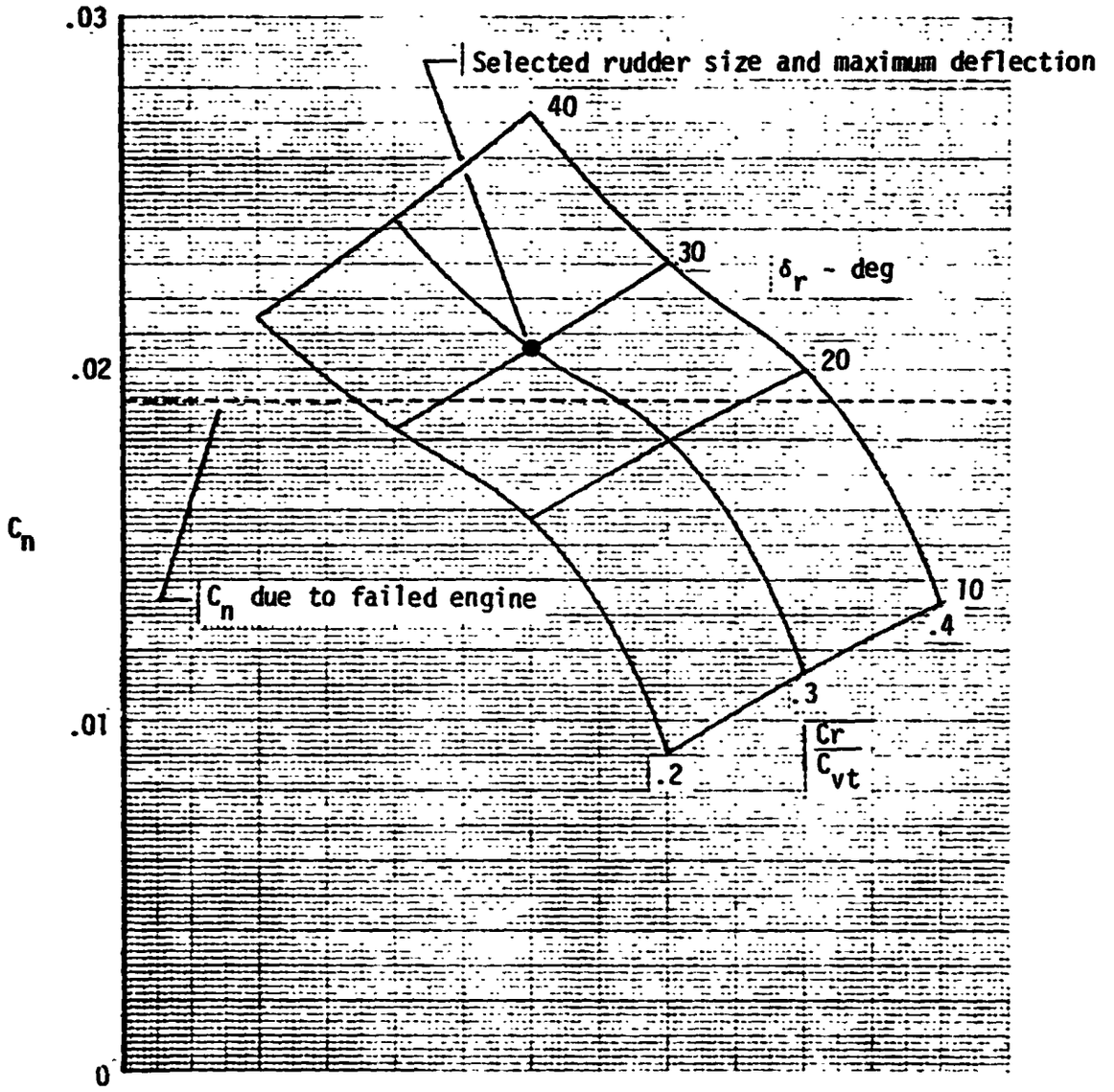

Figure 28. - Estimated directional control capability assuming an engine failure. V = 46.3 m/s (90 kts); S_{vt} = 6.64 m^2 (71.5 ft^2)

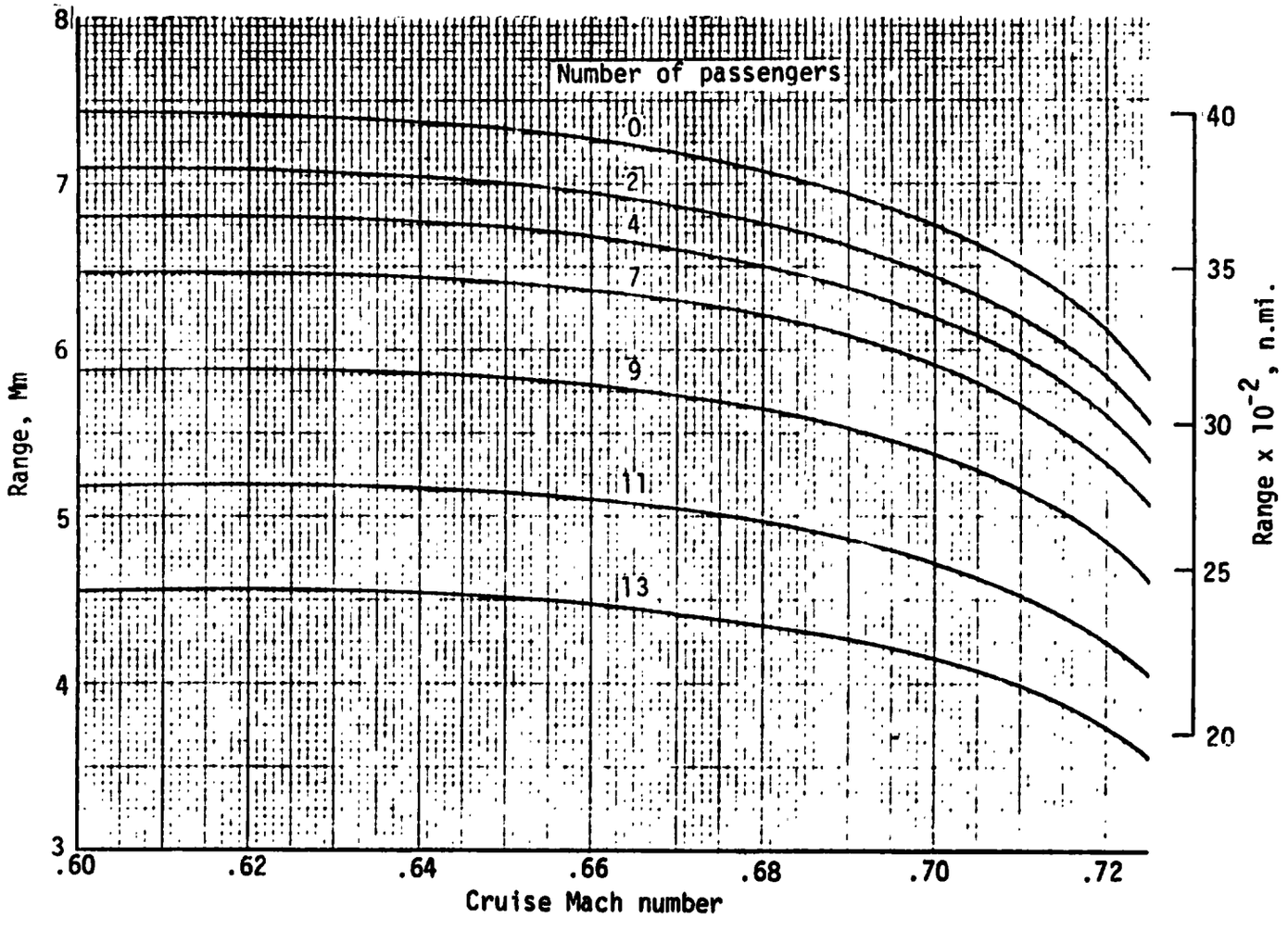

(a) SB-1.

Figure 29. - Range versus cruise Mach number and numbers of passengers. Passenger accommodations adjusted for number of passengers.

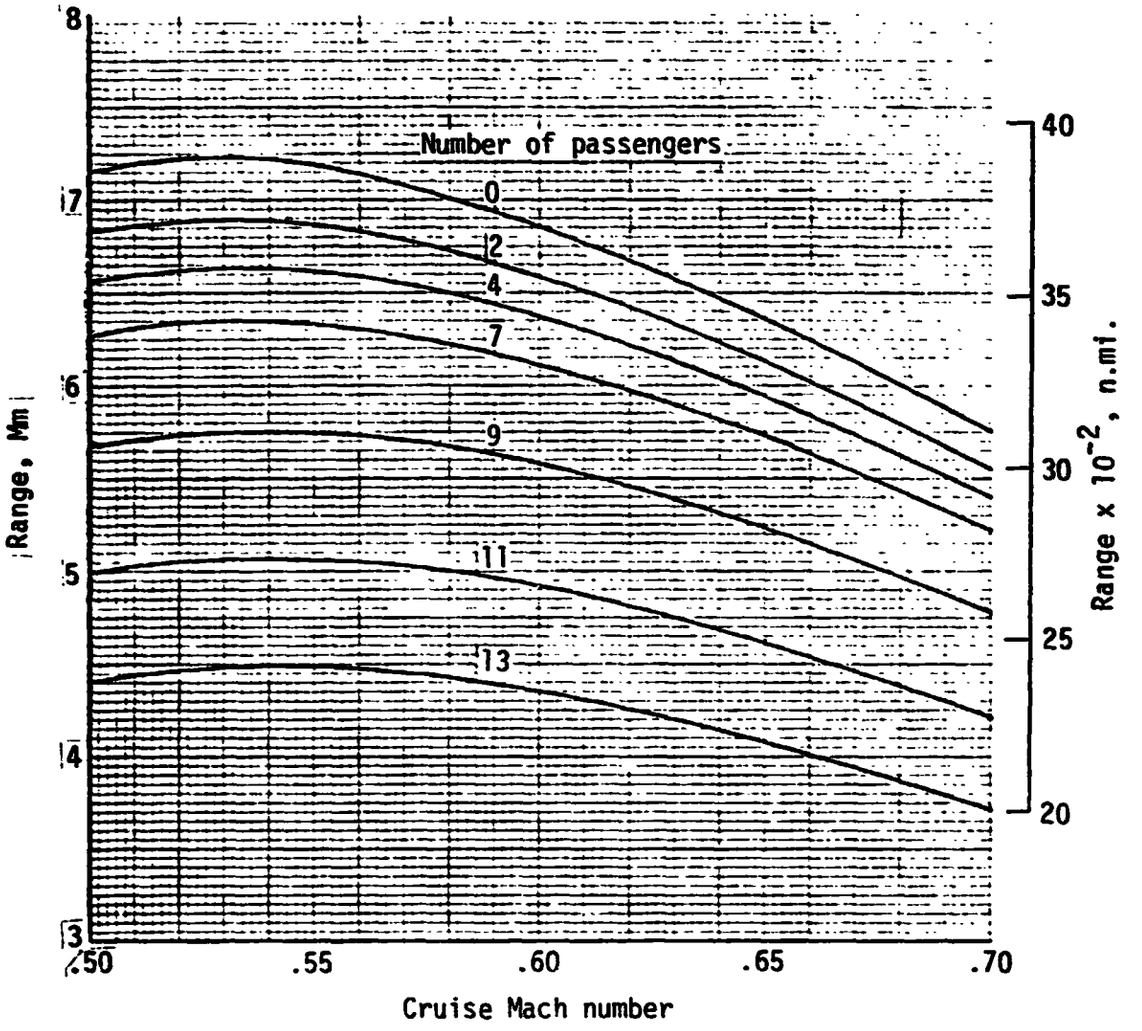

(b) SB-2.

Figure 29. - Concluded.

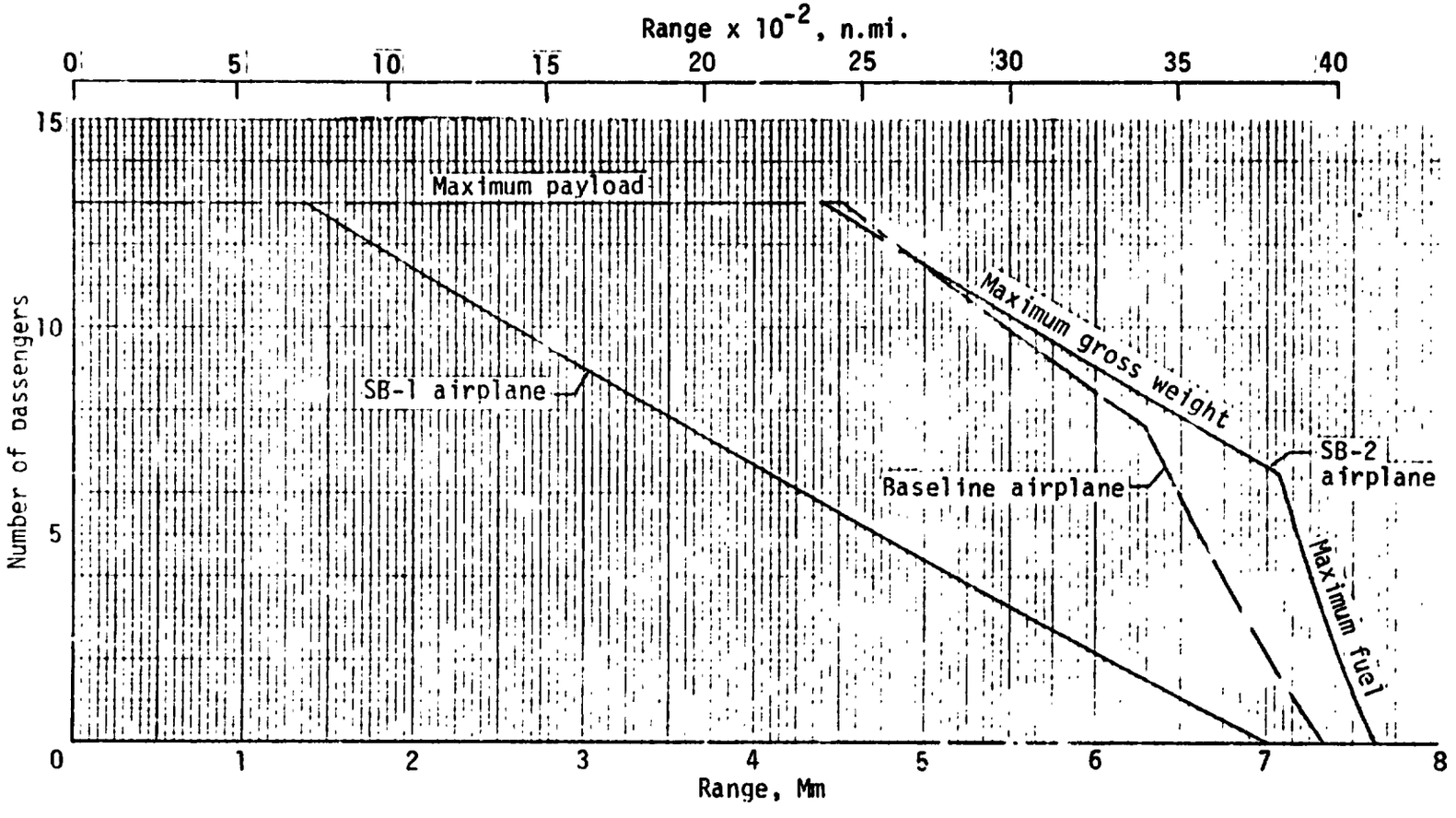

(a) Passenger accommodations adjusted for number of passengers

Figure 30. - Payload versus range at long-range cruise Mach numbers. Maximum gross weight equals 86.3 kN (19 400 lbf) for all models.

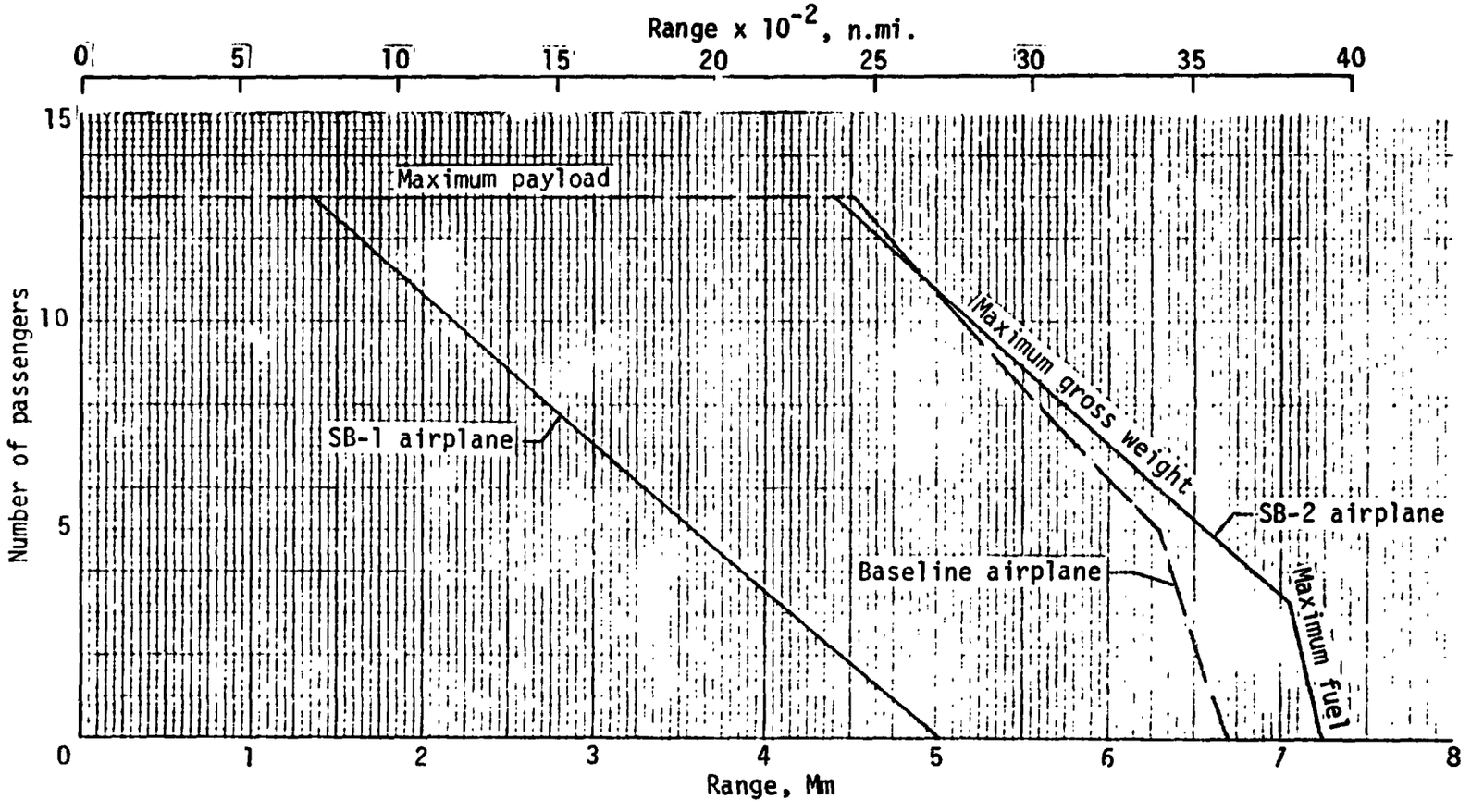

(b) Passenger accommodations for thirteen passengers.

Figure 30. - Concluded.

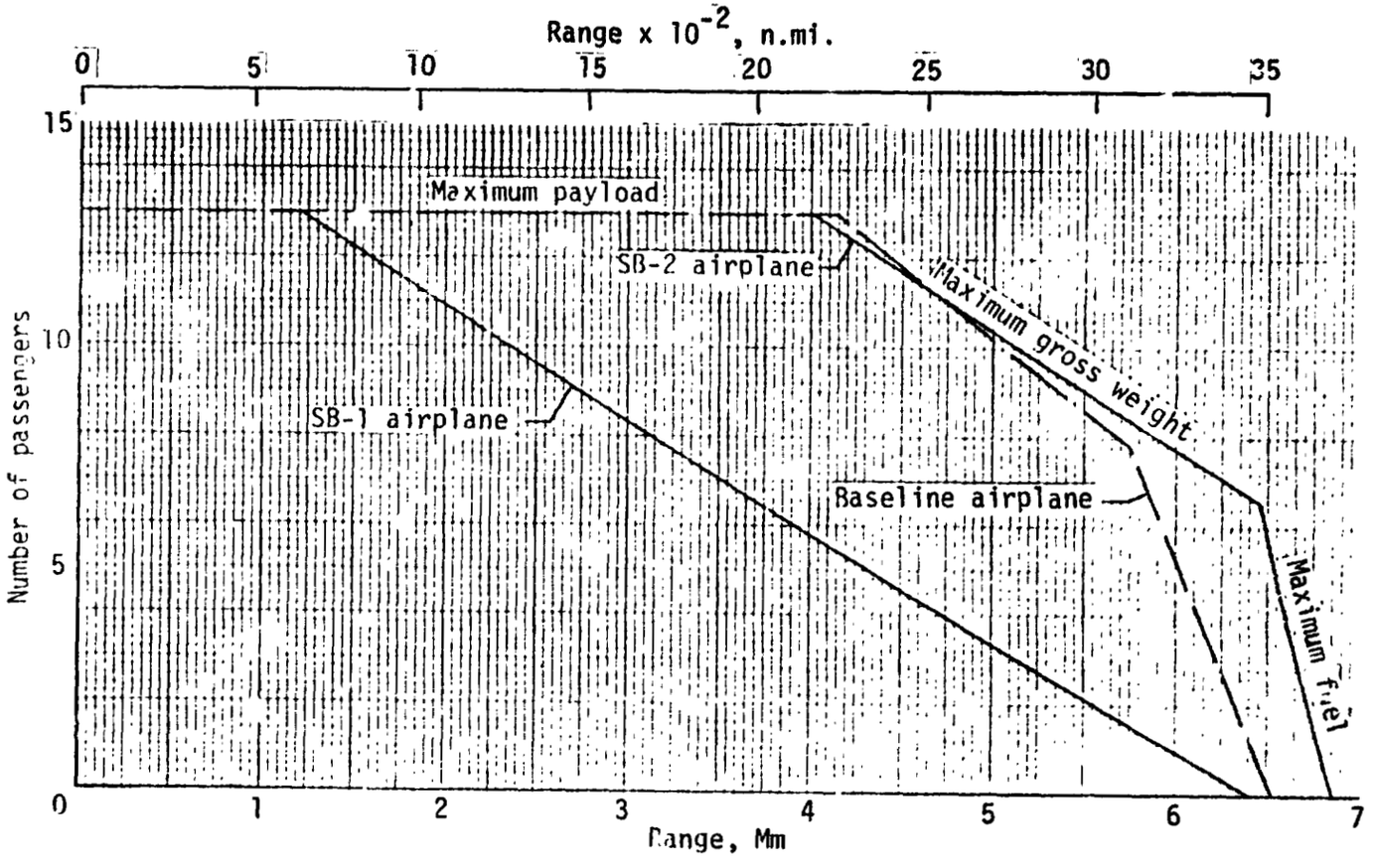

(a) Passenger accommodations adjusted for number of passengers.

re 31. - Payload versus range at high-speed cruise Mach numbers. Maximum gross weight equals 86.3 kN (19 400 lbf) for all models.

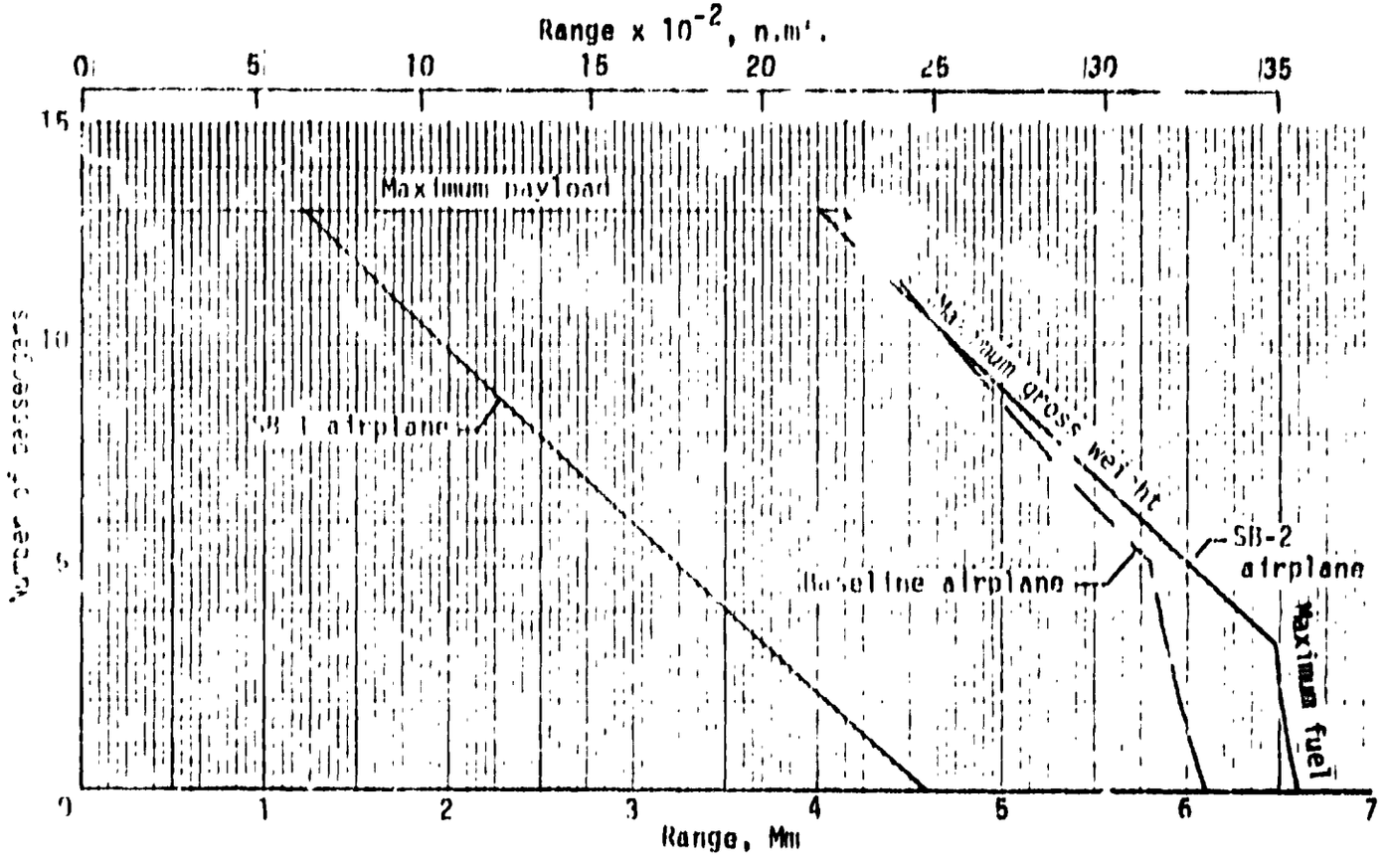

(b) Passenger accommodations for thirteen passengers.

Figure 31. - Concluded.

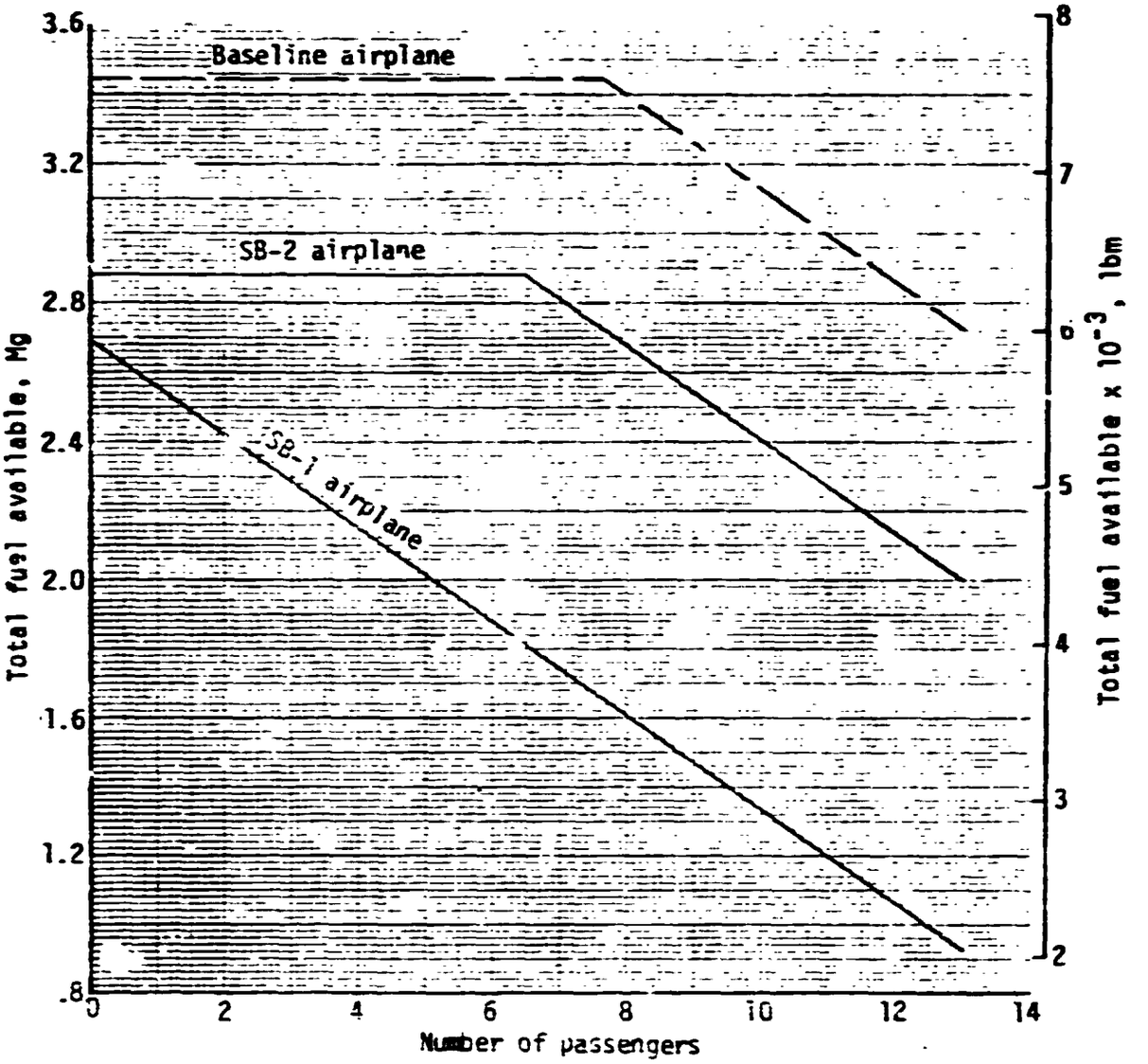

(a) Passenger accommodations adjusted for number of passengers.

Figure 32. - Total fuel available with maximum gross weight equal to 86.3 kN (19 400 lbf).

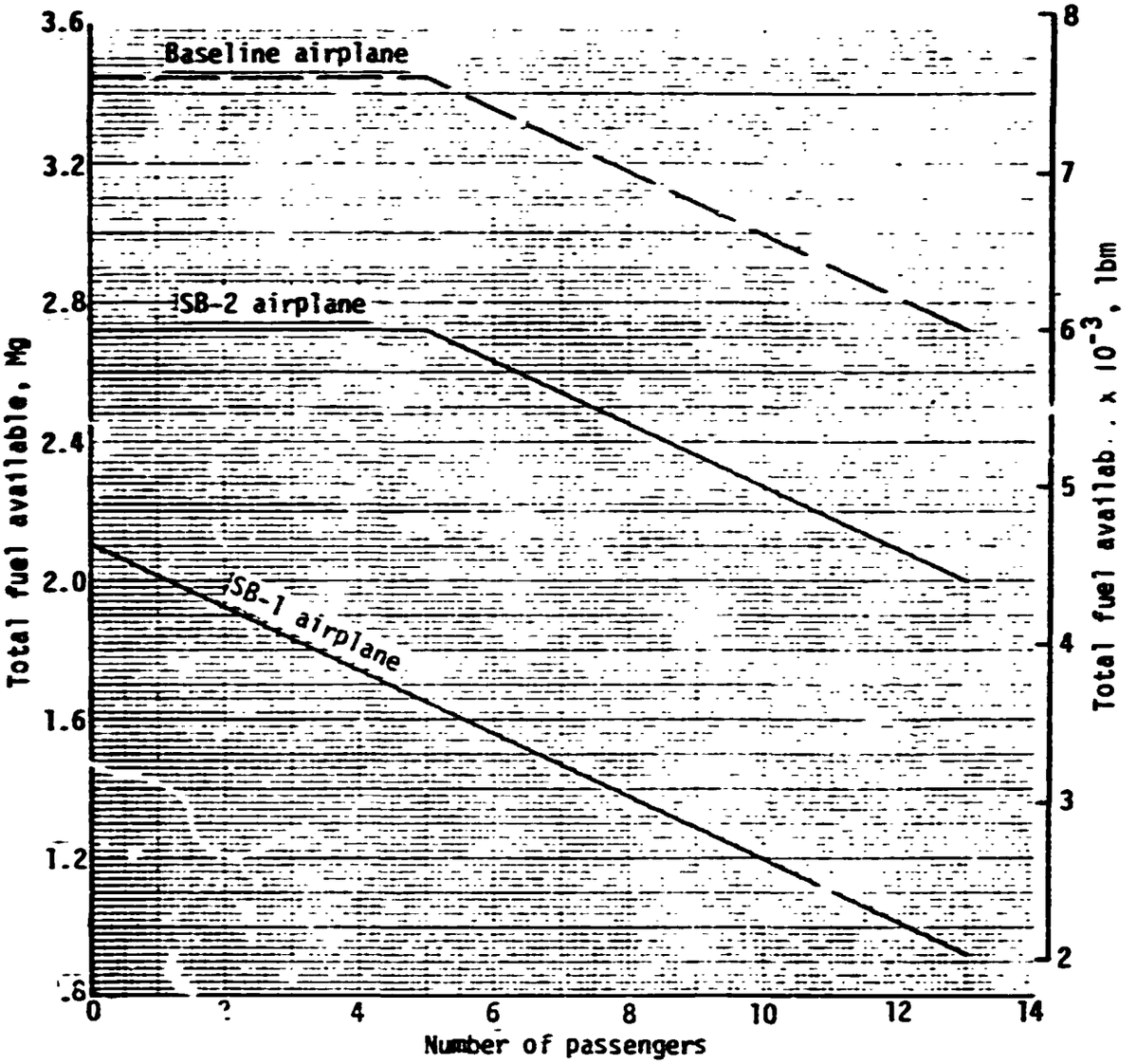

(b) Passenger accommodations for thirteen passengers.

Figure 32. - Concluded.

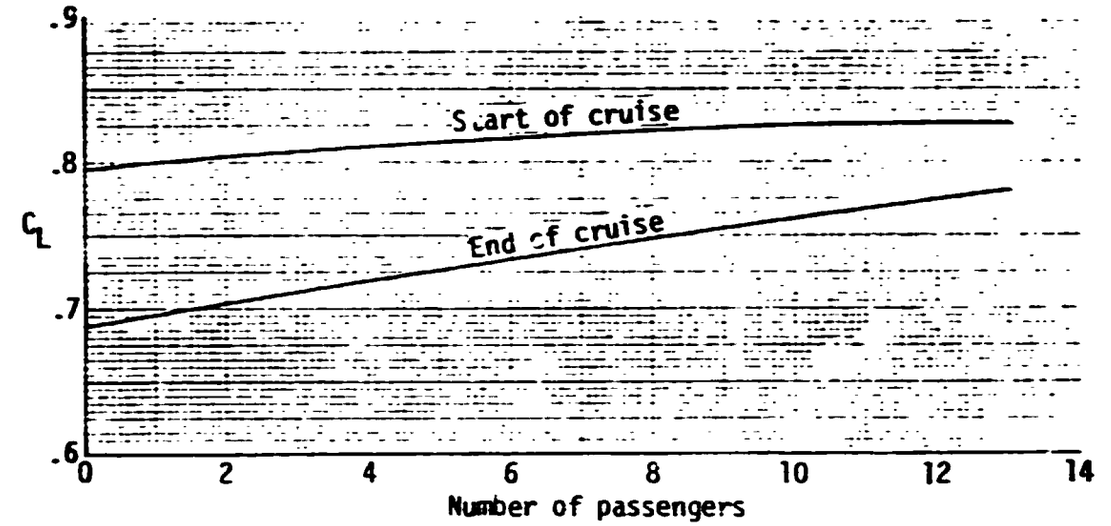

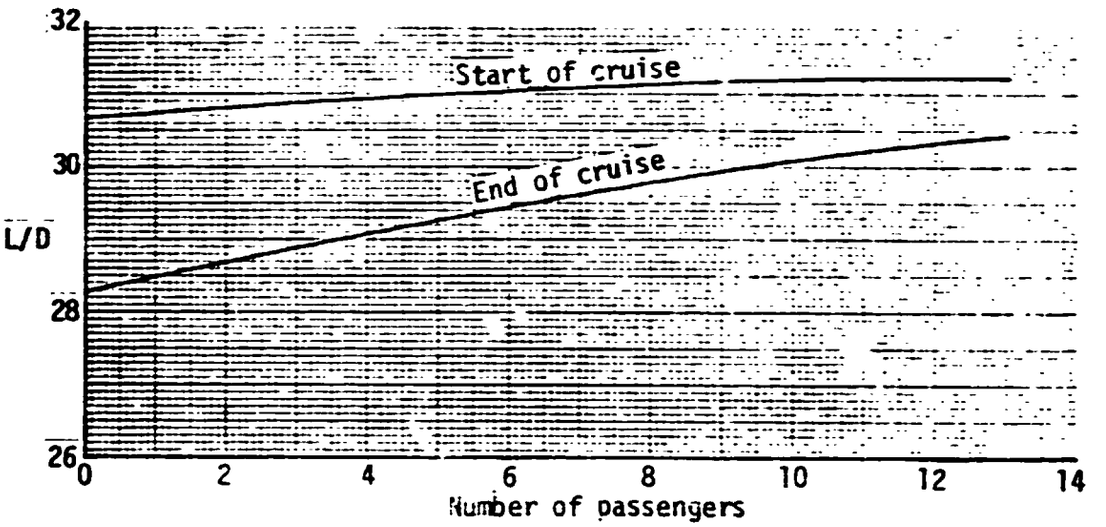

(a) SB-1 at M = .65.

Figure 33. - L/D and C_L versus number of passengers. Passenger accommodations adjusted for number of passengers.

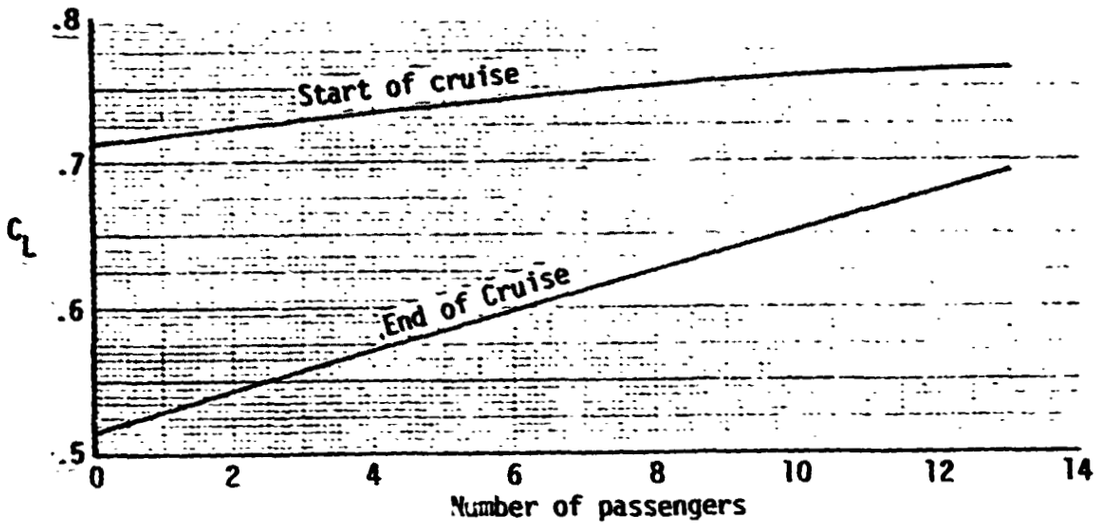

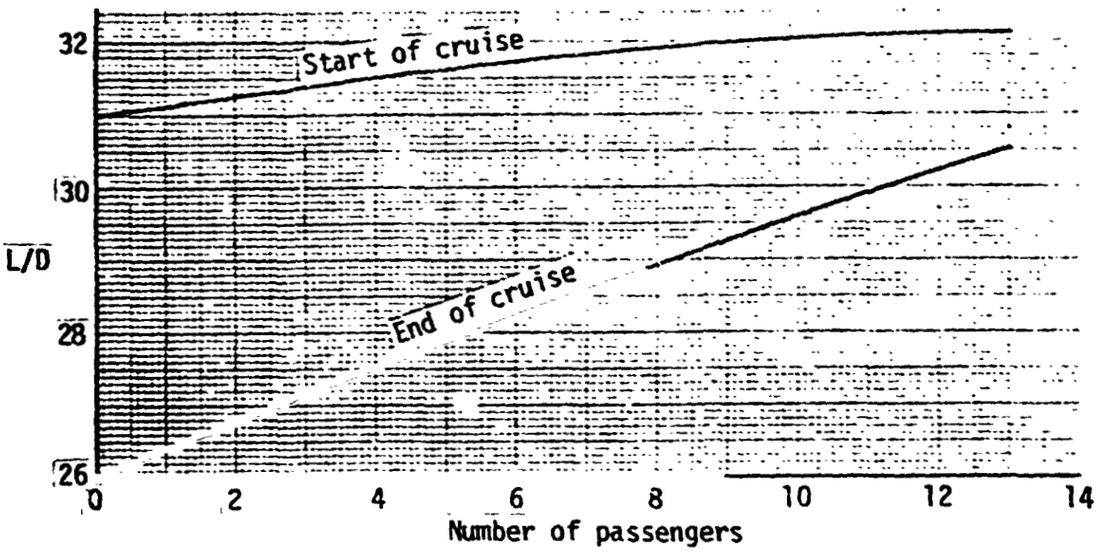

(b) SB-2 at M = 55.

Figure 33. - Concluded.

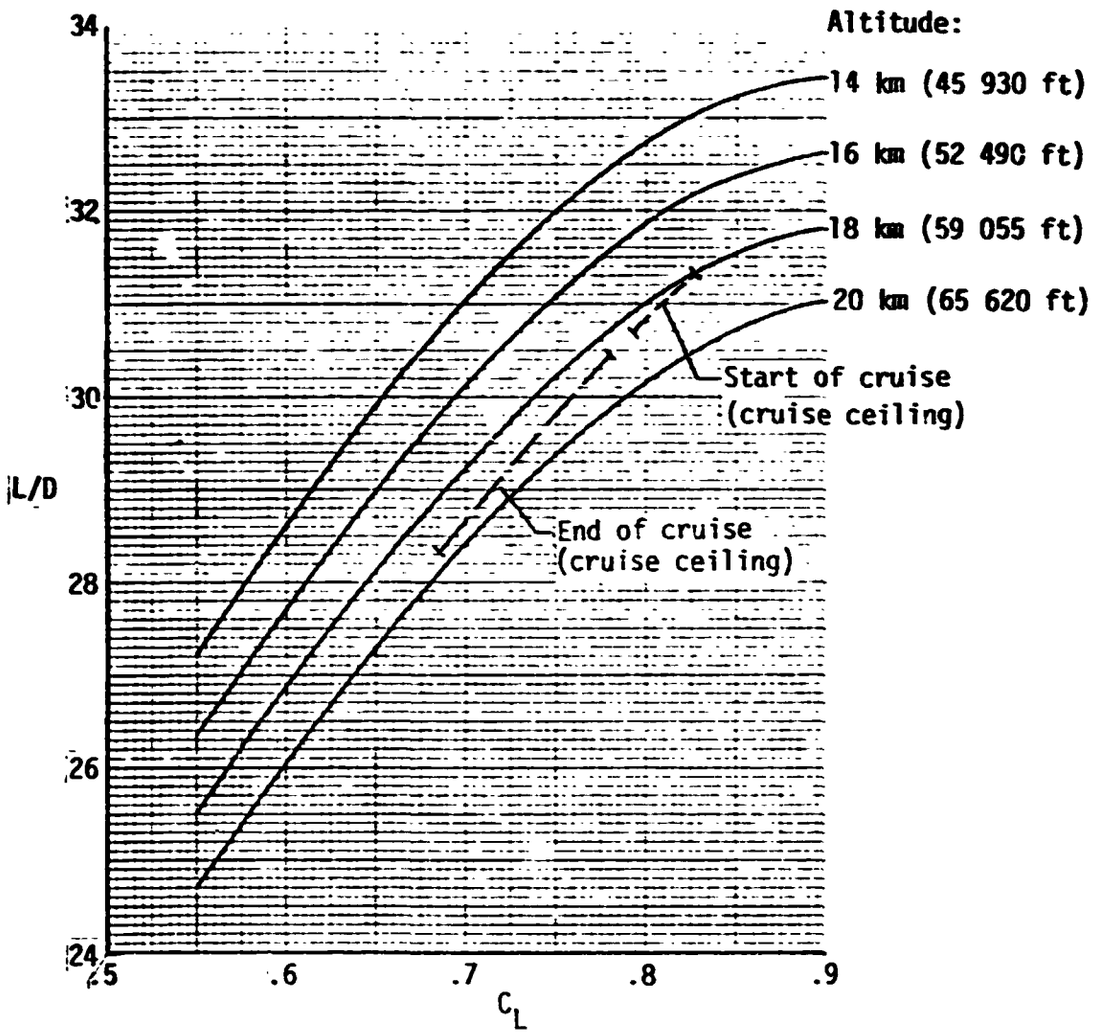

(a) SB-1 at M = .65.

Figure 34. - Cruise lift-drag ratios versus lift coefficient.

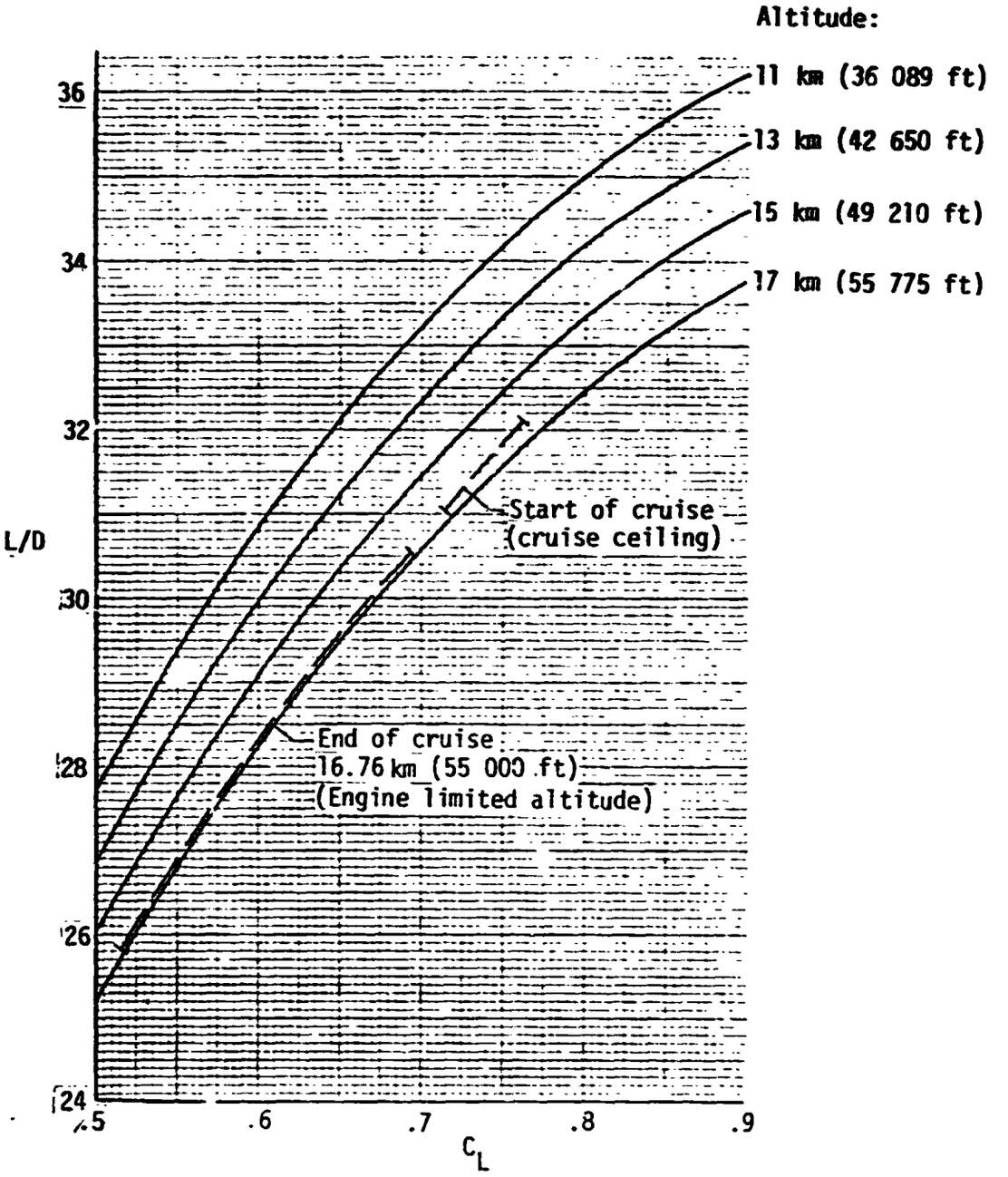

(b) SB-2 at M = .55.

Figure 34. - Concluded.

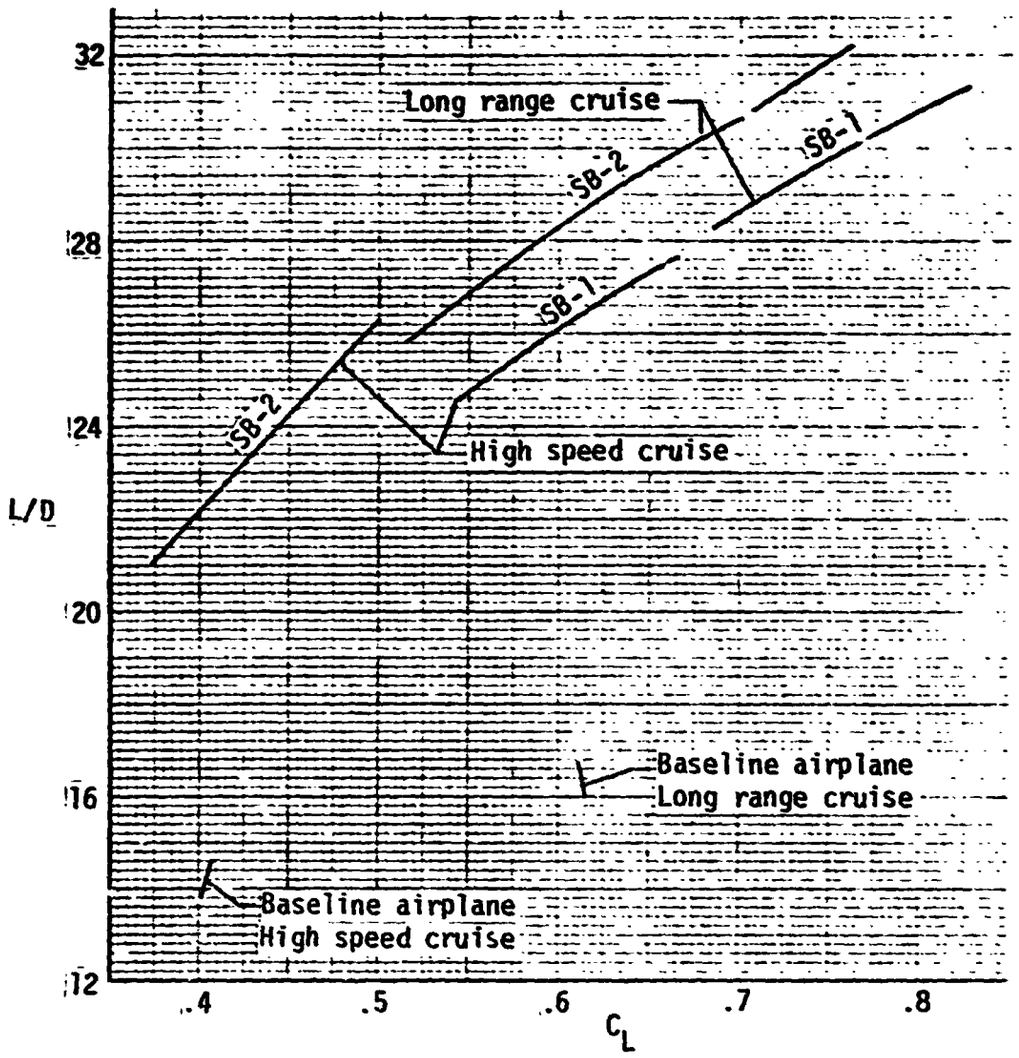

Figure 35. - Comparisons of cruise lift to drag ratios at long range cruise and high speed cruise conditions.

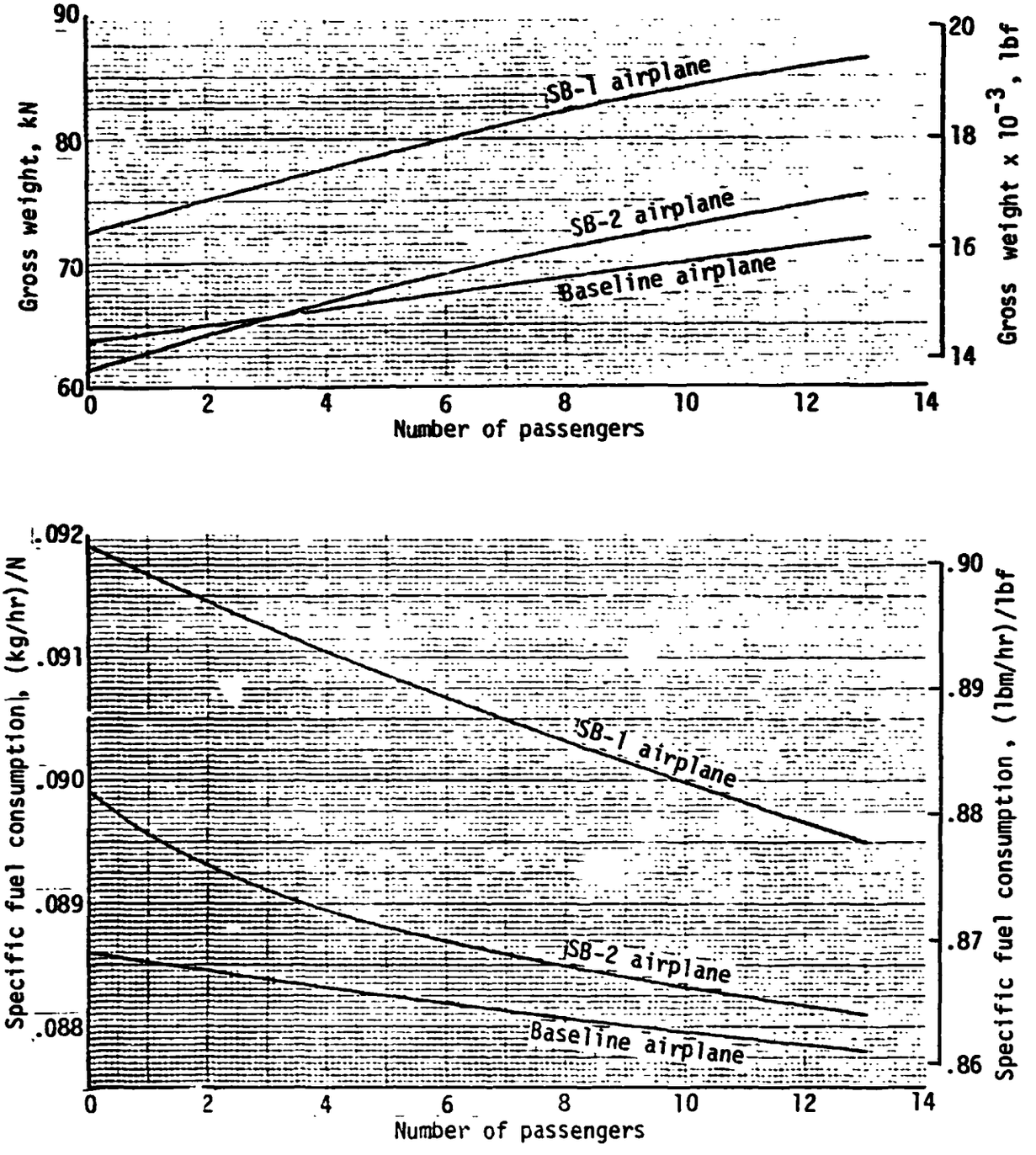

Figure 36. - Comparisons of average cruise gross weight and SFC for baseline range at long-range cruise speed, passenger accommodations adjusted for number of passengers.

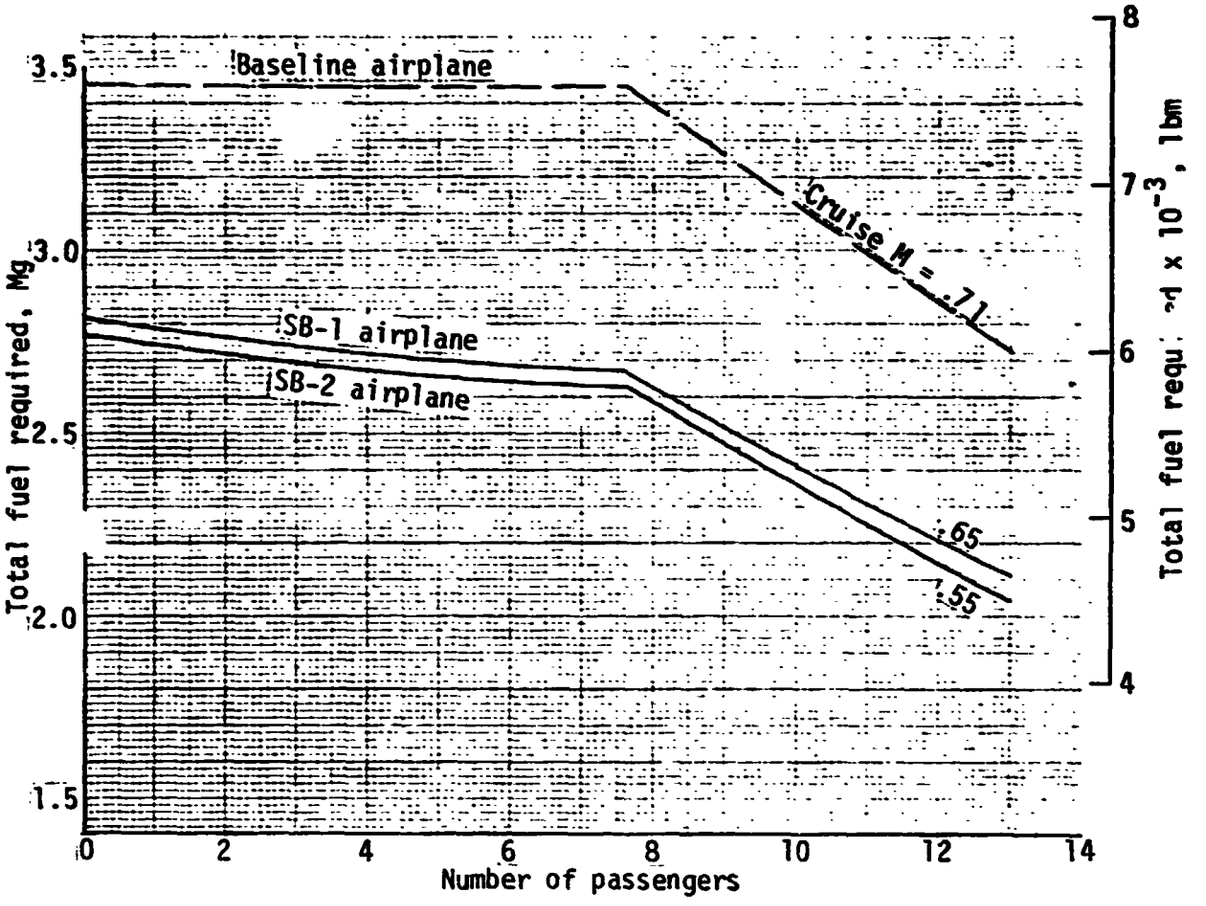

(a) Passenger accommodations adjusted for number of passengers.

Figure 37. - Total fuel required to fly baseline range, at long-range cruise Mach numbers.

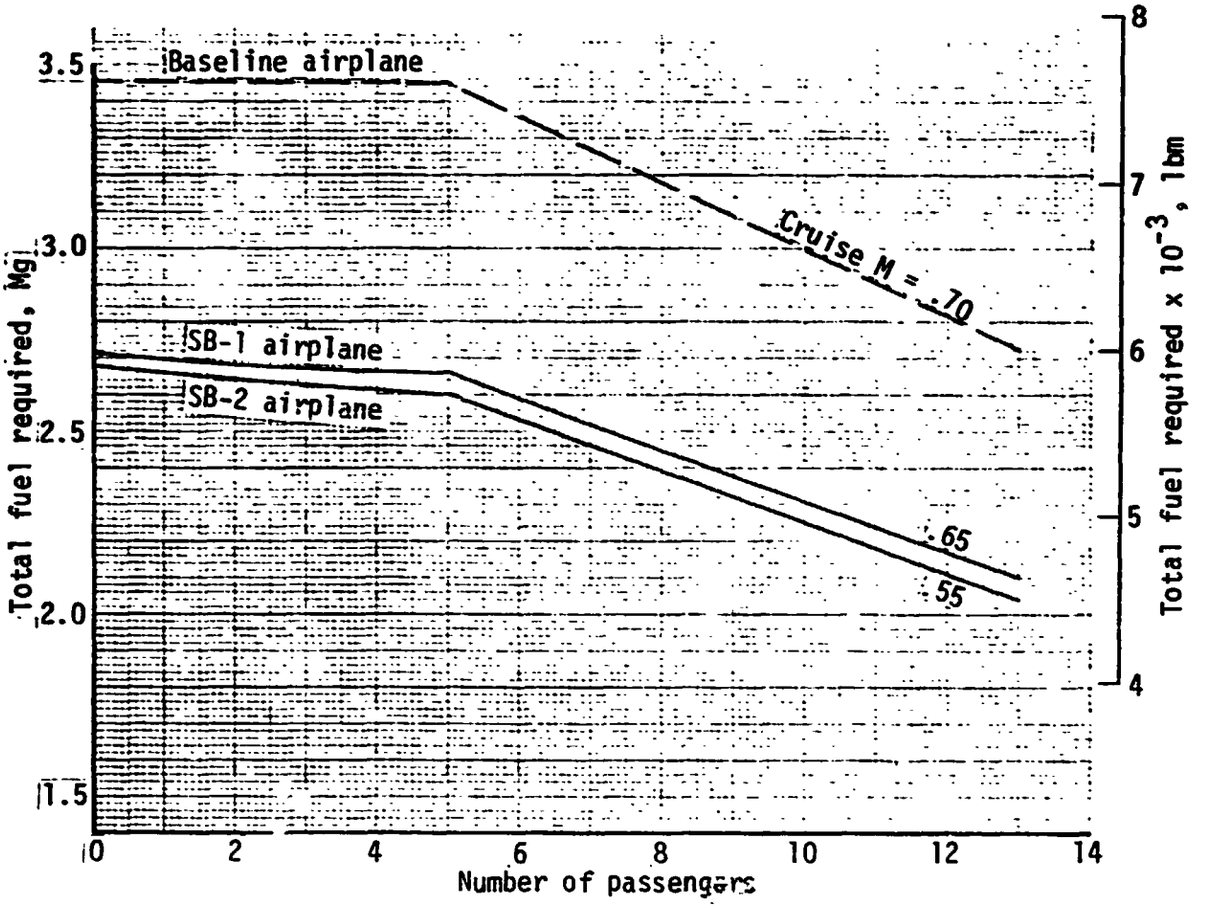

(b) Passenger accommodations for thirteen passengers.

Figure 37. - Concluded.

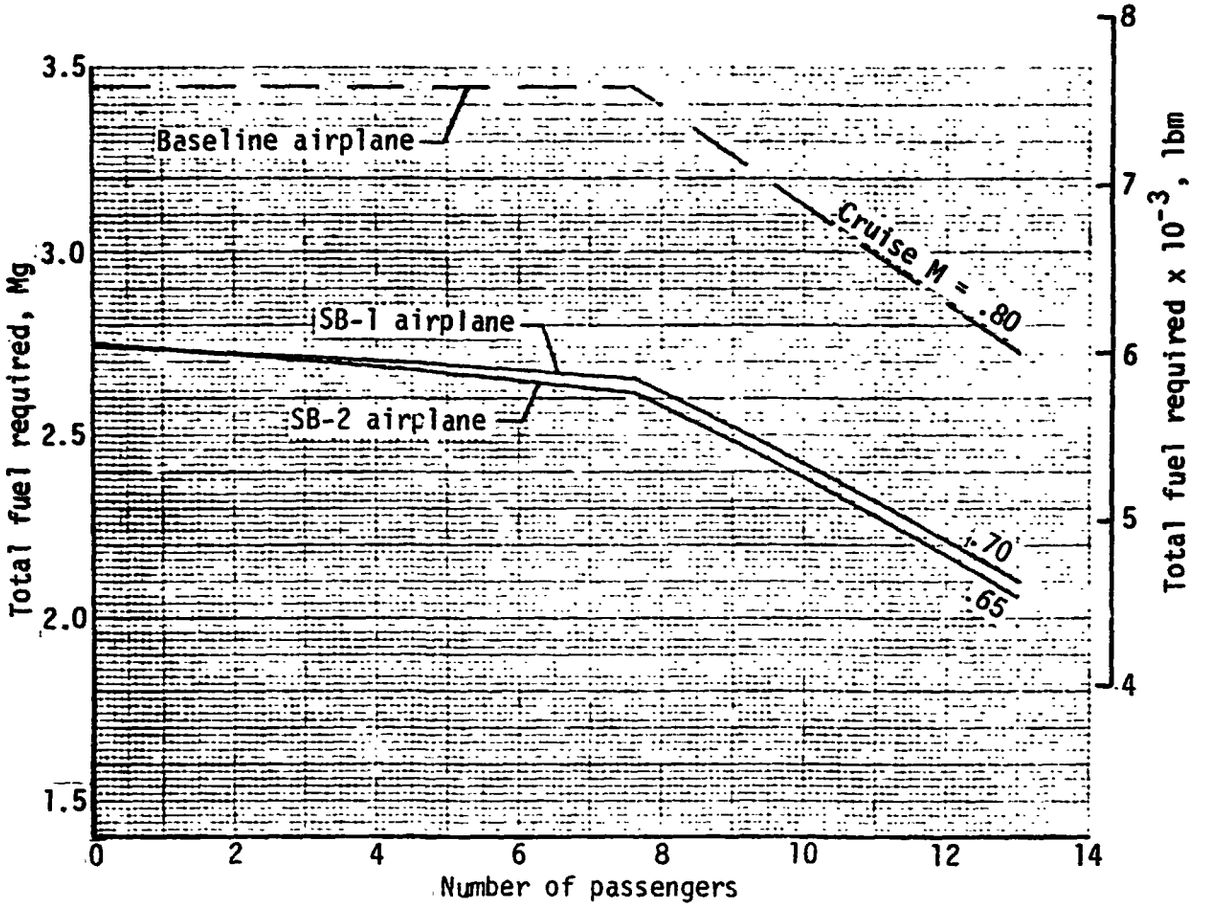

(a) Passenger accommodations adjusted for number of passengers.

Figure 38. - Total fuel required to fly baseline range at high-speed cruise Mach numbers.

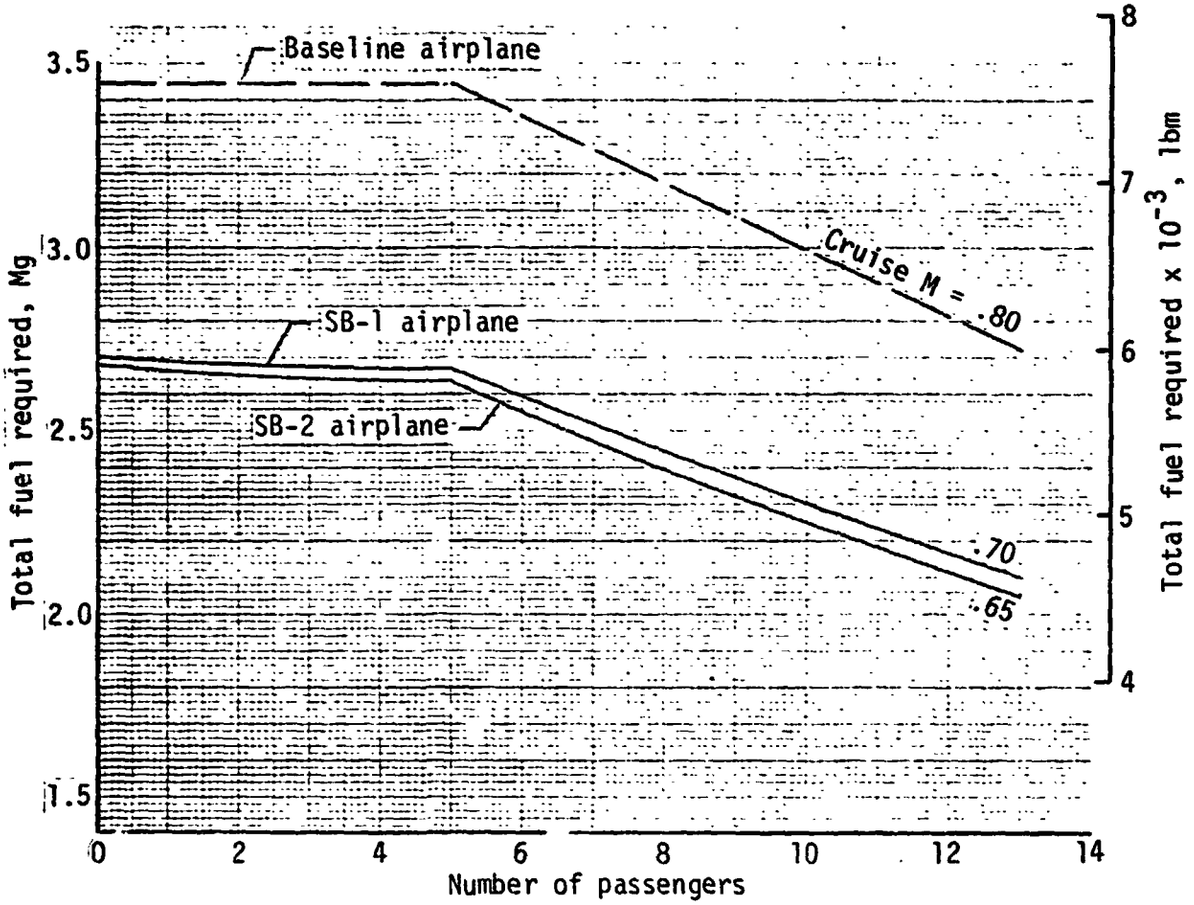

(b) Passenger accommodations for thirteen passengers.

Figure 38. - Concluded.

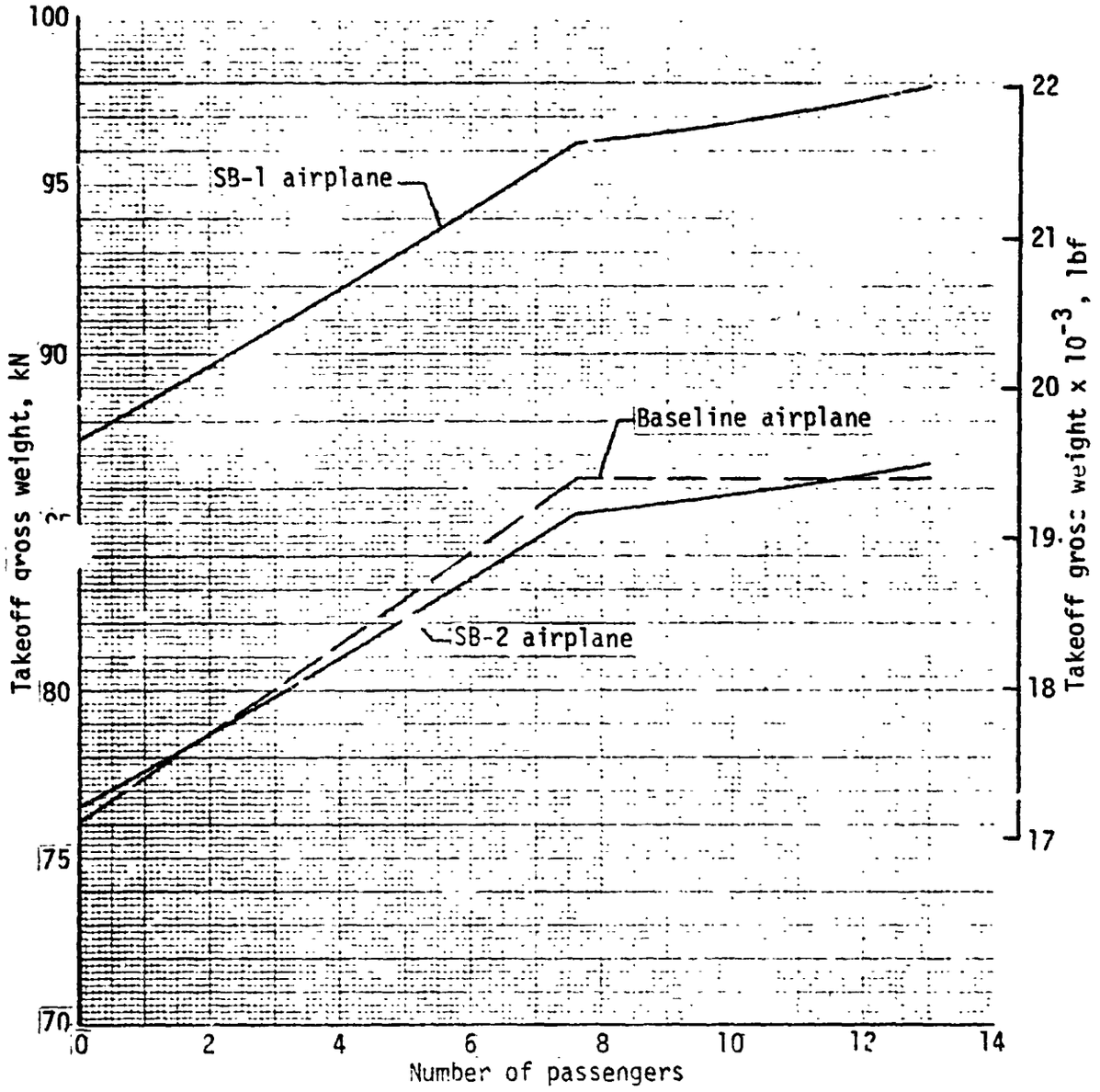

(a) Passenger accommodations adjusted for number of passengers.

Figure 39. - Takeoff gross weight for baseline payload-range missions, at long-range cruise Mach numbers.

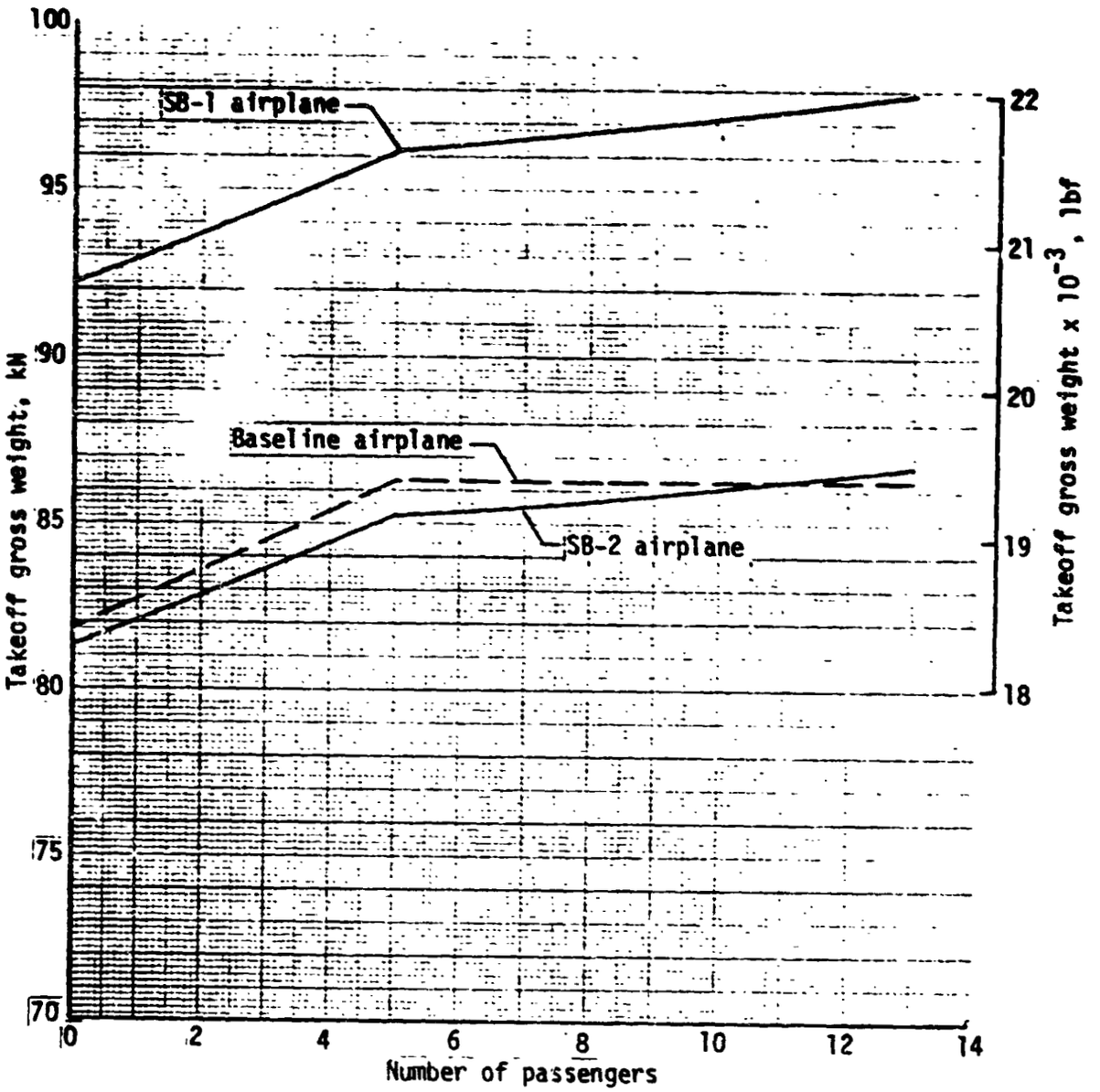

(b) Passenger accommodations for thirteen passengers.

Figure 39. - Concluded.

C-2

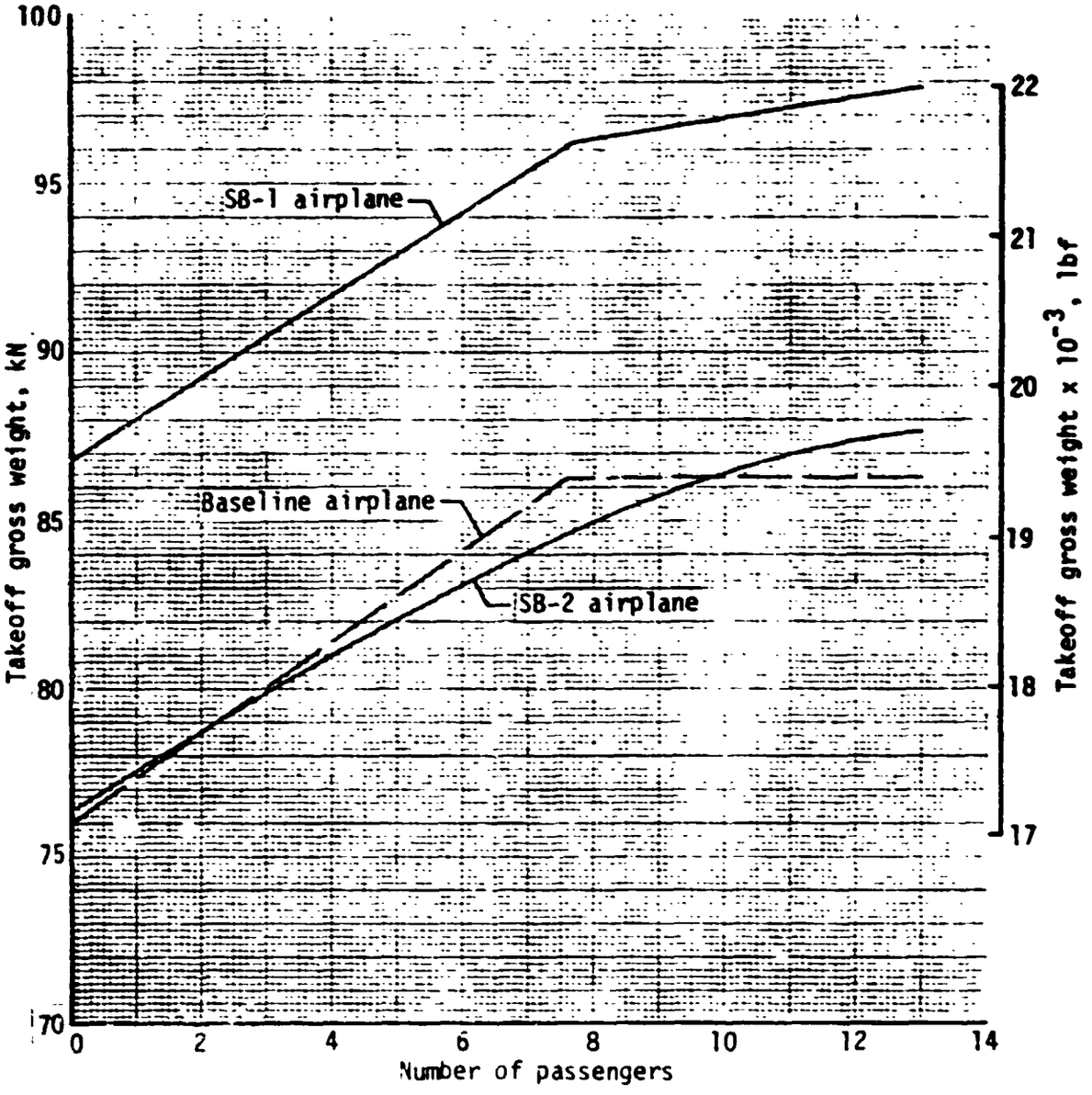

(a) Passenger accommodations adjusted for number of passengers.

Figure 40. - Takeoff gross weight for baseline payload-range missions, at high-speed cruise Mach numbers.

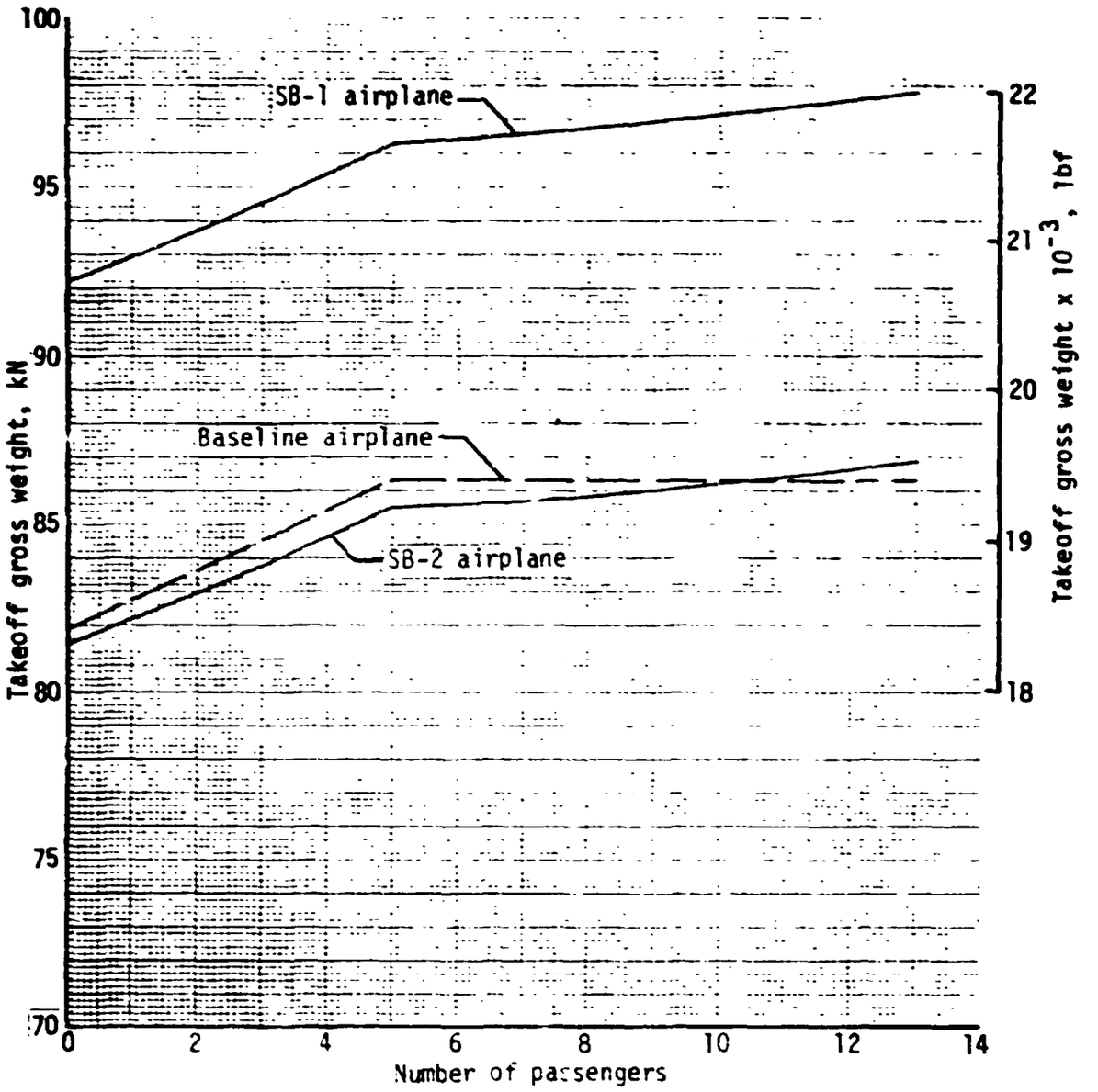

(c) Passenger accommodations for thirteen passengers.

Figure 40. - Concluded.